

## Advances in Molecular Structure and Interaction Studies Using Near-Infrared Spectroscopy

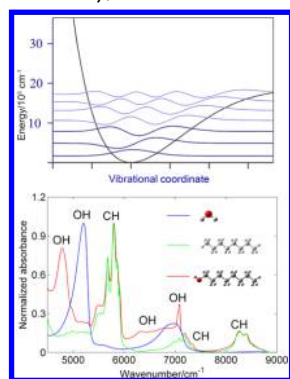
Mirosław Antoni Czarnecki,<sup>\*,†</sup> Yusuke Morisawa,<sup>‡</sup> Yoshisuke Futami,<sup>§</sup> and Yukihiro Ozaki<sup>\*,||</sup>

<sup>†</sup>Faculty of Chemistry, University of Wrocław, F. Joliot-Curie 14, 50-383 Wrocław, Poland

<sup>‡</sup>Department of Chemistry, School of Science and Engineering, Kinki University, Higashi-Osaka, Osaka 577-8502, Japan

<sup>§</sup>Department of Biological and Chemical Systems Engineering, National Institute of Technology, Kumamoto College, Yatsushiro, Kumamoto 866-8501, Japan

<sup>||</sup>Department of Chemistry, School of Science and Technology, Kwansei Gakuin University, Sanda, Hyogo 669-1337, Japan



### CONTENTS

1. Introduction	9707	
2. Principles and Advantages of NIR Spectroscopy	9708	
2.1. Brief History of NIR Spectroscopy	9708	
2.2. Principles of NIR Spectroscopy	9708	
2.3. Importance and Advantages of NIR Spectroscopy with Respect to Physical Chemistry	9709	
3. Spectral Analysis in the NIR Region	9710	
3.1. Classical Methods	9710	
3.2. Two-Dimensional Correlation Spectroscopy	9711	
3.3. Chemometrics	9712	
3.3.1. Principal Component Analysis (PCA)	9712	
3.3.2. Evolving Factor Analysis (EFA)	9712	
3.3.3. Multivariate Curve Resolution (MCR)	9712	
3.3.4. Multivariate Calibration	9713	
4. Applications of NIR Spectroscopy	9713	
4.1. Water	9713	
4.1.1. Structure of Bulk Water	9714	
4.1.2. Interaction of Water with Other Molecules	9716	
4.1.3. Hydration and Physical Properties of Aqueous Solutions	9717	
4.2. Hydrogen Bonding and Molecular Interaction	9718	
4.3. Phase Behavior and Phase Transition	9722	
4.4. Structure of Peptides and Proteins	9722	
4.5. Ionic Liquids	9723	
4.6. Gas-Phase Overtone Spectra	9724	
4.7. Matrix-Isolated Complexes	9725	
4.8. Spectra–Structure Correlations in the NIR Region	9725	
5. NIR Spectroscopy and Quantum Chemical Calculation Studies of Wavenumbers and Intensities of Overtones, Anharmonicities, Vibrational Potential Functions, and Intermolecular Interactions	9727	
5.1. Recent Progress in Quantum Chemical Calculations in NIR Spectroscopy	9727	
5.2. Quantum Chemical Calculation Studies of Wavenumbers and Intensities of Overtones, Anharmonicities, Vibrational Potential Functions, and Intermolecular Interactions	9731	
5.3. Some Examples of NIR Spectroscopy and Quantum Chemical Calculation Studies on Wavenumbers and Absorption Intensities of Overtones and Intermolecular Interactions	9732	
5.3.1. NIR/IR Spectroscopy and a DFT Calculation Study on the Frequencies and Intensities of the Fundamentals and Overtones of the NH Stretching Vibrations of Pyrrole and a Pyrrole–Pyridine Complex	9732	
5.3.2. Quantum Chemical Calculation Study on the Dielectric Constant Dependence of Frequencies and Absorption Intensities of the Fundamental and the First, Second, and Third Overtones of the Stretching Vibration of Hydrogen Fluoride	9735	
5.3.3. Vis/NIR/IR Spectroscopy Studies of Effects of Hydrogen Bonding on the Frequencies and Intensities of the Fundamental and the First, Second, and Third Overtones of the OH Stretching Mode of Phenol and 2,6-Dihalo-genated Phenols	9735	
6. Concluding Remarks	9736	
Author Information	9737	
Corresponding Authors	9737	
Notes	9737	
Biographies	9737	
References	9738	

Received: January 9, 2014

Published: September 10, 2015



## 1. INTRODUCTION

Near-infrared (NIR) spectroscopy involves the spectral region of 12 500–4000  $\text{cm}^{-1}$  (800–2500 nm). This is the region where bands due to electronic transitions as well as those due to overtones and combination modes are expected to appear.<sup>1–10</sup> During the past two decades or so, NIR spectroscopy has made remarkable progress due to advances in instrumentation and spectral analysis. This is true for basic science and in a wide range of practical applications. The purpose of this Review is to give an up-to-date account of the current state-of-the-art applications of NIR spectroscopy with respect to physical chemistry. First, it should be pointed out that this technique incorporates both electronic as well as vibrational spectroscopy.<sup>11–15</sup> From a vibrational spectroscopy perspective, it is concerned only with overtones and combination modes, and hence is more versatile when compared with mid-infrared (MIR) and Raman spectroscopy. NIR spectroscopy is also concerned with electronic transitions, and a number of molecules are found which yield absorption bands due to electronic transitions in the NIR region.<sup>11–15</sup> In general, electronic spectroscopy in the NIR region is usually considered as a simple extension of the spectroscopy in the visible (Vis) region. However, electronic NIR spectroscopy, in fact, has specific properties as will be described later.

The diversity of NIR spectroscopy is reflected in the wide range of spectrometers and instruments available. In the MIR region most of the spectrometers used are Fourier-transform (FT) instruments, whereas in the Vis region scanning dispersive spectrometers are usually employed. For NIR spectroscopy, both FT spectrometers and dispersive spectrometers are commonly used. The dispersive ones with a charge-coupled device detector play an important role in the short-wavelength NIR (SWNIR) region (12 500–9000  $\text{cm}^{-1}$ /800–1100 nm). Portable spectrometers using light fibers are also very popular.

Another notable diversity in NIR spectroscopy is its capability for spectral analysis. Compared with other kinds of spectroscopy, chemometrics is regularly used for NIR spectral analysis.<sup>16–20</sup> In fact, one can confidently say that chemometrics has developed simultaneously with progress in NIR spectroscopy. Two-dimensional (2D) correlation analysis is also often used in NIR spectroscopy.<sup>21–25</sup> Currently, quantum chemical calculations are becoming popular for the analysis of NIR spectra and for investigations on the intensities of overtones, vibrational potentials, and anharmonicity.<sup>26–33</sup> All of these “add-ons” have contributed to the huge versatility in NIR spectroscopy applications, for example, with solids, crystals, fibers, powders, liquids, solutions, and gases. In addition, most kinds of materials, from purified samples to bulk materials, can be subjected to NIR measurements.<sup>1–10</sup>

As mentioned above, this Review is concerned with NIR applications in physical chemistry; hence, we will first describe the principles and advantages of NIR spectroscopy including a brief history. NIR spectral analytical methods, particularly those for bands due to overtones and combination modes, will then be discussed in some detail. This will be followed by a number of examples of physical chemistry applications. The focus throughout the Review will be on the originality and usefulness of NIR spectroscopy in exploring molecular structure and interactions. Only a few measurements involving electronic transitions will be mentioned because examples of applications

to physical chemistry based on electronic NIR spectroscopy are, in fact, very rare.

## 2. PRINCIPLES AND ADVANTAGES OF NIR SPECTROSCOPY

### 2.1. Brief History of NIR Spectroscopy

The history of NIR spectroscopy stretches back to the 1880s, when Abney and Festing measured the spectra of simple organic compounds in the 700–1200 nm (14 286–8333  $\text{cm}^{-1}$ ) region.<sup>34</sup> It was in the 1930s that bands due to the overtones of many compounds were first successfully measured. By the 1940s, a number of papers reporting NIR spectra had been published in scientific journals.<sup>1</sup> In the 1950s, NIR spectroscopy attracted considerable attention with respect to hydrogen bonding and anharmonicity studies. In addition, several good review papers appeared.<sup>35,36</sup> However, further developments were slow, most probably because of the insufficient availability of suitable spectrometers for the NIR region and the difficulty in the spectral analysis. From the 1960s to the 1980s, both MIR and Raman spectroscopy made remarkable progress, as evidenced by their extensive use in chemistry. This success led in some ways to the usefulness of NIR spectroscopy being overlooked.

Interestingly, it was not a spectroscopist but an agricultural engineer who awakened the “sleeping giant” in the 1960s.<sup>37,38</sup> Karl Norris of the United States Department of Agriculture, fittingly called the “father of NIR spectroscopy”, applied this technique to the quality assessments of agricultural products. He proposed the excellent idea of using statistical methods to develop calibrations from NIR data. His idea realized the advantages of NIR spectroscopy in practical applications. A pioneering study on the potential of medical applications of NIR spectroscopy was carried out by Jöbsis.<sup>39</sup> He monitored the redox behavior of cytochrome *c* oxidase *in vivo*. The continued progress of this technique in applications such as agriculture, food engineering, chemical and polymer engineering, and biomedical sciences stimulated a rapid progress in NIR instrumentation and spectral analysis throughout the 1980s and 1990s.<sup>1–10</sup> The applications of NIR spectroscopy in basic sciences such as physical chemistry during the past two decades followed. Thus, this is an example of the rather rare case in spectroscopy where practical applications have inspired applications in the basic sciences.

The renaissance of NIR spectroscopy as a basic spectroscopic technique took place in the 1990s, thanks to the fast development of new NIR spectrometers and the extended use of spectral analysis methods during that period. New technology, particularly FT-NIR instruments, combined with chemometrics, generalized 2D correlation analysis, and quantum chemical calculations, stimulated on the one hand novel studies on overtones and combination modes and their anharmonicity, and on the other hand unique investigations of molecular structures, interactions, reactions, and properties.<sup>1,8</sup> Also very sensitive laser-based techniques (for gas phase) like cavity ring-down have been recently used.<sup>40</sup>

### 2.2. Principles of NIR Spectroscopy

As has been previously mentioned, NIR spectroscopy is concerned with both electronic and vibrational transitions.<sup>1–15</sup> It should be noted that it is rather difficult to differentiate electronic transitions in the Vis region and those in the NIR region. What one can say, however, is that most of the electronic transitions observed in the NIR region are d-d

transitions, charge-transfer transitions, and  $\pi$ – $\pi$  transitions of conjugated systems.<sup>11–15</sup> Another famous electronic transition in the NIR region is that of the O<sub>2</sub> forbidden band first observed by cavity ring-down spectroscopy by O’Keefe and Deacon in 1988.<sup>41</sup> Bands due to electronic transitions observed in the NIR region are, in general, weak. Moreover, overtones and combination modes, arising from so-called forbidden transitions, also yield relatively weak bands.<sup>1–10</sup> The fact that the NIR region is a spectral range of forbidden transitions within the harmonic oscillator approximation makes this region unique and markedly different from the other spectral regions. It is possible, therefore, to make the general statement that the NIR region transmits light well and, consequently, NIR absorption is weak.

Some NIR band characteristics can be summarized as follows:<sup>1–4,8–10</sup>

- (1) NIR absorption band intensities are much weaker than those of MIR absorption bands.
- (2) A number of the bands due to overtones and combination modes overlap each other. In addition, many bands due to Fermi resonance also appear in the NIR region, all of which means that band assignments in this spectral range are not straightforward.
- (3) Bands ascribed to functional groups (e.g., OH, CH, NH) containing a hydrogen atom dominate the NIR spectra. This is partly because the anharmonic constant of an XH bond is large and partly because a fundamental of the XH stretching vibration has a high frequency. One sometimes observes an absorption arising from the second overtone of a C=O stretching vibration in the 5260–5130 cm<sup>–1</sup> region.<sup>42</sup> In contrast, a C=C vibration does not yield bands in the NIR region. Such bonds provide information in the form of combination modes of a C–H group that is linked with a C=C bond.
- (4) As in the case of a MIR spectrum, a hydrogen bond and an interaction between molecules cause a shift and intensity changes for particular bands. This shift for the overtone bands is much larger than that of the corresponding MIR bands.
- (5) XH stretching bands (X = O, N) due to monomeric and polymeric species are better separated in the NIR region than in the MIR region. Even bands assigned to free, terminal XH groups of the linear associates can be identified.<sup>23,43</sup>
- (6) Because of the larger anharmonicity, bands ascribed to the first overtones of the XH (X = O, N) stretching modes of monomeric species exhibit much greater intensity enhancement compared with the corresponding bands of polymeric species.<sup>44</sup>

Functional groups including a hydrogen atom, such as CH, NH, and OH, play important roles in chemical bonding and chemical phenomena such as hydrogen bonding, hydrogen transfer, and tunneling effects. Vibrations of these substituents greatly reflect even subtle changes in the molecular structures and interactions. It can be concluded, therefore, that NIR spectroscopy has unique advantages in the investigation of molecular structures and interactions.

### 2.3. Importance and Advantages of NIR Spectroscopy with Respect to Physical Chemistry

In physical chemistry and molecular science investigations, NIR spectroscopy holds significant unique advantages over MIR and Raman spectroscopy. Of particular importance is the fact that

NIR studies of anharmonicity and vibrational potentials that are essential for understanding molecular structures yield significant data. A combination of NIR data and quantum chemical calculations should lead to further progress in studies of anharmonicity and vibrational potentials. In this Review we will demonstrate the potential of such studies in [section 5](#).

The keywords for MIR and Raman spectra are dipole moment and polarizability, respectively.<sup>1,2,8</sup> On the other hand, anharmonicity of vibrational potential and nonlinearity in the dipole moment function are keywords for understanding NIR spectra in terms of both intensity and frequency. Most of advantages and uniqueness of NIR spectroscopy originate from anharmonicity. One could, in fact, call NIR spectroscopy the “spectroscopy of anharmonicity”. One peculiar characteristic of this technique is that it exhibits distinct types of “selectivity”, which also arise from anharmonicity. The first selectivity means that, with a few exceptions, only those bands due to the overtones and combination modes of XH (X = C, O, N) groups are observed in an NIR spectrum. Bands assigned to overtones and combination modes of C–X and C=X (X = C, N, O) groups are not observed, except for the second overtone of the C=O stretching mode.<sup>42</sup> Thus, information obtained from the NIR spectrum is mainly concerned with hydrogen bonding and the interactions of the XH groups. As a result, it is usually difficult to study the backbone structure of a molecule using NIR spectroscopy. The second selectivity is that the overtones of free XH (X = O, N) groups are much stronger than those of hydrogen-bonded XH groups. Therefore, it is often easier to monitor the process of dissociation of polymeric species into monomeric ones in the NIR region than in the MIR region. This can be achieved by using the first overtone of the OH or NH stretching mode of the monomeric species. A good example is shown in [Figure 1](#), which displays the MIR and NIR spectra of Nylon-12 over a temperature range of 298–453 K. In the MIR spectra a band due to the stretching mode of a free NH is extremely weak or missing at room temperature; it appears only weakly at higher temperatures. In contrast, the NIR spectra show quite different intensity patterns. It should be noted that, at higher temperatures, absorption from the first overtone of the stretching mode of a free NH is stronger than that arising from the hydrogen-bonded species. This example is a good illustration of the second selectivity of NIR spectroscopy and how it can be used to easily identify free species. However, one must be careful about the intensity of a band due to the free NH because it does not always reflect the relative content of the free species. Anharmonicity leads to another kind of selectivity. Overtones of the antisymmetric stretching XH<sub>2</sub> (e.g., CH<sub>2</sub>, NH<sub>2</sub>) modes are much stronger than those of the corresponding symmetric stretching modes. The second and third overtones of the symmetric XH<sub>2</sub> stretching modes often cannot be observed.

NIR spectroscopy is unique also in the separation of bands in the wavenumber direction.<sup>1,2,8,44</sup> Because it deals with overtones, a band shift induced by the formation of a hydrogen bond or other interaction nearly doubles, triples, and so on compared with the corresponding shift in the MIR spectra. Thus, a band due to the free species is more clearly separated from a band of the associated species in NIR spectrum than in MIR spectrum. Thus, it is possible to discriminate even between a band assigned to a free XH group in a monomeric species and that attributed to a terminal free XH group in the linear associates.<sup>23,43</sup> It may also be possible to identify bands due to XH groups in small entities such as dimers, trimers, and



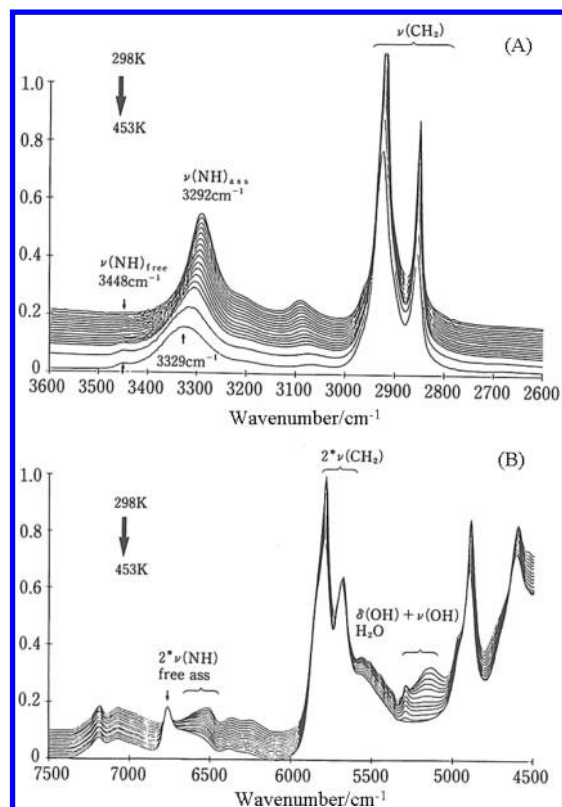


**Figure 1.** Temperature-dependent MIR (A) and NIR (B) spectra of Nylon-12 from 298 to 453 K. Reproduced with permission from H. W. Siesler, from Siesler, H. W. In *Kinsekigai-Bunkouhou* (in Japanese, Near-Infrared Spectroscopy); Ozaki, Y., Kawata, S., Eds.; Gakkai Shuppan Center: Tokyo, 1996 (translated by Y. Ozaki).

tetramers. NIR spectroscopy has been employed to investigate hydrogen bonds, hydration, and self-association of a variety of compounds, from simple molecules such as water and alcohols to complicated ones such as polymers and proteins.<sup>1,2,8,23–33,42–106</sup> From the physical chemistry and molecular science point of view, NIR spectroscopy is useful for the following studies:

- (1) inter- and intramolecular interactions including weak hydrogen bonds such as C–H···O (refs 23,24,30–33,42,43,45,46,50,54,58–67,72–84,88–90)
- (2) dissociation and association processes; determination of association constants<sup>23,50,72–74,80,83,84</sup>
- (3) hydration; solvent–solute interactions<sup>31,32,42,54–67,69,91</sup>
- (4) crystal structures and crystallization processes<sup>45,50,72–74</sup>
- (5) structures of rotational isomers<sup>23,43,73–79,100</sup>
- (6) phase transition and phase separation<sup>23,50,72–74,83–86,91</sup>

### 3. SPECTRAL ANALYSIS IN THE NIR REGION

Spectral analysis relies on band assignments. In the NIR region this is not as straightforward as in the fundamentals region. Yet, a growing number of NIR studies involving a range of compounds appear to be helpful in establishing assignments for most of the spectral features appearing in this spectral region. There are some recent text books which comprehensively cover the characteristic NIR band assignments.<sup>1–3,9</sup> Reliable band assignment is particularly important for the molecular structure and hydrogen bonding investigations since such studies are based on spectra–structure correlations. These can be obtained in two ways: by comparing either the NIR spectra of related

compounds recorded under the same experimental conditions or the spectra of the same compound recorded under different conditions.<sup>107,108</sup> The so-called “perturbation-dependent analysis” is based on monitoring spectral changes induced by variations in temperature, pressure, concentration, pH among others. As in the MIR region, isotopic substitution is also very useful method for establishing band assignments. In the NIR region it is mainly overtones and combinations of X–H vibrations that appear. Hence, after isotope exchange one can expect significant changes in the spectra.<sup>46,107</sup> For example, the separation of water absorption from that of proteins in aqueous solutions is often achieved by using deuterated water as the solvent.<sup>47</sup>

Direct interpretation of NIR spectra of liquid and solid samples provides only limited information due to the overlap of the numerous overtones and combination bands. This means that detailed exploration of these spectra requires, in addition to classical techniques such as the use of difference or derivative spectra, the application of more advanced tools including quantum chemical calculations, 2D correlation analysis, and chemometric methods. Usually, prior to any further analysis, the NIR spectra require pre-processing. Recently, the most common methods of pre-processing NIR spectra were reviewed by Rinnan et al.<sup>109</sup> Another important factor in the recent progress of spectral analysis in NIR spectroscopy is the development of quantum chemical calculations. These calculations are significant not only for spectral analysis but also for physical chemistry studies themselves such as anharmonicity, vibrational potentials, and intensities of overtones. Quantum chemical calculations are described in section 5.

#### 3.1. Classical Methods

The calculation of difference spectra is both a simple and useful method for the analysis of complex spectra. Even small spectral changes not clearly seen in the raw data appear pronounced in the difference spectra. Difference spectroscopy is a very convenient and efficient method for the separation of the solute absorption from that of the solvent. It can also be used to separate the absorptions of different components of the mixture from each other. In the simplest case the subtraction factor is assumed to be 1. In the more advanced mode, however, this factor is optimized by minimizing the difference between the spectra in the selected region containing common bands. The calculation of reliable difference spectra is possible only in the case of high-quality source data. These can be easily measured by using the FT-based instruments.

The resolution enhancement of vibrational spectra can be significantly improved by calculation of the derivative spectra.<sup>110</sup> This method allows the estimation of the number of bands and their positions. In addition, since the broad spectral features appearing in the source data do not occur in the derivative spectra, spectral derivatization can be used for baseline elimination. In general, the higher the order of the derivative, the better is the resolution enhancement. However, in vibrational spectroscopy it is mainly the first and second derivatives that are used since the higher order derivatives require superior signal-to-noise ratio. For this reason, the calculation of the derivative spectra is often coupled with a smoothing procedure. The most popular Savitzky–Golay method is based on the approximation of small amount of the data points (window) by a low-degree polynomial.<sup>111</sup> Interpreting the second derivative spectra requires that one has

to take into account the side lobes appearing on both sides of the main peak.

Fourier self-deconvolution is another method used for resolution enhancement in vibrational spectra.<sup>112</sup> This approach provides a way of computationally resolving overlapped bands that cannot be instrumentally resolved due to their intrinsic bandwidth. By setting appropriate parameters, the width of bands with moderate signal-to-noise ratios ( $\sim 1000$ ) can readily be reduced by a factor of 3. The extent of resolution enhancement strongly depends on the bandwidth and is found to be more effective for narrow bands that result from absorption of monomers and small associates. In contrast, this effect is less important for the broad spectral features originating from the absorption of strongly hydrogen-bonded species.

### 3.2. Two-Dimensional Correlation Spectroscopy

Although the principles of 2D correlation analysis were proposed by Noda already in 1986,<sup>113</sup> the widespread use of this method for various spectral analyses including IR, Raman, and NIR spectroscopy has really only begun since 1993, after the development of the generalized 2D correlation approach.<sup>114</sup> This method made it possible to deal with any type of perturbation, including concentration, temperature, pH, pressure, and so on.<sup>21,22</sup> In addition, hetero-correlation between distinct spectral methods has also become feasible. By correlating MIR or Raman spectra, where the band assignments are well established, with NIR spectra one can determine reliable band assignments in the NIR region. The main advantage of using the 2D correlation approach for the analysis of NIR spectra is the resulting resolution enhancement of heavily overlapped NIR bands. One of the first applications of this method was devoted to the temperature-dependent spectral changes of oleyl alcohol.<sup>23</sup> As a result of resolution enhancement and the selective correlation of the vibrational peaks, it was possible to explore the molecular mechanism of temperature-induced changes of oleyl alcohol in much more detail than previously.

The idea of 2D correlation spectroscopy is based on the application of the external perturbation which induces the selective intensity changes at individual wavenumbers that are monitored by a relevant electromagnetic probe.<sup>22,113,114</sup> From the single spectra a perturbation-ordered matrix is assembled, and then the data are subjected to typical pretreatment such as denoising, baseline correction, and normalization.<sup>43,48</sup> Next, the dynamic spectrum ( $\mathbf{A}_d$ ) is computed by subtracting the reference spectrum from each of the individual spectra. Finally, the 2D correlation spectra are calculated as follows:<sup>22,114</sup>

$$\mathbf{syn} = \frac{1}{n-1} \mathbf{A}_d^T \cdot \mathbf{A}_d \quad (1)$$

$$\mathbf{asyn} = \frac{1}{n-1} \cdot \mathbf{A}_d^T \cdot \mathbf{H} \cdot \mathbf{A}_d \quad (2)$$

where  $n$  is the number of the spectra in the data set, and **syn** and **asyn** are the synchronous and asynchronous spectra. **H** is the Noda–Hilbert transformation matrix:

$$\mathbf{H} = \begin{cases} 0 & \text{if } i = j \\ 1/(\pi(i-j)) & \text{otherwise} \end{cases} \quad (3)$$

It is important to note that eqs 1 and 2 are correct for the row-oriented data. It is also possible to perform 2D correlation analysis in the perturbation direction. This approach is called

“sample–sample correlation” and was first proposed by Šašić et al.<sup>49–51</sup> In principle, this method differs from the classical generalized 2D correlation analysis by the order of the matrix multiplication:

$$\mathbf{syn}' = \frac{1}{m-1} \mathbf{A}_d \cdot \mathbf{A}_d^T \quad (4)$$

$$\mathbf{asyn}' = \frac{1}{m-1} \mathbf{A}_d \cdot \mathbf{H} \cdot \mathbf{A}_d^T \quad (5)$$

Here,  $m$  is the number of wavenumbers in the spectrum. In contrast to the classical wavenumber–wavenumber 2D correlation analysis, the sample–sample correlation provides information on perturbation-dependent dynamics.

The detailed properties of the synchronous and asynchronous spectra have been discussed in depth elsewhere.<sup>22,114</sup> Hence we present only a brief outline. Typical simulated synchronous and asynchronous 2D correlation spectra are displayed in Figure 2. The diagonal peaks of the synchronous spectrum (power spectrum) are always positive and correspond to the overall magnitude of spectral changes at individual wavenumbers. A positive synchronous cross-peak at  $(\nu_i, \nu_j)$  implies that the spectral changes at these two wavenumbers are in the same direction, whereas a negative synchronous cross-peak shows the opposite. The presence of the cross-peak at

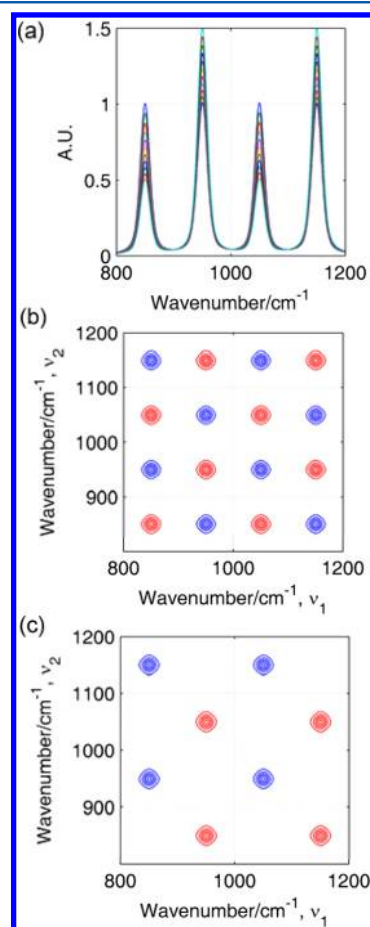


**Figure 2.** (a) Synthetic spectra with four peaks. The peaks at 850 and 1050  $\text{cm}^{-1}$  are exponentially decreasing in intensity, while the peaks at 900 and 1100  $\text{cm}^{-1}$  are exponentially increasing in intensity. Synchronous (b) and asynchronous (c) 2D correlation spectra constructed from the data shown in panel a.

$(\nu_i \nu_j)$  suggests that the bands at  $\nu_i$  and  $\nu_j$  originate either from the same molecular fragment or from two different groups interacting with each other. In contrast, the asynchronous spectrum gives information about how much the spectral changes at two distinct wavenumbers are dissimilar to each other. To ensure easy interpretation of the asynchronous spectra, the asynchronous intensity at  $(\nu_i \nu_j)$  is often multiplied by the sign of the synchronous intensity at  $(\nu_i \nu_j)$ :

$$\text{asyn}(\nu_i, \nu_j) = \text{asyn}(\nu_i, \nu_j) \cdot \text{sign}(\text{syn}(\nu_i, \nu_j)) \quad (6)$$

This way a positive asynchronous cross-peak at  $(\nu_i \nu_j)$  implies that the intensity changes at  $\nu_i$  appears earlier (or faster) than those at  $\nu_j$ , while negative peaks suggest the opposite. The asynchronous spectrum is a very powerful tool for resolving heavily overlapped peaks since it shows a cross-peak at  $(\nu_i \nu_j)$  if the spectral changes at  $\nu_i$  and  $\nu_j$  vary out of phase for few values of the perturbation or respond in a different way. The existence of the asynchronous peak at  $(\nu_i \nu_j)$  suggests that the spectral changes at  $\nu_i$  and  $\nu_j$  are due to various molecules or distinct fragments of the same molecule responding differently to the common perturbation.

While the calculation of 2D correlation spectra is relatively simple,<sup>43</sup> the correct interpretation of these spectra is, on the other hand, sometimes a challenging task.<sup>52,53,115</sup> The rules for interpretation of the synchronous and asynchronous spectra work correctly for the peaks with the intensity changes only. They fail if the intensity changes are accompanied by a significant band shift or width changes.<sup>22,114</sup> These distortions may strongly influence 2D correlation spectra by developing the artificial peaks that must be discriminated from the true ones. Fortunately, computer simulations are a helpful tool for the elucidation of the origin of 2D correlation peaks. The characteristic patterns of the synchronous and asynchronous contour plots generated by the noise, baseline fluctuations, bandwidth, and position changes are well known due to systematic simulations studies.<sup>52,53,115</sup>

### 3.3. Chemometrics

Based on mathematics and statistics, chemometrics consist of numerous procedures for experimental design, multivariate classification, and calibration.<sup>16–20,116–120</sup> The first applications of chemometrics in chemistry focused on the quantitative analysis and classification of different kinds of samples. With growing interest in hydrogen bonding and structural studies, chemometrics became a powerful tool for the deeper exploration of NIR spectra. In contrast to the 2D correlation approach, chemometrics can provide both qualitative and quantitative results on the species present in the system under study.

**3.3.1. Principal Component Analysis (PCA).** The main purpose of chemometrics is based on the fact that experimental data include a large amount of redundant information that can be substantially reduced without much loss of information. The reduced data, often called the latent variables, are easier to understand and interpret since the residual contains mainly noise, baseline fluctuations, and other irrelevant information. PCA is the most important and effective technique for multivariate analysis and finding these latent variables (principal components).<sup>121,122</sup> Many other chemometric procedures rely on PCA. Prior to analysis the data matrix ( $\mathbf{X}$ ) is usually mean-centered and sometimes normalized. PCA decomposes  $\mathbf{X}$  into a sum of products of orthogonal scores ( $\mathbf{t}_i$ ) and orthonormal loadings ( $\mathbf{p}_i$ ):

$$\mathbf{X} = \sum_i^N \mathbf{t}_i \cdot \mathbf{p}_i^T + \mathbf{E} \quad (7)$$

where  $N$  is the number of the principal components, and  $\mathbf{E}$  is the residual matrix (mainly noise). PCA attempts to explain  $\mathbf{E}$  as much as possible using the minimum number of principal components. Hence, the fundamental problem in using PCA is the selection of the correct number of  $N$ , which is equal to rank of  $\mathbf{E}$ . To date, numerous methods for the selection of  $N$  have been developed, but they are all more or less subjective. Simultaneously, based on PCA, one can identify different classes of the samples and the outliers. In spite of its great usefulness, the principal components (latent variables) represent only the pure mathematical models, and they do not have a direct chemical meaning like results obtained from the other chemometrics methods.

**3.3.2. Evolving Factor Analysis (EFA).** EFA is a method for the examination of multivariate data that are ordered.<sup>123</sup>

This approach can be applied for the estimation of the range of existence of each of the components present in the data set. The basic idea of EFA is to determine the singular values of the data matrix as the new samples (rows) are added. The analysis is started with the first sample, and then the successive samples are added to the data (forward analysis). It is also possible to perform EFA in the opposite direction, i.e., starting with the last sample (backward analysis). The analysis is continued until all the samples in the data set are included. Next, the singular values are plotted against the ordered variable. The appearance of a new factor in the data corresponds to a substantial increase in the singular values above the values due to the noise level. On the other hand, the backward analysis reveals the disappearance of the factors from the data matrix. In principle, EFA provides information on the windows of presence of all independently varying factors. However, the analysis is difficult if the ranges of presence of the individual components are highly overlapped.

**3.3.3. Multivariate Curve Resolution (MCR).** The main aim of MCR is the resolution of spectra of pure components from the overlapped spectra of their mixtures.<sup>124,125</sup> In contrast to PCA, by imposing restrictions on the solutions, MCR yields results that have actual physical and chemical meaning. Frequently, non-negativity of the spectral and concentration profiles is assumed, as sometimes are unimodality or closure. The formal equation for this procedure has the form

$$\mathbf{X} = \sum_i^N \mathbf{c}_i \cdot \mathbf{s}_i^T + \mathbf{E} \quad (8)$$

where  $N$  is the number of components, and  $\mathbf{E}$  is the residual matrix. Here,  $\mathbf{c}_i$  and  $\mathbf{s}_i$  are the concentration and spectral profiles of the pure components present in the system. The spectral profiles have chemical meaning and are related to the spectra of the pure components in the mixture. The concentration profiles are also related to the actual concentrations. Applying additional limitations, one can obtain the real spectra and concentrations of all components present in the system. To perform MCR, at first one has to estimate the number of significant components. Usually this information is obtained from either PCA or EFA. Next, the initial concentrations or spectral profiles for each component have to be evaluated. The best results are achieved if the spectra have regions of one-component absorption (selective regions) for each of the constituents. In this case, the concentration profiles



for each of the components can be estimated from the selective regions. Unfortunately, in the NIR region this situation is rare, and the estimation of the initial profiles is achieved by EFA or other more sophisticated methods.

**3.3.4. Multivariate Calibration.** Multivariate calibration correlates the concentration of all constituents or their physical/chemical properties to a measured response of the multicomponent system.<sup>126,127</sup> Among the many multivariate calibration methods, such as classical least-squares, inverse least-squares, and principal component regression, one, namely partial least-squares (PLS), dominates due to excellent performance and easily available software. Latent variables in PLS are obtained simultaneously with the calibration model. This way each latent variable is a linear combination of the original variables. Often these variables are rotated to provide maximum correlation with the spectral changes due to this variable. Multivariate calibration includes several steps: building a model, testing the quality of the model, predicting the unknown properties (often concentration) from the spectra, and checking the quality of the prediction by comparing it with the results obtained by the reference method. The relationship between the measured responses ( $y$ ) and the data matrix ( $X$ ) has the following form:

$$y = X \cdot b + f \quad (9)$$

Here,  $b$  is a vector of regression coefficient, and  $f$  is a vector of residuals. The above equation represents soft modeling, since the vector  $b$  has to be determined without much prior knowledge of the studied system. In PLS, the regression vector  $b$  is calculated from the latent variables ( $T$ ) that are often obtained from PCA:

$$y = T \cdot q + f \quad (10)$$

Here  $q$  includes the regression coefficients for the columns of  $T$ . The solutions of eqs 9 and 10 have the form

$$b = (X^T \cdot X)^{-1} \cdot X^T \cdot y \quad (11)$$

and

$$q = (T^T \cdot T)^{-1} \cdot T^T \cdot y \quad (12)$$

By defining the generalized inverse ( $X^+$ ), the above equation takes a simpler form:

$$b = X^+ \cdot y \quad (13)$$

The regression coefficients can be used on the test data ( $X_t$ ) to predict the concentrations or the other properties of the components:

$$\hat{y} = X_t \cdot b \quad (14)$$

In the PLS method the measured property  $y$  does not need to be correlated with all the spectral variables. If the measured property is related to a specific functional group then the correlation will be limited to a narrow range of the spectrum. Therefore, the selection of the proper spectral range is of a great importance for successful analysis. The selection of the optimal spectral range for PLS can be achieved by a so-called “target projection graph” showing the covariance between the predicted values of  $\hat{y}$  and the spectral changes at each wavenumber.<sup>116–118</sup> Recently, new methods such as “mowing window PLS regression” have been developed to improve PLS performance by searching for the most informative spectral

regions.<sup>128</sup> The flexibility of PLS makes it a helpful tool for both the quantitative and qualitative analysis of NIR spectra.

## 4. APPLICATIONS OF NIR SPECTROSCOPY

### 4.1. Water

Water has very strong absorption in the MIR region and, hence, NIR spectroscopy has often been applied for the study of pure water and aqueous solutions.<sup>54–57</sup> NIR spectra of water (Figure 3a) are dominated by the  $\nu_2 + \nu_3$  (5100–5300  $\text{cm}^{-1}$ ) and  $\nu_1 + \nu_3$

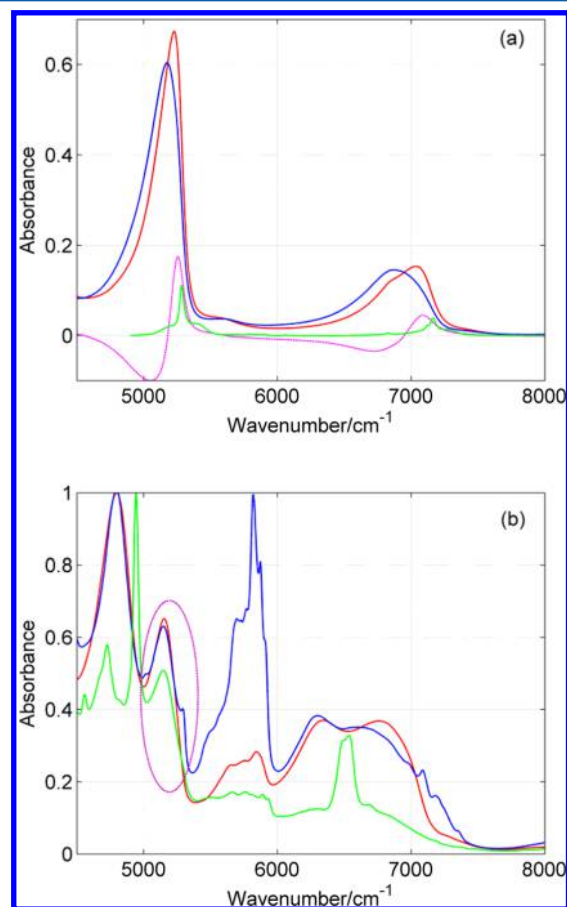


**Figure 3.** (a) NIR spectra of pure water at 20 (blue) and 80 °C (red), the difference spectrum (dashed magenta line), and the spectrum of water in  $\text{CCl}_4$  (green). (b) Normalized (to unity) NIR spectra of binary mixtures of water with *n*-butyl alcohol (blue), ethylene glycol (red), and 1,3-aminopropanol (green). The dashed ellipse (magenta) highlights location of the  $\nu_2 + \nu_3$  band.

(6800–7200  $\text{cm}^{-1}$ ) combination bands (where  $\nu_1$  is symmetric OH stretching,  $\nu_2$  is OH bending, and  $\nu_3$  is antisymmetric OH stretching). Especially useful is the  $\nu_2 + \nu_3$  band of water that is located in a region free from the other overtones and combination bands (Figure 3b). It is of particular importance to note that the absorption of this band is also well separated from the OH absorption of other compounds. In contrast, the OH absorption from water and alcohols often heavily overlaps in the MIR region. Hence, by using NIR spectroscopy, one can examine the state of water in OH-containing solvents such as alcohols or diols. The spectral parameters of both combination bands of water are sensitive to temperature, pressure, pH, and contaminations. Therefore, they are good markers of the changes induced by these perturbations.

**4.1.1. Structure of Bulk Water.** In spite of numerous studies using various experimental and theoretical methods, the structure of liquid water is still far from being really understood. The information and data provided by many different authors do not form a uniform picture. In fact, they often contradict each other. The current models describing the structure of liquid water can be divided into two groups: *mixture models*, where the structure of water is an equilibrium consisting of a few specific structural units (mostly two or three),<sup>129–137</sup> and *continuum models*, where the structure of water is a network of tetrahedrally hydrogen-bonded molecules of water with a continuous distribution of distances, angles, and energies.<sup>138–142</sup>

The majority of classical MIR and Raman studies on the structure of water have been based on the decomposition of the spectra using curve-fitting or MCR techniques. All these results support the validity of the mixture model.<sup>130–135</sup> Sometimes the mixture is composed of different species of fixed structure (e.g., dimers, trimers, tetramers, and so on),<sup>130</sup> but mostly the components of the mixture are different kinds of substructures which differ in the average number of hydrogen bonds per water molecule.<sup>131–136</sup> Wouterson et al. used femtosecond MIR pump–probe spectroscopy in a study of liquid water.<sup>137</sup> Their evidence points toward two-component structures with respect to orientational dynamics. Strongly hydrogen-bonded water relaxes through a slow reorientational process. On the other hand, the fast process dominates for weakly hydrogen-bonded water.

MIR studies of liquid water by Max and Chapados suggest that there are no free OH groups in liquid water.<sup>143</sup> On this basis the authors concluded that monomers, dimers, trimers, oligomers, and cyclic structures are absent in the bulk water. However, the authors do not support the validity of any particular water structure model. Ratcliffe and Irish measured the Raman spectra of liquid H<sub>2</sub>O, D<sub>2</sub>O, and HDO in solution (10%) of H<sub>2</sub>O or D<sub>2</sub>O up to 300 °C.<sup>141</sup> The spectral changes were interpreted in terms of a continuum model, but the authors did not discard the mixture model which assumes the presence of weak and strong hydrogen-bonded oscillators. More conclusive are the 2D vibrational spectroscopic studies by Eaves et al.<sup>142</sup> These results reveal that the continuum model is more appropriate. Studies by Zhukovskii also show that the absorption contours of liquid water can be satisfactorily described on the basis of the statistical distribution of the oscillators with respect to the hydrogen bond energies.<sup>144</sup> This is another argument supporting the validity of the continuous model of liquid water. Efimov and Naberukhin calculated MIR and Raman spectra of normal and heavy water within the framework of the fluctuation hypothesis.<sup>139</sup> The authors show that it is not necessary to assume the existence of discrete aggregates in the liquid water. They also suggest that the decomposition of the vibrational spectra into various components by using the curve-fitting is in fact an inadequate approach. This conclusion is in line with the simulation studies on the origin of spectral variations.<sup>145</sup> As shown, the linear combination of contributions from a few neighboring peaks with a fixed position may generate identical pattern as the position shift for a single peak. This model can easily be extended into two or more spectral components. If the separation between the peaks is substantially reduced then the mixture model can be easily converted into the continuous one. Hence, it seems that the results obtained from the vibrational spectra of hydrogen-bonded liquids strongly depend

on the method of decomposition of the spectra and the means used in their interpretation.

The presence of so many conflicting results on the structure of liquid water, as obtained from the analysis of MIR and Raman spectra, did not discourage researchers from undertaking similar efforts in the NIR region. Of particular interest is the comparison of the picture obtained from the analysis of the fundamentals with that derived from the overtones and combination modes. NIR studies on the structure of liquid water are not as numerous as those from the MIR region, but recently several papers worth mentioning have been published.<sup>54–57</sup> Segtnan et al. studied the temperature-dependent (6–80 °C) NIR spectra of water using the combination of 2D correlation spectroscopy and PCA.<sup>54</sup> It was demonstrated that more than 99% variability in the spectra is due to the two bands at 6707 and 7082 cm<sup>−1</sup>. The bands results from the weakly and strongly hydrogen-bonded water. These two different species are closely correlated with each other; i.e., the population of one species increases at the expense of the other species. This suggests the validity of the two-state model of liquid water. However, the presence of a weak spectral feature near 6954 cm<sup>−1</sup>, whose population changes slightly during the temperature rise, indicates that this model is still not perfectly fulfilled. This conclusion was confirmed by the application of the self-modeling curve resolution (SMCR) approach to the spectra of water recorded at different temperatures.<sup>55</sup> The two-state model thus appears to be acceptable at higher temperatures; the residuals are as small as 0.4%. As the temperature decreases, this model is gradually degraded, and the water structure resembles a quasi-lattice with broken bonds. Any ambiguity in the above findings may arise from the rank deficiency of the data matrix. To resolve this ambiguity Czarnik-Matusiewicz et al. concatenated the MIR and NIR spectra of water measured from 25 to 80 °C.<sup>56</sup> The results of MCR analysis on the augmented data matrix reveals the presence of two structural constituents of water with the linear intensity changes in opposite directions (Figure 4). At low and high temperatures the structure of water is dominated by one of these two components. On the other hand, a 2D IR-NIR hetero-correlation analysis shows the three kinds of water with different degrees of hydrogen bonding. The species absorbing at the lowest frequency was assigned to symmetrically hydrogen bonded water. The second component was attributed to water involving asymmetrical hydrogen bonding. Here some of the tetrahedral bonds were broken. On the other hand the highest frequency absorption was assigned to the OH group not involved in hydrogen bonding. These three spectral components result from the presence of two structural components whose relative populations vary linearly with the temperature. Also this result supports the validity of the two-state model of liquid water. Three different spectral components were also resolved in the temperature-dependent (20–80 °C) NIR spectra of water.<sup>57</sup> The band positions determined from the asynchronous spectrum were found to be 5262, 5193, and 5084 cm<sup>−1</sup>. The highest and the lowest frequency components were assigned as described in a previous paper.<sup>56</sup> The intermediate component weakly changed its population with the temperature and was attributed to interstitial water. It was suggested that the interstitial water promotes the transition from the stronger to the weaker hydrogen-bonded species.

A combined analysis of the MIR and NIR spectra of water and alcohols by Luck has shown the presence of three kinds of OH groups: strongly (cooperatively) hydrogen-bonded, weakly



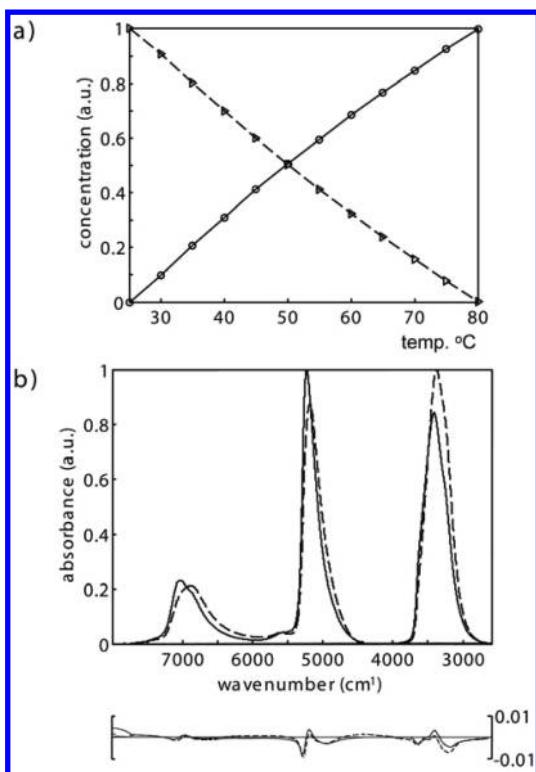


**Figure 4.** Optimized pure concentration profiles (a) and spectral profiles (b) of water by means of the MCR-ALS method applied to the row-wise augmented matrix for two selected components. Reprinted with permission from ref 56. Copyright 2005 Elsevier.

(non-cooperatively) hydrogen-bonded, and nonbonded.<sup>146</sup> The equilibrium between these three water species is responsible for the observed anomalous properties of water. The author emphasizes the importance of the cooperativity effect and the presence of the nonbonded OH groups for producing the properties of liquid water. Due to the cooperativity effect, the hydrogen bonding in liquid water is 250% stronger when compared with that between the monomers in solution. The population of the nonbonded OH groups in liquid water, estimated from NIR spectra, was found to be 10% at 0 °C and to increase with the temperature. The presence of the free OH groups in liquid water is seen clearly only in NIR and Raman spectra.<sup>57,146</sup> However, it should be remembered that in the MIR region this band does not occur or is very weak.<sup>143</sup> This results from the fact that the free OH and weakly hydrogen-bonded OH have the stronger overtones compared with the more associated species that dominate the MIR spectra.<sup>147,148</sup>

Difference and double-difference DOD and HOH stretching overtone ( $2\nu_{OD}$  and  $2\nu_{OH}$ ) spectroscopy and decomposition with curve-fitting made it possible to discriminate the three different kinds of interstitial water structures (Figure 5) responsible for its high density, compressibility, and fragility.<sup>149</sup> The baseline-corrected and normalized overtone spectra were resolved for up to six vibrational components in liquid water from ambient to 300 MPa pressure. Comparing the results obtained with the structural data (X-ray, neutron scattering) and molecular dynamics (MD) simulations for liquid water, the authors assigned the resolved components to a basic Ih icelike substructure, temperature-dependent remote interstitial defects due to tetrahedral displacements, interstitial defects (quasiplanar noncyclic tetramers), and the interstitial defects created at higher pressures (cubic water octamers). These results support

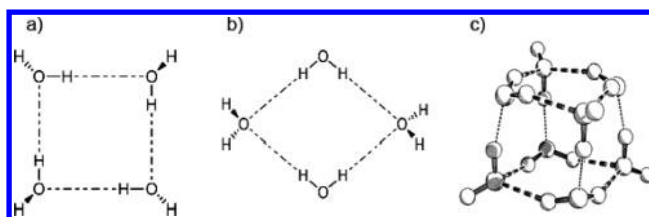


**Figure 5.** (a) Cyclic and (b) noncyclic planar water tetramers with single-donor/single-acceptor and double-donor/double-acceptor H-bonding arrangements. (c) A water cube octamer, which consists of two rings of the type shown in panel a and two rings of the type shown in panel b. Reprinted with permission from ref 149. Copyright 2004 Wiley-VCH Verlag GmbH & Co. KGaA.

the “second critical point” hypothesis and indicate that the two-state model is insufficient in providing acceptable explanation of the structural, thermodynamic, and transport properties of liquid water. Near the critical solution temperatures ( $>300$  °C) and high pressures ( $\sim 400$  atm), water reveals quite different properties from those of ambient water. For example, it becomes a good solvent for nonpolar compounds and a poor solvent for ionic compounds.<sup>150,151</sup> The temperature- and pressure-induced changes in the solubility phenomena of aqueous solutions result from variations in water structure and hydrogen bonding. Jin and Ikawa studied the unusual properties of water at high temperatures (100–400 °C) and pressures (20–400 bar) by monitoring the spectral changes of the  $\nu_1+\nu_3$  combination band of water from 6200 to 7800  $\text{cm}^{-1}$  (Figure 6).<sup>152</sup> The authors stress the advantages of spectral

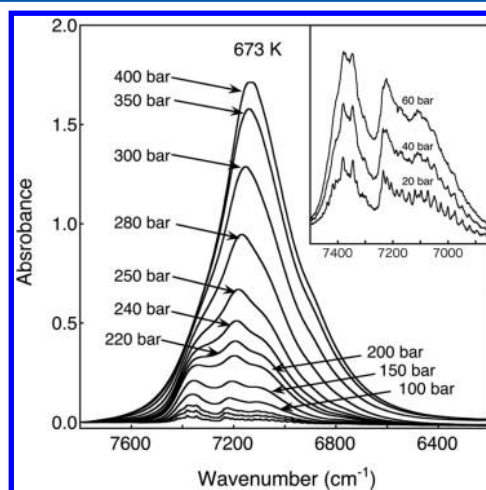


**Figure 6.** Effect of pressure on the NIR OH stretching absorption of water at 673 K. Reprinted with permission from ref 152. Copyright 2003 AIP Publishing LLC.

measurements in the overtone region over the fundamental one. These advantages permitted to measure the spectral profile over a wide range of densities, from the gas phase to a liquid-like density. The ratio of hydrogen-bonded formation strongly depends on the molar density, regardless of the temperature. At 400 °C and 400 bar, a significant amount of water molecules can rotate quite freely, although they also experience frequent collisions with other molecules. From the van't Hoff's plot, the enthalpy of dimerization has been determined to be  $15 \pm 3$  kJ/mol.<sup>152</sup>

In conclusion, most of the former NIR studies on the structure of liquid water provide evidence for the validity of the

mixture model, predominantly supporting two components. Nevertheless, the presence of the third structural component is also very likely. It seems that this simplified picture results from limitations in the applied methods of data analysis. In particular, it should be stated that the use of curve-fitting may lead to incorrect conclusions since the results obtained from this method depend on an almost arbitrary selection of the number of the spectral components and their parameters. Yet, curve-fitting is seldom used for the analysis of NIR spectra. Rather, chemometric methods and 2D correlation approaches dominate. Unfortunately, these methods, in particular MCR, also provide information on a finite number of species; therefore, they also favor the mixture models. Thus, it seems safe to suggest that further studies on the structure of liquid water are still necessary before the debate can be finalized.

#### 4.1.2. Interaction of Water with Other Molecules.

From NIR measurements, one can determine not only the concentration of water but also information on the character of its interactions with other components in its environment. The molar absorptivity of the  $\nu_2 + \nu_3$  band, determined from water concentrations from 0.01 to 0.06 mol·dm<sup>-3</sup> was found to be constant ( $336 \pm 4$  dm<sup>3</sup>·mol<sup>-1</sup>·cm<sup>-1</sup>) in several organic solvents such as toluene, acetone, methyl ethyl ketone, ethyl acetate, acetic acid, and *N*-methylpyrrolidinone.<sup>153</sup> The  $\nu_2 + \nu_3$  combination band of water in this spectral region appears free from any other significant absorption. Therefore, its molar absorptivity can be determined with a high accuracy. The shape and position of this band indicate the number of hydrogen bonds created by molecules of water to the other molecules. Water that is a donor to atoms not easily polarized (e.g., the oxygen in carbonyl groups) absorbs from 5260 to 5240 cm<sup>-1</sup>. Water donating one hydrogen bond to a moderately polarized atom (the oxygen in water) absorbs in the 5130–5175 cm<sup>-1</sup> region, and water donating two hydrogen bonds to easily polarized atoms (the oxygen in a water-like environment) absorbs in the region 5000–5020 cm<sup>-1</sup>. Results indicate that in none of the solvents studied by the authors even a small amount of water seems to be in a water-like environment.<sup>153</sup>

Binary mixtures of water with alcohols and bifunctional molecules have a complex structure since molecules of water can be bound in many different ways. The hydration process is closely related to the size and shape of the solute molecules. At the same time, the molecules of water modify the structure of the organic phase. Systematic examinations of the effect of temperature and water content on the NIR spectra of binary mixtures of water and aliphatic alcohols,<sup>58–63</sup> diols,<sup>64,65</sup> aminoalcohols,<sup>66</sup> and diamines<sup>67</sup> were undertaken by Czarnecki et al. As shown in Figure 7, the normalized NIR spectrum of pure 2-propanol is the same as the spectral profile (resolved by MCR) of 2-propanol in the mixture with water (the water-poor region:  $0 \leq X_{\text{H}_2\text{O}} \leq 0.5$ ). Similar results were obtained for the other mixtures studied.<sup>58–67</sup> Thus, one can conclude that the addition of a small to moderate amount of water has a negligible effect on the structure of the organic phase. This suggests that the molecules of the solvent in the mixture are in almost the same environment as the molecules in a pure liquid phase. In the water-poor region, the molecules of water predominantly act as double proton donors, and this bonding is stronger than that found in bulk water. This is evidence of its highly cooperative character. The spectra shown in Figure 7 provide evidence for this conclusion. Here the  $\nu_2 + \nu_3$

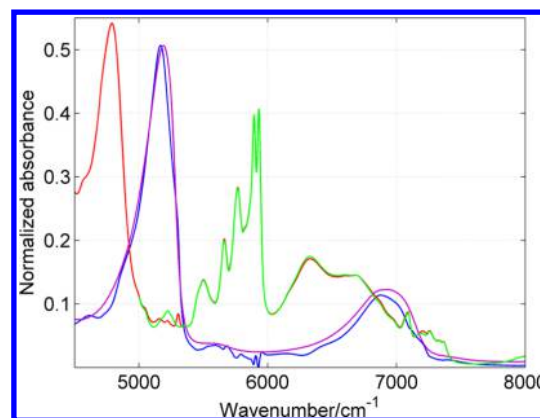


**Figure 7.** Normalized spectra of bulk 2-propanol (green) and bulk water (magenta) together with the spectral profiles of 2-propanol (red) and water (blue) obtained from the MCR of concentration-dependent spectra of 2-propanol/water mixture.

combination band of bulk water is blue-shifted with respect to that in the spectral profile of water in the mixture. The movement of the alcohol associates with respect to each other breaks some of the bonds between the molecules of water and the associates, thus increasing the population of the free OH groups from the water. This increase is clearly seen in going from *n*-butyl to *tert*-butyl alcohol (Figure 8): the higher the extent of self-association, the lower the population of the free OH groups of water. The relatively small amount of these groups in the cyclohexane/water mixture (Figure 8D) is due to the high viscosity of cyclohexanol, which tends to stabilize the interactions between cyclohexanol and water.<sup>63</sup> In contrast to the alcohol/water mixtures, in the mixtures of water with bifunctional molecules, the concentration of singly bonded water is negligible as a result of the high degree of self-association. The one-bonded water band at 5300 cm<sup>-1</sup> clearly seen for alcohols<sup>58–62</sup> is not observed for diols<sup>64,65</sup> (Figure 8E), aminoalcohols,<sup>66</sup> and diamines.<sup>67</sup> Increasing the water content ( $X_{\text{H}_2\text{O}} > 0.3$ ) is correlated with the creation of small water clusters. The water–water interactions in these clusters are weaker compared with those in bulk water. The variations in temperature or water concentration have a minor effect on the intensity and position of the C–H stretching bands. This suggests that, in the water-poor region, the hydrophobic effects are insignificant, and the properties of the mixtures are controlled by hydrogen bonding through the OH or NH groups. NIR study of water/methanol binary mixtures reveals a red-shift by about 30 cm<sup>-1</sup> for the first overtone of the CH<sub>3</sub> group.<sup>68</sup> However, this shift is small at both ends of the concentration scale. The authors suggested that the methyl group of the methanol is involved in the direct C–H...O interaction with water.

The combination of NIR spectroscopy and multivariate model-based regression has been applied to the elucidation of species present in alcohol/water mixtures.<sup>154</sup> It has been reported that there are four species present in the mixtures: alcohol, water, and 1:1 and 1:*n* alcohol/water complexes. The last complex appears in the water-rich region, and its stoichiometry depends both on the concentration and size of the alcohol. The number of water molecules surrounding the hydrophobic part of the alcohol increases from 5 for methanol to 14 for 1-propanol. Puxty et al. connected a high-performance chromatography pump with the NIR flow cell to gain a better

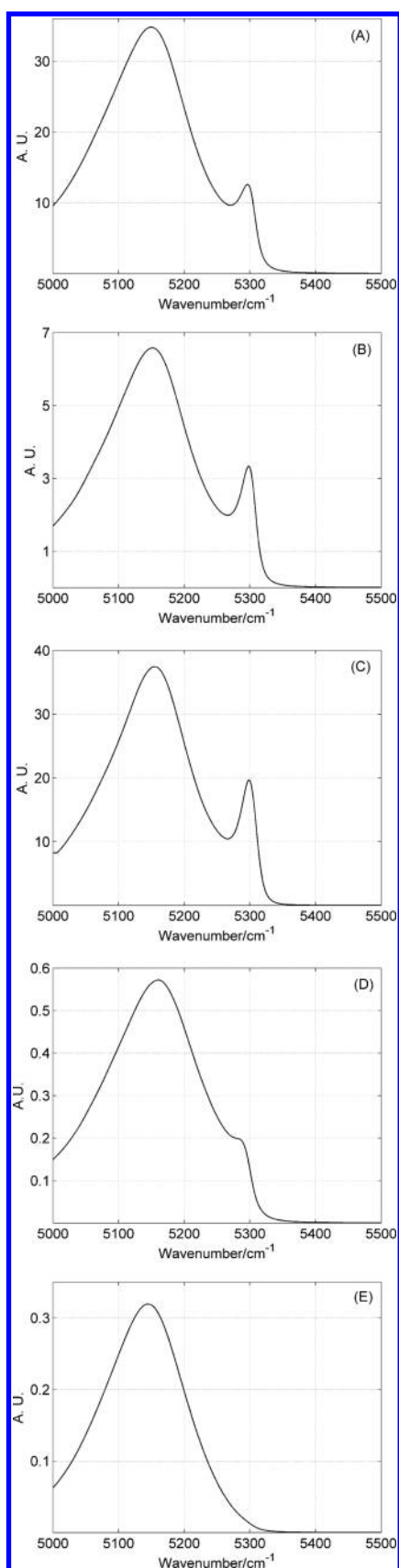


**Figure 8.** Power spectra of binary mixtures of water with (A) *n*-butyl alcohol, (B) *sec*-butyl alcohol, (C) *tert*-butyl alcohol, (D) cyclohexanol, and (E) 1,3-propanediol obtained from concentration-dependent NIR spectra.

compositional resolution.<sup>155</sup> This way, the methanol/water mixture was resolved into a five components: pure methanol, pure water, and 1:1, 1:4, and 1:9 methanol/water complexes whose relative populations depend on the composition of the mixture. Onori and Santucci studied the dynamical and structural properties of water/alcohol mixtures by using a range of experimental methods, including NIR spectroscopy.<sup>156</sup> It was shown that below the concentration threshold level, the molecules of alcohol are separated by “water cages”, where the short-range order of water molecules is different from that in the bulk water. Alcohol–alcohol interactions appear when all the molecules of water are engaged in the hydration of the molecules of alcohol. The authors concluded that the principal mechanism by which short-chain alcohols (from methanol to butanol) influence this micellization process is through their effect on the structure of water phase. Comparing the numerous NIR results for binary mixtures of organic solvents with water, Chen et al. concluded that the solubility of water in the organic solvents depends mainly on the population and distribution of the polar groups from the organic solvent.<sup>65</sup> On the other hand, the distribution of these groups is determined by the length and the structure of the hydrocarbon chain.

**4.1.3. Hydration and Physical Properties of Aqueous Solutions.** Jin and Ikawa measured the NIR spectra of water/benzene mixtures at high pressures (100–400 bar) and temperatures (200–400 °C).<sup>157</sup> The concentrations and densities of water and benzene in the mixtures (*in situ*) were determined from the integrated intensities of the first overtones of the OH and CH stretching modes, respectively. The authors proved that these values cannot be obtained in the two-phase regions by other techniques such as gas chromatography or Karl Fischer titration. It was found that, on mixing, an enormous volume growth occurs in the region enclosed by an extended line of the three-phase equilibrium curve and one-phase critical curve of the mixtures and the gas–liquid equilibrium curve of water. As shown, the size of the relative volume variation increases as the benzene mole fraction in the mixtures decreases. This suggests that a small concentration of benzene in water leads to variation in the fluid density from a liquid-like to a gas-like condition close to the critical point. Similar NIR and UV studies of water/benzene mixtures at high temperatures (50–400 °C) and pressures (50–400 bar) showed that the asymmetry in mutual solubilities of such water/benzene systems one can explain by the cavity-based model.<sup>158</sup> The solubility of benzene in water is much smaller compared with that of water in benzene. This observation was explained by the large difference in the molecular size between water and benzene. The pressure effect on the mutual solubilities is in the opposite direction and results from the variation in isothermal compressibility between benzene and water.

The hydration properties of trimethylamine-*N*-oxide (TMAO) and *tert*-butyl alcohol (TBA) were explored by examination the concentration-dependent intensity changes of the  $\nu_2 + \nu_3$  combination band of water at 25 °C.<sup>159</sup> The TMAO molecules have a tendency to stabilize the ordered water structure and do not self-associate. Consequently, the TMAO hydration number does not depend on the concentration. On the contrary, the TBA molecules perturb the structure of water to a smaller extent, but they do have a tendency to self-association. Therefore, the TBA hydration number strongly depends on the mole fraction. Hence, one can expect that the processes dominated by the hydrophobic effect, such as protein



folding or micellization of surfactants, will be modified by TMAO and TBA in different ways.

Iwamoto applied the hydrophobic isolation (HI) method coupled with both MIR and NIR spectroscopy to the study of the hydration properties of the C=O group.<sup>69</sup> An *N,N*-dialkyl amide  $[(\text{CH}_3\text{CH}_2\text{NCO}(\text{CH}_2)_{10}\text{CH}_3)]$  and an alkyl ester  $[\text{CH}_3(\text{CH}_2)_8\text{COOCH}_3]$  were isolated in *n*-heptane. At low concentrations of either the amide or ester in heptane (<5% v/v) water forms singly bonded hydrates  $[\text{C}=\text{O}\cdots\text{H}-\text{O}-\text{H}]$ . When the concentration increases above 5%, double-bonded hydrates  $[\text{C}=\text{O}\cdots\text{H}-\text{O}-\text{H}\cdots\text{O}=\text{C}]$  appear in the solution. An analysis of the frequency shift  $[\nu(\text{OH})_{\text{free}} - \nu(\text{OH})_{\text{bonded}}]$  and hydration constant  $[\text{C}=\text{O} + \text{H}_2\text{O} \leftrightarrow \text{C}=\text{O}\cdots\text{H}-\text{O}-\text{H}]$ , used as a measure of the hydration power, clearly indicates that the amide C=O has a much stronger hydration ability compared with the ester C=O, ketone C=O, or ether C—O.<sup>70</sup> This result suggests that the amide C=O is responsible for the high hydration ability of proteins. Similar studies on the hydration properties of the OH (2-nonanol) in a hydrophobic medium (*n*-heptane) demonstrated that an isolated OH at concentrations below 2% (v/v) forms an  $\text{HO}\cdots\text{HOH}$  hydrogen bond. In contrast, above 2%, OH is hydrated in the form of  $\text{OH}\cdots\text{OH}_2$ .<sup>71</sup> This means that, depending on the concentration, the OH can act as either a donor or an acceptor with respect to water. The NIR region gives information on the hydration of water that is more reliable since the combination bands of water are much better separated compared to the overlapping fundamental bands.

The state of water confined in Aerosol-OT–hydrocarbon–water reverse micelles was studied using small-angle X-ray and NIR spectroscopy.<sup>160</sup> The pair-distance distribution obtained from the X-ray experiment permitted a detailed description of the topology of these systems to be achieved and revealed deviations from monodispersed spherical water pools for the longer chain aliphatic hydrocarbons. The band due to the first overtone of the OH stretching vibration has a fine structure that reflects the variations in the hydrogen bonding upon confinement. At all hydration states the experimental spectra were successfully reconstructed by a linear combination of the three Gaussian peaks, representing the basis spectra for core (in the interior of the micelle) and shell (close to the interface) water. The authors emphasize that the spectral decomposition in the NIR region is more reliable compared with the MIR data due to the better separation of the NIR bands. In addition, more convenient optical path lengths (of order 1 cm) can be used in the NIR region.

The effect of different ions on the structure and hydrogen bonding of water has been the subject of several NIR spectroscopic studies.<sup>161,162</sup> The shape of the water  $\nu_2+\nu_3$  band appears to be very sensitive to the  $\text{NaClO}_4$  concentration.<sup>161</sup> The width of this band in the saturated solution is twice as narrow compared with that in the spectrum of the bulk water. This effect was attributed to changes in the population of water molecules with different numbers of hydrogen bonds. Another NIR study using the spectrum of excess partial molar absorptivity for the  $\nu_2+\nu_3$  band has shown that the  $\text{Cl}^-$  ion has an unlike effect on the structure of water compared with  $\text{Br}^-$  and  $\text{I}^-$  ions.<sup>162</sup> However, the nature of this effect is yet to be elucidated. The same experimental approach was applied in a study of aqueous acetonitrile and acetone.<sup>163</sup> The plots of the excess molar absorptivity for both solutions show two peaks located at 5020 and 5230  $\text{cm}^{-1}$ . However, there is an obvious difference in the mole fraction relationship for both solutes.

The molecules of acetonitrile enhance the hydrogen bond network in their immediate vicinity, whereas the molecules of acetone form hydrogen bonds directly to the existing water network.

Takeuchi et al. investigated the structure of  $\text{H}_2\text{O}$  clusters adsorbed on  $\text{TiO}_2$  surfaces by NIR spectroscopy.<sup>164–166</sup> The examinations of the  $\nu_2+\nu_3$  band suggested that  $\text{H}_2\text{O}$  molecules adsorbed on a  $\text{TiO}_2$  surface form clusters because of the high surface tension of  $\text{H}_2\text{O}$  resulting from the intermolecular hydrogen bonding. The bonded  $\text{H}_2\text{O}$  in the bulk part of the cluster and the  $\text{H}_2\text{O}$  free from hydrogen bonding in the outside spherical part of the cluster can be clearly recognized. Moreover, the authors also evidenced that the relaxation of the surface energy accompanying the adsorption of  $\text{H}_2\text{O}$  on the  $\text{TiO}_2$  surface leads to stabilization of the adsorption states of the hydrogen-bonded  $\text{H}_2\text{O}$  molecules. In contrast, the non-bonded molecules of  $\text{H}_2\text{O}$  became less stable than the molecules in the bulk  $\text{H}_2\text{O}$ .

## 4.2. Hydrogen Bonding and Molecular Interaction

The absorption of the free OH is much more pronounced in the overtone region compared with the MIR range. One can, therefore, determine its molar absorptivity with a high accuracy. Yet, the first OH overtone of aliphatic alcohols overlaps with the  $2\nu(\text{C}-\text{H})+\delta(\text{C}-\text{H})$  combination bands. To obtain the net intensity of the OH band, one first has to eliminate the absorption from the C—H. Iwahashi et al. proposed subtraction of the spectrum of the deuterated (OD) analogue of alcohol.<sup>72</sup> In this way it was possible to evaluate the intensity of the first overtone of the OH stretching band and calculate the mean association number for three butyl alcohols. As expected, this value increases with growing concentration and decreasing temperature. The mean association number is found to decrease with branching of the alcohol. Another method of removing the C—H absorption was applied for the study of the temperature-dependent (25–75 °C) NIR spectra of *cis*-9-octadecen-1-ol.<sup>167</sup> These contributions were canceled by subtraction of the spectrum of 1-bromo-*cis*-octadecene from the spectra of the alcohol. From the difference spectra, the authors determined an average association number for this alcohol. This value strongly depends on the temperature decreasing from 4 at 25 °C to 2 at 75 °C. More drastic changes were observed for the association constant (*K*). Relatively low *K* value appears to be responsible for the high self-diffusion and the low viscosity of *cis*-9-octadecen-1-ol.

Stordrange et al. examined the self-association of aliphatic alcohols in  $\text{CCl}_4$  solutions from 0.01 to 1.0 M using NIR spectroscopy and chemometrics methods such as PCA, EFA, and MCR.<sup>168</sup> The results from PCA and EFA indicated the presence of three different species for all of the alcohols studied over the whole concentration range. The concentration and spectral profiles of these species calculated from MCR were used to obtain the association numbers and equilibrium constants. The authors suggested the existence of equilibrium among monomers, linear associates, and cyclic associates for all the alcohols studied. The increase in concentration led to an increase in the average size of the associates and shifted this equilibrium toward the cyclic associates. The average size of the cyclic associates is higher than that of the linear ones. In addition, it was concluded that the associates of the branched alcohols are smaller than those of the *n*-alcohols.

Due to strong absorption IR measurements of pure liquids in the transmission mode are difficult. In this case very short

pathlengths of the order 1–2  $\mu\text{m}$  are required. These pathlengths are easily achieved using attenuated total reflectance (ATR) technique. But the raw ATR spectra have to be subjected to numerical correction which requires knowledge of the refractive index of both the windows and the sample. A problem is that some samples may be absorbed onto the ATR crystal and also aggressive liquids may damage the gaskets. In contrast, NIR transmission spectroscopy is free from these disadvantages. NIR absorptions are much weaker and more convenient for spectral measurements. Yet, the NIR spectra are complex due to heavy overlap of the overtones and various combination bands. Hence, obtaining useful information from NIR spectra involves using of resolution enhancement methods such as 2D correlation analysis. This method was applied for the first time by Noda et al. in the study of the thermal changes in NIR spectra of neat *cis*-9-octadecen-1-ol.<sup>23</sup> As a result of the resolution enhancement in 2D NIR correlation spectra the peak at  $7090\text{ cm}^{-1}$  was resolved into two additional components located at  $7070$  and  $7115\text{ cm}^{-1}$ . These components were assigned to distinct rotational isomers of the OH ( $7090$  and  $7115\text{ cm}^{-1}$ ) and to the free end OH groups in the open-chain associates of *cis*-9-octadecen-1-ol ( $7070\text{ cm}^{-1}$ ). A synchronous peak at  $7090/10380\text{ cm}^{-1}$  correlates the first and second overtones of the OH stretching mode of the monomeric alcohol. At the same time, no appreciable asynchronous intensity in this spectral region is observed. Hence, one can conclude that both the correlated bands originate from the same molecular fragment. Identical correlation patterns were also observed for other alcohols (Figure 9). Thus, by correlating the various fundamentals and overtones or different overtones, one can establish reliable band assignments in the NIR region.

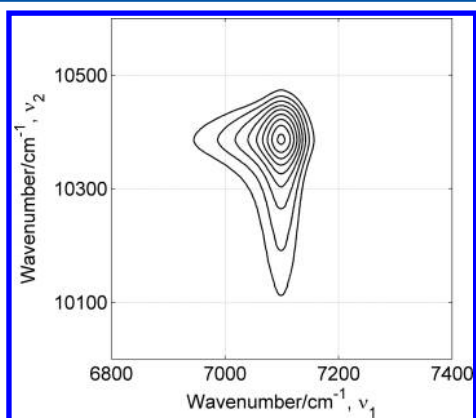


**Figure 9.** Localized view of the off-diagonal position of a synchronous 2D NIR spectrum of *n*-butyl alcohol constructed from temperature-dependent (20–80 °C) spectra.

A paper by Noda et al.<sup>23</sup> stimulated similar studies of other alcohols, including butanols,<sup>73,74</sup> decanol,<sup>75</sup> octanols,<sup>76–79</sup> and cyclohexanol.<sup>63</sup> As can be seen from Figure 10, a relationship exists between the shape of the asynchronous spectra and the degree of hydrogen bonding.<sup>79</sup> The more associated the alcohol, the weaker intensity of the monomer peak. In the case of highly associated alcohols such as 1-butanol, this peak does not occur at all (Figure 10A). Similar correlations between the strength of the hydrogen bonds and the intensity and position of the OH peaks can be observed in the power spectra (diagonal of the synchronous spectrum), as shown in Figure 11.

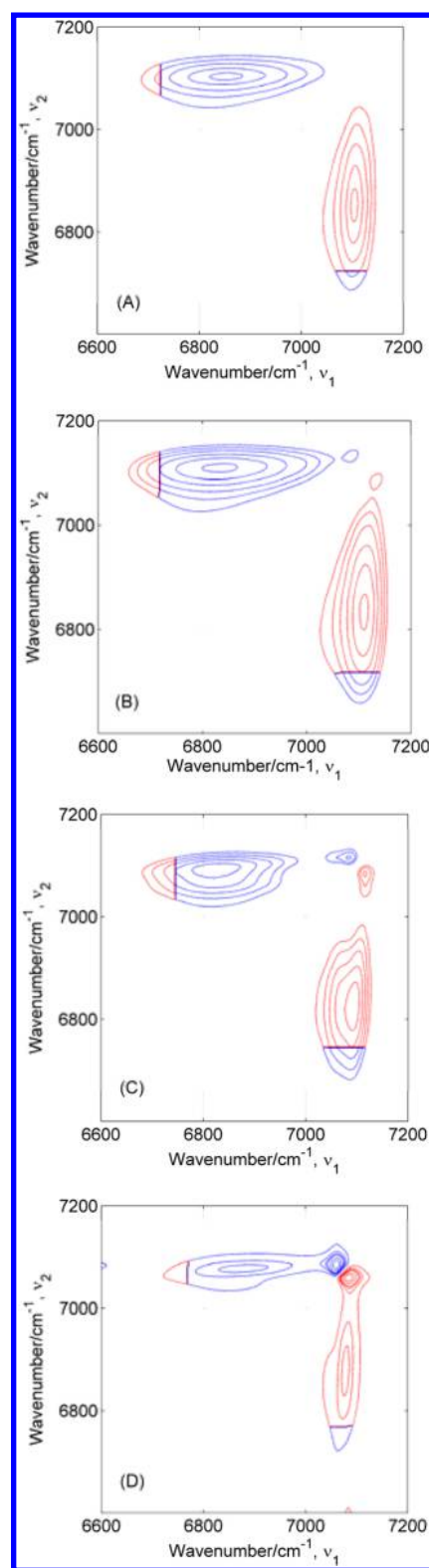


**Figure 10.** Temperature-dependent asynchronous 2D NIR correlation spectra of pure liquid (A) *n*-butyl alcohol, (B) *iso*-butyl alcohol, (C) *sec*-butyl alcohol, and (D) *tert*-butyl alcohol.

The intensity of the bonded OH decreases on going from 1-butanol to *tert*-butanol, whereas the intensity of the free OH is seen to increase. The stronger hydrogen bonding is, the more red-shifted is the band due to the bonded OH. In contrast, the band position of the free OH shows the opposite trend. A

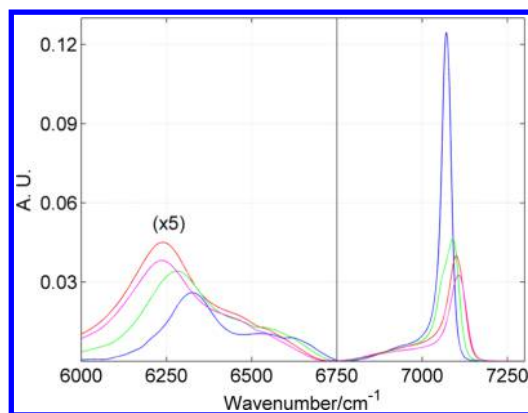


**Figure 11.** Power spectra obtained from temperature-dependent synchronous 2D NIR correlation spectra of pure liquid *n*-butyl alcohol (red), *iso*-butyl alcohol (magenta), *sec*-butyl alcohol (green), and *tert*-butyl alcohol (blue).

comparison of the results for different aliphatic alcohols reveals that the strength of the hydrogen bonding weakens with an increase in both the alcohol order and the chain length. The presence of distinct asynchronous peaks is evidence that the thermal breaking of the associates does not lead directly to the monomers but involves formation of the smaller species like oligomers. The connection of the NIR spectroscopy with the dielectric methods provided more detailed information on the hydrogen bonding in neat octyl alcohols and in  $\text{CCl}_4$  solutions.<sup>77</sup> As was shown, at relatively low concentrations the cyclic species with the dipole moment close to zero dominate. An increase in the concentration of alcohol shifts this equilibrium toward the creation of the linear species, and this trend is more apparent for the straight-chain alcohols. On the other hand, the branching enhances the tendency for the formation of cyclic associates.

The spectra of chiral and racemic alcohols are expected to show some differences resulting from the chiral discrimination effect. It has been reported that such a difference exists in the MIR spectra of chiral and racemic butan-2-ol in  $\text{CCl}_4$ .<sup>169</sup> An analysis of the MIR and NIR spectra of (*R*)-, (*S*)-, and (*RS*)-butan-2-ol as a function of concentration failed to confirm previous findings.<sup>80</sup> The spectra of pure chiral and racemic butan-2-ol were found to be indistinguishable. Analogous results were obtained for pure liquid (*R*)-(-)-octan-2-ol, (*S*)-(+)-octan-2-ol, as well as the racemic mixture.<sup>78</sup> Both the NIR and 2D correlation spectra of pure enantiomers and the racemic mixture were also very similar. This observation allows us to conclude that the chiral discrimination effect, if it exists, is too small to be observed in either the MIR or NIR spectra of aliphatic alcohols.

Hydrogen bonding in liquid and supercritical 1-octanol and 2-octanol has been studied using both MIR and NIR spectroscopy.<sup>170</sup> The estimation of the amount of the free OH groups was based on the quantitative analysis of the intensity of the fundamental, first, and second overtones of the OH stretching vibration. All three results were very similar and demonstrate that, in the liquid octyl alcohols under ambient conditions, the population of the free OH groups is around 5% but increases up to 70–80% at 340 °C. In the supercritical domain it remains around 80% and reaches 96% in the gas phase. As expected, due to steric hindrance, the amount of the free OH is always greater in 2-octanol compared with 1-octanol

under the same conditions. This confirms the results from the NIR and dielectric measurements of liquid octanols.<sup>77</sup>

Recently, Kuen and Feierabend studied solute–solvent interactions and self-association of methanol in aprotic solvents ( $\text{CCl}_4$ ,  $\text{CHCl}_3$ ,  $\text{CH}_2\text{Cl}_2$ , and  $\text{C}_6\text{H}_6$ ) by using cavity-enhanced overtone spectroscopy.<sup>171</sup> The concentration relationship of the integrated intensity of the third overtone of the free OH indicates that the degree of the nonspecific interaction increases with rising solvent dielectric constant ( $\epsilon$ ). Only in the case of benzene the authors observed the presence of a specific H– $\pi$  interaction. The concentration dependence of the free  $3\nu_{\text{OH}}$  and  $4\nu_{\text{OH}}$  transition intensities indicates the following order of self-association:  $\text{CH}_2\text{Cl}_2 \sim \text{CHCl}_3 < \text{C}_6\text{H}_6 < \text{CCl}_4$ .

The presence of two or more functional groups in chemical compounds may lead to a variety of intra- and intermolecular interactions. This is particularly true if the groups can be both acceptors and donors, such as OH or amine. MIR and NIR studies give no evidence that ethylene glycol (EG),<sup>65</sup> 1,2-propanediol (12PD),<sup>64</sup> and propanediamines<sup>67</sup> in the liquid phase form intramolecular hydrogen bonds. On the other hand, a substantial population of 1,3-propanediol (13PD)<sup>64</sup> and aminoalcohol<sup>66</sup> molecules in diluted  $\text{CCl}_4$  solution participate in intramolecular hydrogen bonding. With an increase in concentration the population of the molecules with the intramolecular hydrogen bonds decreases at the expense of the molecules involved in the intermolecular hydrogen bonding. Another vibrational (NIR, IR) spectroscopic study of a series of diols in *n*-heptane solutions reveals that the strength of the intramolecular hydrogen bonding increases from that in the five-membered ring of a 1,2-diol to the seven-membered ring of a 1,4-diol.<sup>81</sup> It was shown that the creation of the hydrogen bond does not influence the vibrational properties of the OH acceptor, but it does appreciably affect the OH donor. The intensity of the first overtone OH donor band is significantly reduced as the strength of the hydrogen bond increases. The structures of EG, 12PD, and 13PD in the liquid phase are determined by the numerous interactions through the OH groups, including the bifurcated bonds which are responsible for the high viscosity of diols.<sup>64,65</sup> On the other hand, the combined density functional theory (DFT) calculations and NIR measurements provide evidence that in both liquid amino alcohols and their mixtures with water, the cyclic dimers dominate (Figure 12).<sup>66</sup> The molecules of 1,2-aminoalcohols create the dimers through the intermolecular O–H $\cdots$ N hydrogen bonds, while molecules of 1,3-aminoalcohols may create two kinds of dimers in which the intermolecular hydrogen bonds O–H $\cdots$ N are stabilized by the intramolecular N–H $\cdots$ O bond. DFT calculations show that the dimers with the O–H $\cdots$ N bonds are about 1.4 kcal/mol more stable than those with the N–H $\cdots$ O bonds. Both kinds of 13PD dimers can be transformed into each other by the rotation of the OH and  $\text{NH}_2$  groups. In the condensed phase the dimers can create bigger associates through the additional N–H $\cdots$ O intermolecular hydrogen bonds.<sup>66</sup>

Carboxylic acids form very stable centrosymmetric cyclic dimers. The dimers are present even at elevated temperatures, in dilute solutions, and in the gas phase. The temperature- and concentration-dependent dissociation of the fatty acid dimers into the corresponding monomers has been studied by NIR spectroscopy.<sup>82–87</sup> The application of FT-NIR instruments for studies in the thermal changes (15–92 °C) of octanoic acid made it possible to propose a reliable method for the determination of the intensity of the first overtone of the free



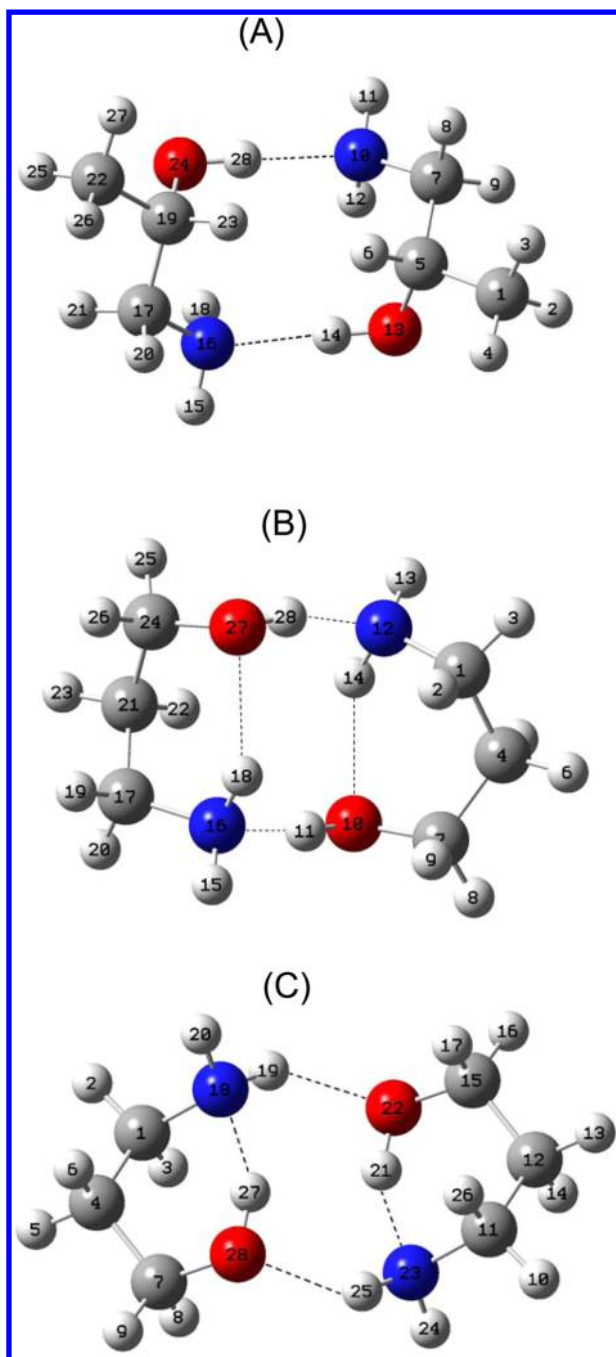


**Figure 12.** Optimized (DFT) structures of dimers of 1,2-aminopropanol (A) and 1,3-aminopropanol (B,C). Reproduced with permission from ref 66. Copyright 2010 Society for Applied Spectroscopy.

OH group in the pure liquid phase and in  $\text{CCl}_4$  solutions.<sup>82</sup> Next, these values were used for the calculation of the molar absorptivities and the population of the free OH groups as a function of the temperature. It appears that, even at 92 °C, most of molecules of octanoic acid form cyclic dimers, and the population of the free OH does not exceed 17%. The direct breaking of the dimers of fatty acids into the monomers involves the existence of two distinct bands due to the OH group, while the dissociation through the open dimers involves the presence of four bands (Figure 13A). *Ab initio* and semiempirical molecular orbital studies reveal that the open dimers of carboxylic acids are far less favored than the cyclic

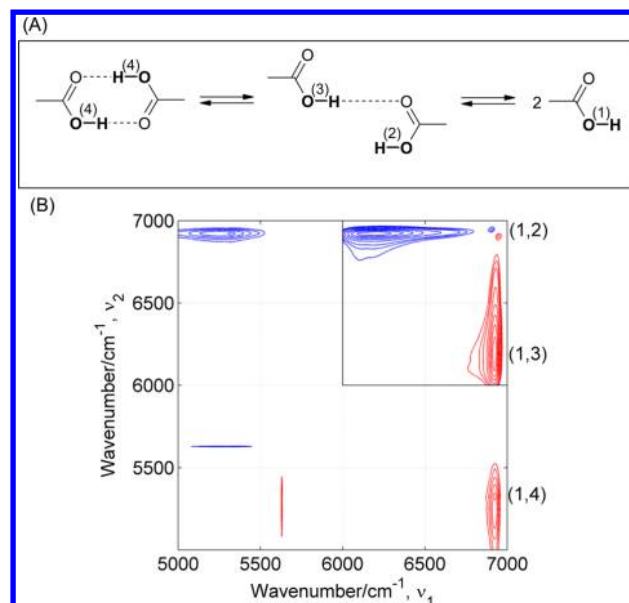


**Figure 13.** (A) Schematic diagram of breaking of the dimer of carboxylic acid into monomers with indication of different types of OH. (B) Asynchronous 2D NIR correlation spectrum constructed from the temperature-dependent spectra of pure liquid octanoic acid. On the right side are shown the types of OH contributing to particular correlation peaks.

ones.<sup>172,173</sup> As a result, the intermediate species are not observed in conventional vibrational spectra. Careful analysis of the temperature-dependent 2D NIR asynchronous spectrum of octanoic acid evidences the presence of four distinct OH peaks (Figure 13B), located at 6919 (monomer, free OH), 6902 (open dimer, free OH), 6390 (open dimer, bonded OH), and near 5300 cm<sup>-1</sup> (cyclic dimer, bonded OH).<sup>87</sup> The band due to the cyclic dimer is very broad, and in the synchronous spectrum (Figure 3a in ref 87) it extends from 4700 to 5700 cm<sup>-1</sup>. The resolution enhancement in 2D NIR correlation spectra made possible to confirm that the thermal breaking of the dimeric species of octanoic acid into the monomers proceeds through the open dimers.

As the simplest model compound of the peptide linkage the molecule of *N*-methylacetamide (NMA) was widely studied using both experimental and theoretical methods. However, the NIR spectroscopic studies of NMA were limited due to difficulties in analyzing the spectra using classical methods. Therefore, Liu et al. employed 2D correlation analysis in studies of the temperature-dependent (30–90 °C) changes in the NIR spectra of neat NMA.<sup>88</sup> In the asynchronous spectra the authors resolved five peaks at 6790, 6650, 6510, 6440, and 6250 cm<sup>-1</sup>. The peaks were assigned to the NH groups of the monomer, free end NH groups in the open-chain dimers and oligomers, as well as to the hydrogen-bonded NH groups in the dimers and higher associates. The analysis over smaller temperature intervals has shown that the breaking of the higher NMA associates leads to the creation of monomers and smaller sized associates. The relative rate of these changes depends on the temperature. A similar conclusion was reached from NMA data obtained from the combined MIR and NIR studies.<sup>89</sup> A re-examination of liquid NMA by NIR spectroscopy has revealed additional information on the band assignment and molecular mechanism of thermal changes.<sup>90</sup> It has been shown that some of the asynchronous peaks are due

to the temperature-induced frequency shift, and this assumption was confirmed by computer simulations. The temperature rise causes a decrease in the total amount of hydrogen bonds. But on the contrary to the aliphatic alcohols,<sup>58–63</sup> the mean strength of these bonds remains the same. This means that the molecules of NMA in the liquid phase are more associated than the molecules of alcohols. The amount of monomers in liquid NMA is small hence the band at  $6770\text{ cm}^{-1}$  was assigned to the free end N–H groups in the open-chain associates. The monomer band was observed at  $6808\text{ cm}^{-1}$  in dilute  $\text{CCl}_4$  solution.<sup>90</sup>

### 4.3. Phase Behavior and Phase Transition

Ikehata et al. developed a new and interesting NIR spectroscopy application.<sup>91</sup> The authors examined the phase behavior of a triethylamine/water system by monitoring the changes in the position of the first overtone of the C–H stretching modes ( $6000\text{--}5500\text{ cm}^{-1}$ ) as a function of the temperature and concentration. This shift is related to specific physical properties like density and viscosity, and hence can be readily used as a probe of the phase behavior. It appears that, although the position of this band shifts to lower wavenumbers with increasing temperature for completely miscible mixtures and for far-off-critical mixtures, this effect is relatively small. The magnitude of this shift at the critical point (32.1 wt%) was found to be notably greater compared with the off-critical mixtures. Hence, one can conclude that the microscopic association of nonpolar triethylamine species is responsible for the phase separation in systems with the lower critical mixing temperature. This work demonstrates the great potential of NIR spectroscopy for the exploration of the phase behavior of complex systems.

Iwahashi et al. studied the thermal breaking ( $8.6\text{--}84.4\text{ }^\circ\text{C}$ ) of the dimers of *cis*-9-octadecenoic acid into monomers in the pure liquid state using NIR spectroscopy.<sup>83,84</sup> The band due to the free OH was not observed in the fundamental region. In contrast, this band clearly appears in the overtone region (at  $6915\text{ cm}^{-1}$ ) even at temperatures close to the melting point. Its intensity was found to increase with the rise in temperature. The temperature relationship of the degree of dissociation determined from the intensity changes of the first overtone of the free OH shows two inflection points at  $30$  and  $55\text{ }^\circ\text{C}$  (Figure 14). The presence of these two inflection points was explained by formation of the three different structural units in liquid *cis*-9-octadecenoic acid. From the melting point to  $30\text{ }^\circ\text{C}$ , the structure is dominated by quasi-smectic liquid crystal clusters. At  $30\text{ }^\circ\text{C}$ , these clusters become less ordered, and at  $55\text{ }^\circ\text{C}$ , the disordered quasi-smectic structure undergoes a transition to an isotropic liquid. The monomers, which exist as impurities, initiate the transitions in the pure liquid *cis*-9-octadecenoic acid and cause additional breaking of the dimers. The presence of these transition points in the temperature-dependent NIR spectra of neat *cis*-9-octadecenoic acid was later confirmed by 2D sample–sample and wavenumber–wavenumber correlation analysis.<sup>50</sup> In addition, results from the newly developed analytic geometric approach<sup>85</sup> and moving window 2D NIR correlation analysis<sup>86</sup> supported these conclusions.

### 4.4. Structure of Peptides and Proteins

In order to retain the native structure of biologically important samples they are usually examined in aqueous solutions. Unfortunately, water absorption in the MIR region is very strong, and transmission measurements are challenging. On the

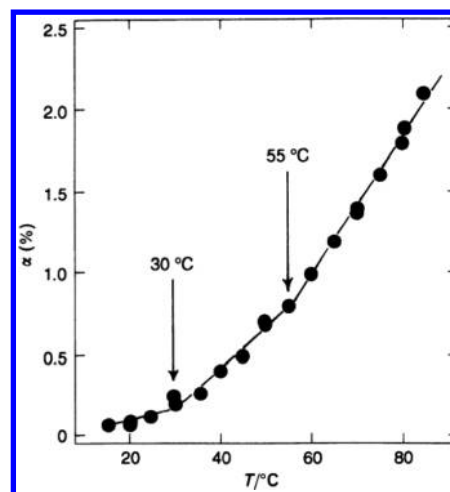


**Figure 14.** Temperature dependence of the degree of dissociation for *cis*-9-octadecenoic acid in the liquid state. Reproduced with permission from ref 84. Copyright 1995 the Royal Society of Chemistry.

other hand, reflection methods such as ATR suffer from the interaction of the sample with the surface of the crystal. Hence, transmission NIR spectroscopy appears to be an excellent alternative for the examination of the properties of bulk samples. As mentioned before, the NIR spectra of aqueous solutions are complex, and any comprehensive analysis includes both classical methods as well as 2D correlation analysis and chemometric methods. The secondary structure of proteins and the molecular mechanism of structural changes during the denaturation process are fundamental problems in this field; therefore, it is not surprising that numerous NIR spectroscopic studies have been undertaken to explore these questions.

NIR and MIR spectroscopy individually have limited ability in the structural resolution enhancement when applied to aqueous protein solutions. However, the simultaneous application of both spectral regions overcomes this problem by providing the high discriminating power needed to recognize the protein structural conformations. Navea et al. reported the combined MCR-ALS analysis of NIR and MIR spectra for the elucidation of the temperature-dependent structural changes of  $\beta$ -lactoglobulin in  $\text{D}_2\text{O}$ .<sup>174</sup> This approach allowed for the resolving of the spectra of all the protein conformations, including intermediates, as well as the corresponding pure concentration profiles (Figure 15). In Figure 15b is shown the spectral range of  $4000\text{--}8000\text{ cm}^{-1}$ , which includes the first overtones of the N–H stretching band and the second-order combination bands (free NH stretching + the first overtone of amide II, a combination of amide A and amide II). The results obtained by the authors support the mechanism proposed in the literature for the temperature-dependent denaturation of  $\beta$ -lactoglobulin as a two-step process evolving from the native conformation to a molten globule state which passes through an R-type transition form. Only the combined use of MIR and NIR techniques made discrimination of the three pure conformations of  $\beta$ -lactoglobulin involved in the process of the thermal denaturation possible.

Absorption of proteins in aqueous solutions is significantly weaker than the absorption from water. To enhance the sensitivity and the resolution of the raw NIR spectra, Wang et al. applied 2D NIR correlation spectroscopy for examination of the heat denaturation of ovalbumin in aqueous solutions,<sup>92,93</sup> as

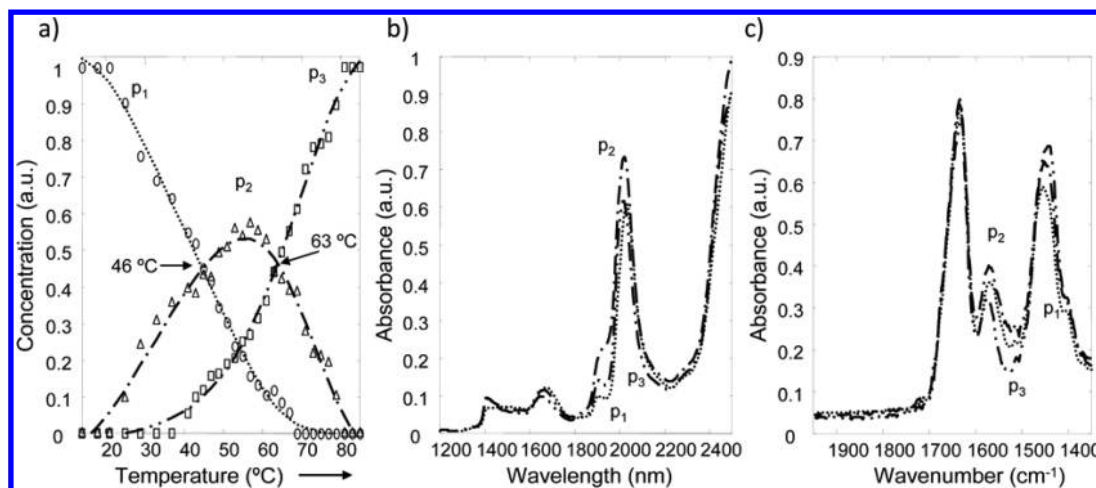


**Figure 15.** Graphical description of the temperature-dependent conformational transitions of  $\beta$ -lactoglobulin (p1, native conformation; p2, R-type state; p3, molten globule state). (a) Evolution of the concentration profiles. (b) Pure NIR spectra. (c) Pure MIR spectra. Reproduced with permission from ref 174. Copyright 2003 American Chemical Society.

well as pH-induced variations in the structure of serum albumin.<sup>93</sup> An analysis of the NIR spectra recorded from 45 to 80 °C has shown that the hydration of ovalbumin is unchanged up to 67 °C, and the protein remains in the native state. From 67 to 69 °C, a rapid change in the hydration state starts, and this induces the unfolding of the secondary structure of the ovalbumin. This process then gradually continues until 80 °C, where the next abrupt change, due to the complete denaturation of the protein, is observed. The 2D NIR correlation spectra of serum albumin over a pH range of 2.4–8.0 reveal clear pH-dependent changes in the hydration and surroundings of the amide groups.<sup>93</sup> Murayama et al. compared the results of a classical spectral analysis (difference and second derivative spectra), PCA, and 2D correlation analysis of NIR spectra of aqueous solutions of human serum albumin from 0.5 to 5.0 wt%.<sup>94</sup> As they demonstrated (Figures 4–6 in ref 94), the first loading plots are very similar to a slice of the synchronous spectra, while the second loading plots resemble a slice of the asynchronous spectra. Generalized 2D correlation spectroscopy yields information on the selective correlation of the peaks and the sequence of the intensity changes taking place during the measurements. On the other hand, PCA allows classification of the samples and is less sensitive to noise in the data. The authors state that both 2D correlation analysis and PCA give similar information on the spectral changes and lead to a better understanding of the NIR spectra of proteins.

Wang et al. measured the photoacoustic NIR spectra of powdered homo-polypeptides with an aim to better understand the structure of larger biomolecules.<sup>175</sup> These studies provided detailed spectral assignments in the NIR region based on the MIR frequencies and on the local mode framework. It was demonstrated that the regions where dominate the side chain vibrations are sensitive to the primary structure of the proteins and the chemical environment of the side chains. On the other hand, the vibrations of the backbone are sensitive to the secondary structure of the proteins. Robert et al. recorded the NIR spectra of 12 model proteins in the solid state and assigned the main bands using a comparison with the corresponding MIR data.<sup>176</sup> The bands at 4606 (2172 nm) and 4369  $\text{cm}^{-1}$  (2289 nm) appeared to be characteristic of the  $\alpha$ -helix structure. The bands observed at 4535 (2205 nm), 4417

(2264 nm), and 4323  $\text{cm}^{-1}$  (2313 nm) were attributed to the  $\beta$ -sheet, while the 4415  $\text{cm}^{-1}$  (2265 nm) band was assigned to an unordered structure. The second derivative spectra reveal the characteristic peaks that can be used for discrimination between myoglobin,  $\beta$ -lactoglobulin, and  $\beta$ -casein. The NIR spectra of a range of proteins (bovine serum albumin, lysozyme, ovalbumin,  $\gamma$ -globulin,  $\beta$ -lactoglobulin, myoglobin, cytochrome c) were explored as a potential analytical method for studies of the secondary structure of proteins in different physical states.<sup>177</sup> The second derivative of the NIR spectra of proteins in aqueous solutions and in freeze-dried solids revealed some bands in similar positions in the combination (4000–5000  $\text{cm}^{-1}$ ) and the first overtone (5600–6600  $\text{cm}^{-1}$ ) regions. The characteristic bands for the  $\alpha$ -helix and  $\beta$ -sheet were identified and assigned. It was shown that, after freeze-drying, the proteins generally preserved their native structures. Yet some decreases in the  $\alpha$ -helical structure and an increase in unordered  $\beta$ -sheet structures were observed. All these results confirm the potential of NIR spectroscopy as a nondestructive tool for the exploration of the secondary structure of proteins.

#### 4.5. Ionic Liquids

Although MIR and Raman spectra are sensitive to changes in hydrogen bonding, the studies on ionic liquids (ILs) using these techniques are limited, particularly in the molecular solvent-rich region. This results from strong absorption of these systems and lack of a noninvasive and no-sample-pretreatment technique. In contrast, NIR spectroscopy overcomes these problems. In addition, it is sensitive to vibrations of the C–H, O–H, and N–H groups. Recently, Wu et al. reported the first applications of NIR spectroscopy for probing the intermolecular interactions in IL/water mixtures.<sup>178–180</sup> The differences in the NIR spectra of pure 1-butyl-3-methylimidazolium tetrafluoroborate ([Bmim]BF<sub>4</sub>) and 1-allyl-3-methylimidazolium chloride ([Amim]Cl) were assigned to different conformations of both ILs.<sup>178</sup> As observed, the position of the anion with respect to the imidazolium cation is different in these two ILs. It follows, therefore, that they interact with water in different ways. In contrast, the NIR spectra of aromatic groups were similar irrespective of the water content. As was shown, water prefers to interact with BF<sub>4</sub><sup>−</sup>, while Cl<sup>−</sup> prefers to interact with the aromatic C–H. These results suggest that even a small amount of water is able to break the



supramolecular structure of ILs. Another NIR spectroscopic study of the intermolecular interactions between ([Bmim]-BF<sub>4</sub>)<sup>179</sup> ILs and water/ethanol mixture revealed that the supramolecular structure of the [Bmim]BF<sub>4</sub> was destroyed when the water mole fraction exceeds 0.3979. Addition of ethanol leads to the formation of hydrogen bonds with water and weakens the interaction between water and [Bmim]BF<sub>4</sub>. Both water and ethanol prefer to create hydrogen bonds with the H2 proton on the imidazolium ring, rather than the H4 or H5. A similar observation was made for [Amim]Cl/H<sub>2</sub>O, where there is evidence for the creation of C<sub>2</sub>-H...O hydrogen bonds with the ethanol molecules.<sup>180</sup> In contrast, ethanol does not form hydrogen bonds with any of the imidazolium C-H groups of [Bmim]BF<sub>4</sub>. In the case of both ILs, the ethanol molecules were able to change the interaction between the cations and water as well as between the anions and water by forming C-H...O bonds with the cations and strong hydrogen bonds between the anions and the OH group of ethanol. These studies have shown that NIR spectroscopy is useful for the exploration of such intermolecular interactions and aggregation processes in ILs.

#### 4.6. Gas-Phase Overtone Spectra

The overtone spectra of X-H stretching vibrations in the gas phase are sensitive to the bond properties. They can be applied to the examination of fine effects in the molecular structure and conformations. The OH and SH stretching overtone spectra of alcohols, thiols, diols, dithiols, and mercaptoalcohols in the gas phase have all been studied by Howard, Kjaergaard, and co-workers with the aim of probing weak inter- and intramolecular interactions as well as spectra-structure correlations in the NIR region.<sup>181–185</sup> It is hard to observe the red-shift and intensity changes of weakly hydrogen-bonded systems in the fundamentals region due to overlap with bands from the free species. Hence, the higher vibrational overtones are more convenient as a tool for probing the weak interactions since the small frequency and anharmonicity changes are more pronounced in the higher overtones region (Figure 16). The results obtained suggest that the structure of simple diols at room temperature is dominated by two conformers with intramolecular hydrogen bonding.<sup>181,182</sup> The strength of this hydrogen bonding increases on going from 1,2-ethanediol to 1,4-butanediol, and this increase is correlated with the broadening of the stretching transition of the bonded OH.<sup>182</sup> In the higher overtone region ( $n = 4,5$ ) at elevated temperatures, a third conformer, without hydrogen bonding, was detected.<sup>181</sup> The studies provide evidence of the resonance coupling between the CH and OH stretching states in EG when these groups are in the *trans* configuration. The intensities of the SH stretching vibrations in thiols are an order of magnitude weaker than the CH and OH stretching vibrations in the alcohols. This results from the low anharmonicity of the SH stretching vibration and relatively small dipole moment derivatives.<sup>183</sup> Both the overtone spectra and the theoretical calculations reveal that the most stable conformer of 2-mercaptoethanol forms weak hydrogen-bond-like OH...S interactions, similar to OH...O in EG.<sup>184</sup> On the other hand, SH...O intramolecular hydrogen bonding was not observed. As expected, the two thiol groups of 1,2-ethanedithiol do not interact with each other.

In the higher overtone region the vibrations are very well described by the local mode model (LMM) and are less coupled to other modes and to each other. Thus, the LMM parameters provide bond-specific information somewhat differ-

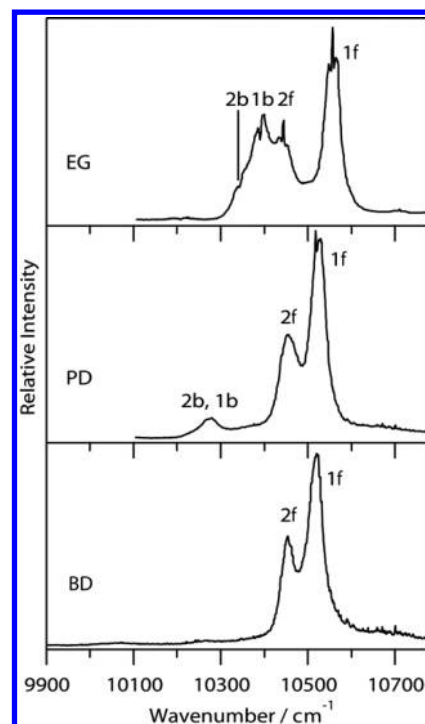


**Figure 16.** Vapor-phase overtone spectra of ethylene glycol (EG) (20 °C), 1,3-propanediol (PD) (20 °C), and 1,4-butanediol (BD) (40 °C) in the  $\Delta\nu(\text{OH})$  3 region. Reproduced with permission from ref 182. Copyright 2006 American Chemical Society.

ent from that available from normal-mode spectra. The CH stretching higher overtones ( $n = 2-6$ ) of alkenes<sup>185,186</sup> and naphthalene<sup>187</sup> in the gas phase have been measured and compared with the high-level theoretical calculations of anharmonic spectra. It was shown that the experimental spectra in the higher overtone region are well reproduced by a simple Morse oscillator LMM. The spectral differences in the higher overtone regions that might not be observed in normal-mode spectra allow the discrimination of similar compounds or similar bonds in the same compound. For example, due to a better separation of the bands in the higher overtone regions, it was possible to resolve the two nonequivalent C-H bonds in naphthalene.<sup>187</sup>

Thomsen et al. studied intramolecular interaction in 2-aminoethanol and 3-aminopropanol by using gas-phase MIR and NIR spectra.<sup>188</sup> The authors observed hydrogen-bond-like interactions in both aminoalcohols. However, the red-shift of the bonded OH and the intensity increase of the fundamental transition indicate that the intramolecular hydrogen bonding is stronger in 3-aminopropanol. Atoms-in-molecules analysis gives evidence that the hydrogen bond is present in 3-aminopropanol but not in 2-aminoethanol. In contrast, a noncovalent interactions study reveals the presence of intramolecular hydrogen bonding in both compounds.

Vapor-phase overtone spectra were applied to determine the molecular structure and interactions in complexes: methanol-trimethylamine (MeOH-TMA),<sup>27</sup> methanol-dimethylamine (MeOH-DMA),<sup>189</sup> and TMA-dimethyl sulfide.<sup>190</sup> For the first time was observed the combination transition involving one quantum of OH stretching mode and one quantum of in-plane COH bending mode.<sup>27</sup> The values of enthalpy determined from the temperature-relationship of the integrated intensity of the OH stretching mode indicate that the

interaction between MeOH and TMA is slightly stronger than that between MeOH and DMA.<sup>189</sup> The theoretical value of  $\Delta G$  calculated from a DFT thermal correction joined with a correlated coupled cluster electronic energy agrees well with the experimental estimations of  $K_p$  and  $\Delta G$ . Another study of the gas-phase overtone spectra ( $n = 1-4$ ) reveals that the CH peaks are better resolved after deuteration of the methyl groups. This indicates that the lone pair facilitates the coupling between methyl groups in TMA and dimethyl sulfide.<sup>190</sup>

Havey and Vaida measured the MIR and NIR spectra of a homologous series of organic acids [ $\text{CH}_3(\text{CH}_2)_n\text{COOH}$ ,  $n = 1-5$ ] in the vapor phase.<sup>191</sup> A comparison of the intensities and positions of the OH and CH oscillators reveals interesting trends with acid chain length. In the fundamental region the CH bands are more intense compared with the OH ones, and this trend is more evident for short-chain acids. The situation is reversed in the first overtone region. One possible explanation is that the CH stretching vibration is more harmonic and a lower energy transition compared with the OH stretching mode. The coupling and energy flow between the CH and OH oscillators seem to play important roles in the energy transfer to other vibrational modes and may result in the appearance of a series of combination bands in the NIR spectra.

#### 4.7. Matrix-Isolated Complexes

Using NIR and MIR spectroscopy, Perchard et al. studied the effect of hydrogen bonding on the anharmonicity and intensity of OH oscillators in methanol trapped in nitrogen, argon,<sup>192</sup> and neon<sup>193</sup> matrixes, and water trapped in nitrogen,<sup>194</sup> argon,<sup>195</sup> and neon<sup>196-198</sup> matrixes. These are the first NIR applications for the study of matrix-isolated H-bonded aggregates. Most of the monomer and dimer bands of methanol were identified on the basis of  $^{16}\text{O}/^{18}\text{O}$  or  $^{12}\text{C}/^{13}\text{C}$  isotopic shifts. Subsequently, the anharmonicity parameters were determined from the positions and intensities of these bands. Obviously, it is impossible to obtain this information from MIR spectra alone. The estimated intensity ratio of  $\nu_1^{\text{OH}}/\nu_2^{\text{OH}}$  was found to be greater than 1000 for the polymers, 400 for the proton donor in the dimer, and around 20 for the monomer. An opposite trend was observed for the bending mode. There are several reasons for the noticeable differences between the spectra of the proton donor and the proton acceptor molecules of the dimer. First of all, it results from the variations in the dipole moment function when the H-bonds are created and, to a lesser extent, from the Fermi resonance and the mechanical decoupling. The  $\nu_1$  band of the proton donor strongly absorbs in the fundamental region, while the related  $2\nu_1$  band is not observed. This confirms the intensity weakening of the first overtone of the hydrogen-bonded oscillator. This effect was observed both for the dimers and larger polymers and confirmed Low and Kjaergaard's theoretical predictions.<sup>26</sup>

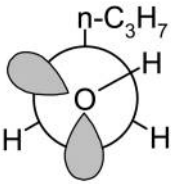
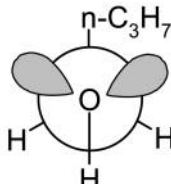
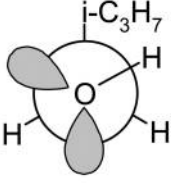
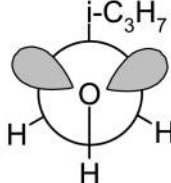
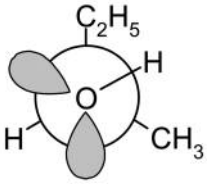
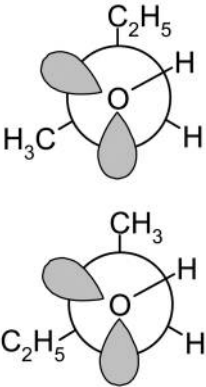
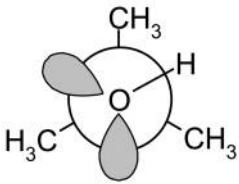
The NIR and MIR spectra of water ( $^{16}\text{O}$  and  $^{18}\text{O}$ ) in nitrogen matrixes were measured in the 8000–80  $\text{cm}^{-1}$  range.<sup>194</sup> Concentration and annealing effects make it possible to distinguish the bands due to the monomer, dimer, and polymer presence. In the vibrational spectrum of water in  $\text{N}_2$  matrixes, 25 and 19 transitions for the monomer and dimer, respectively, were observed. As in the case for methanol, in spite of strong absorbance in the fundamental region, the first overtone of the hydrogen-bonded OH was not observed. This weakening was explained by strong variations in the second derivative of the dipole moment with respect to the stretching coordinate of the hydrogen-bonded OH. The next paper in that

series was dedicated to the analysis of the IR and NIR spectra of  $\text{H}_2^{16}\text{O}$  and  $\text{H}_2^{18}\text{O}$  in argon matrixes at different molar ratios.<sup>196</sup> At low water content quasi-freely rotating monomers dominate. Also in an Ar matrix, the first overtone of the hydrogen-bonded OH (proton donor) was not observed. In contrast, a significant increase in the intensity of the  $\nu\text{OH}_b + \nu_2$  combination band appears in the NIR spectrum. Both features, assigned as a property of hydrogen bonding, result from enormous changes in the dipole moment function involving hydrogen-bonded OH. The vibrational spectrum of water dimers in a neon matrix was compared with the anharmonic *ab initio* calculations.<sup>196,197</sup> Using an improved experimental method the initial results<sup>196</sup> were subsequently reexamined, and this allowed the spectra up to the Vis to be recorded.<sup>197</sup> The authors identified 23 intramolecular transitions for the proton acceptor and 22 transitions for the proton donor. The observed and calculated anharmonic frequencies were found to be in a good agreement. As was also shown, a significant reduction of the Fermi coefficients is necessary to correctly describe the relative intensities of the interacting levels. The vibrational properties of the proton acceptor are very similar to that of the monomer, whereas the stretching harmonic frequency of the proton donor is red-shifted by 50  $\text{cm}^{-1}$ . The related anharmonicity shows a decrease due to the partial decoupling between the two oscillators. The same group examined the matrix spectra of water trimers from 11000 to 90  $\text{cm}^{-1}$ .<sup>198</sup> Although previous calculations suggested that the three water molecules in the trimer are nonequivalent, the experimental results did not support this conclusion and provided evidence for weak intermolecular couplings leading to quasi-degeneracy of the corresponding vibrations. It was shown that the neon matrixes induce small perturbations of the vibrational frequencies that can be applied to test the performance of the new Gaussian versions to reproduce the anharmonicity of the vibrations and the effects of hydrogen bonding.<sup>196</sup> A comprehensive analysis of the vibrational states of a molecule requires both MIR and NIR measurements as well as advanced theoretical calculations.

#### 4.8. Spectra–Structure Correlations in the NIR Region

To better understand correlations between the spectra and the structure in the NIR region, Iwamoto et al. undertook systematic studies of a series of compounds including aliphatic and aromatic hydrocarbons, halogen derivatives of hydrocarbons, alcohols, and other common organic solvents.<sup>95-98</sup> It has been demonstrated that, in the NIR region, absorption of alcohols (1-nonanol, 2-nonanol) and of the hydrophobic solvent (*n*-heptane) can be separated by a simple subtraction of the corresponding spectra. This procedure works well down to very low concentrations (0.1% v/v), where the OH groups are nonbonded, giving rise to a sharp band near 7100  $\text{cm}^{-1}$ . The OH groups of the alcohol appear to be unperturbed by intermolecular interactions with *n*-heptane, whereas in  $\text{CCl}_4$  and in particular in 1-chlorooctane solutions, these groups are red-shifted, indicating the presence of weak  $\text{O}-\text{H}\cdots\text{Cl}$  interactions.<sup>95</sup> A comparison of the MIR and NIR spectra of alcohols recorded at the same concentrations reveals that the relative intensities of various hydrogen-bonded species are quite different in the two spectral regions. Therefore, MIR and NIR spectra provide complementary information on the hydrogen bonding. The overtone and combination bands from the CH stretching  $\{\nu(\text{CH})\}$  and deformation  $\{\delta(\text{CH})\}$  vibrations were examined in  $\text{CHX}_3$ ,  $\text{CHX}_2-\text{CHX}_2$ , and  $\text{CHX}_2-\text{CX}_2-\text{CHX}_2$

Table 1. Newman Projections of the OH Rotational Conformers of Butyl Alcohols, Positions of the  $\nu_{\text{OH}}$  and  $2\nu_{\text{OH}}$  Bands ( $\text{cm}^{-1}$ ), Relative Integrated Intensities of Both Conformers ( $A_g:A_t$ ),  $\Delta H_{\text{T-G}}$  ( $\text{kJ}\cdot\text{mol}^{-1}$ ), and the Anharmonicity Constants<sup>a</sup>

<b>n-butanol</b> $A_g:A_t=1:1.6$ $\Delta H = 2.0$ $B_g/B_t = -85.0/-85.0$	gauche, 3627/7083 	trans, 3640/7109 
<b>iso-butanol</b> $A_g:A_t=1:2.6$ $\Delta H = 2.9$ $B_g/B_t = -85.0/-85.5$	gauche, 3628/7086 	trans, 3642/7112 
trans, 3609/7043 	gauche, 3628/7084 	<b>sec-butanol</b> $A_t:A_g=1:5.1$ $\Delta H = 1.9$ $B_g/B_t = -87.5/-86.5$
3617/7060 	<b>tert-butanol</b> $B = -86.5$	

<sup>a</sup>Anharmonicity constants  $B = \nu^{02}/2 - \nu^{01}$ , where  $\nu^{01}$  and  $\nu^{02}$  are positions of the fundamental and the first overtone, respectively, for gauche ( $B_g$ ) and trans ( $B_t$ ) conformers ( $\text{cm}^{-1}$ ). Reproduced with permission from ref 100. Copyright 2006 Elsevier.

halogen derivatives of alkanes from 3500 to 10 000  $\text{cm}^{-1}$ .<sup>96</sup> Other studies were dedicated to the overtones and the combination bands of the  $\text{CH}_2$  in  $\text{CH}_2\text{X}_2$ ,  $\text{CH}_2\text{XCHX}_2$ , and  $\text{CH}_3(\text{CH}_2)_5\text{CH}_3$ .<sup>97</sup> All bands appearing in this region were assigned to one of the five groups:  $\{\nu(\text{C-H})+\delta(\text{C-H})\}$ ,  $\{\nu(\text{C-H})+2\delta(\text{C-H})\}$ ,  $\{2\nu(\text{C-H})\}$ ,  $\{2\nu(\text{C-H})+\delta(\text{C-H})\}$ , and  $\{3\nu(\text{C-H})\}$ . The overtones and combination modes of various halogen-substituted hydrocarbons have characteristic positions and intensities in the NIR spectra and provide information on the structure of the hydrocarbon chain. It has been suggested that the first-order combination modes include the combined information on the  $\nu(\text{C-H})$  and  $\delta(\text{C-H})$  vibrations. The characteristic spectral windows free from any significant absorption were also localized. These windows are

most useful for examination of other functional groups such as OH, NH, or SH. The NIR absorption of the C-H stretching modes of hydrogen atoms attached to  $\text{C}=\text{C}$  or  $\text{C}\equiv\text{C}$  bonds usually appear at higher frequencies. Hence absorption of these groups can be easily distinguished from the usually strong aliphatic C-H absorption.<sup>98</sup> Most importantly, solvents with functional groups like COO, CON,  $\text{C}\equiv\text{N}$ ,  $\text{C}=\text{O}$ , or  $\text{S}=\text{O}$  have a strong absorption in the fundamental region that often disturb the absorption from the solute. In contrast, these groups only weakly contribute to NIR spectra; therefore, NIR spectroscopy is a more convenient technique for the exploration of reactions and molecular interactions in organic solvents with these functionalities.



The rotation of an OH group around a C–O bond is responsible for the presence of different conformers, and this effect is known as “rotational isomerism”. An analysis of the MIR and NIR spectra of various alcohols has demonstrated that the position of the  $\nu_{\text{OH}}$  and  $2\nu_{\text{OH}}$  bands results mainly from the conformer type (Table 1).<sup>100</sup> The inductive effect of the methyl groups in the  $\alpha$ -position shifts the  $\nu_{\text{OH}}$  and  $2\nu_{\text{OH}}$  bands to higher frequencies. However, the effect of the methyl groups in the  $\beta$ -position is minimal. On the other hand, the relative populations of individual conformers depend strongly on the steric effects of the substituents both in the  $\alpha$ - and  $\beta$ -positions. This study clearly shows that rotation around the C–C axis has a small effect on the position of the OH stretching band in aliphatic alcohols.

Parker et al. reported an application where absorption intensities in chemical analysis proved useful.<sup>199</sup> The NIR spectra of 43 aliphatic hydrocarbons were recorded in the 3900–6000  $\text{cm}^{-1}$  range. The authors demonstrated that by using principal factor analysis the experimental spectra of related compounds can be represented as the sum of a limited series of group spectra. These group spectra were calculated from the eigenspectra (scores) and eigenvectors (loadings) of the covariance matrix of the spectral data. This means that the group spectra in the region of the first overtones and combination bands can be derived with a good approximation from the basic structural units present in the corresponding spectra of pure hydrocarbons. This way all the spectral features in NIR range can be explained and reliably assigned. Recently, similar studies were performed on MIR and NIR spectra of *n*-alkanes and 1-chloroalkanes.<sup>200</sup> Using MCR-ALS approach the authors obtained the group spectra for the C–H stretching vibrations of *n*-alkanes and 1-chloroalkanes from the fundamental to the fourth overtones. An application of 2D correlation analysis and chemometrics methods made it possible to separate the contributions from the terminal and midchain  $\text{CH}_2$ . The spectral prediction based on the group spectra appears to be very efficient in the overtones region. The prediction and correlation of the chemical and physical properties of mixtures using NIR spectroscopy is also of practical meaning. For example, Kelly et al. reported a positive correlation between the octane number and the methyl group content as well as the degree of branching.<sup>201</sup>

## 5. NIR SPECTROSCOPY AND QUANTUM CHEMICAL CALCULATION STUDIES OF WAVENUMBERS AND INTENSITIES OF OVERTONES, ANHARMONICITIES, VIBRATIONAL POTENTIAL FUNCTIONS, AND INTERMOLECULAR INTERACTIONS

### 5.1. Recent Progress in Quantum Chemical Calculations in NIR Spectroscopy

Today, quantum chemical calculations have made marked progress in applications to vibrational spectroscopy, electronic spectroscopy, and many others. They have become popular also in NIR spectroscopy; one can calculate wavenumbers and absorption intensities of the overtones of XH ( $X = \text{C}, \text{O}, \text{and N}$ ) vibrations. Even those of combination bands have become feasible. It is possible to estimate anharmonicity of vibrational potential function from quantum chemical calculations. The most important progress is the improvement in the calculation rate for a single central processing unit (CPU) and that of calculation systems due to advances in the technique of parallel computing. Such progress has made possible calculations that

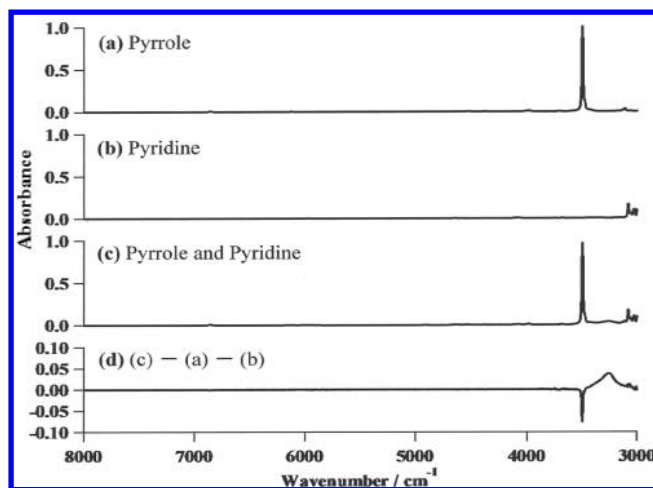


**Figure 17.** FT-NIR/IR spectra of (a) pyrrole, (b) pyridine, and (c) pyrrole + pyridine  $\text{CCl}_4$  solutions. (d) Difference spectrum (c) – (a) – (b). Concentrations of pyrrole and pyridine were 0.04 M for all solutions. Reproduced with permission from ref 30. Copyright 2009 Elsevier.

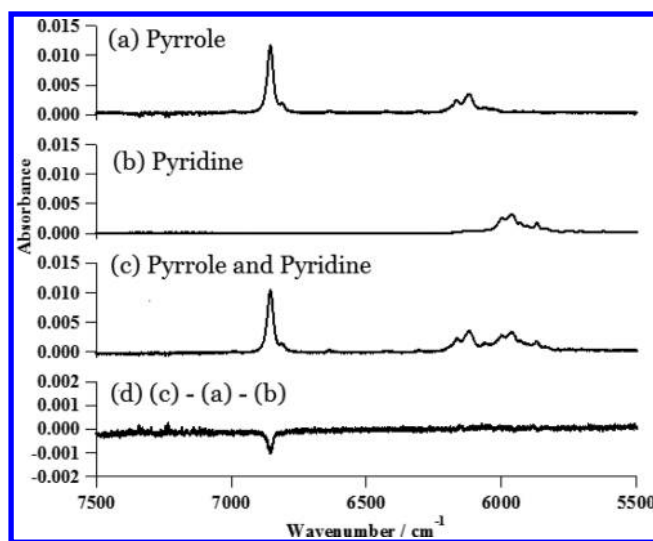


**Figure 18.** FT-NIR spectra in the NH stretching overtone region of (a) pyrrole, (b) pyridine, and (c) pyrrole + pyridine  $\text{CCl}_4$  solutions. (d) Difference spectrum (c) – (a) – (b). Concentrations of pyrrole and pyridine were 0.04 M for all solutions. Reproduced with permission from ref 30. Copyright 2009 Elsevier.

previously were considered difficult. Moreover, there has also been development in quantum chemical calculations such as DFT calculations that can yield better results by the calculation cost which is nearly equivalent to that for Hartree–Fock calculation. It has become possible to perform quantum chemical calculations involving the anharmonicity of molecular vibrations thanks to the development of software such as Gaussian03, GAMESS, and Multimode.

The Lennard-Jones and Morse potentials are well known as approximation functions considering anharmonicity for the potential of a diatomic molecule. For MD simulations the former is often used, while for quantum chemical calculations the latter is more popular. In the case of a diatomic molecule, one can develop vibrational energy levels and wave functions analytically by approximating a vibrational potential using the Morse potential. Moreover, if one increases the number of

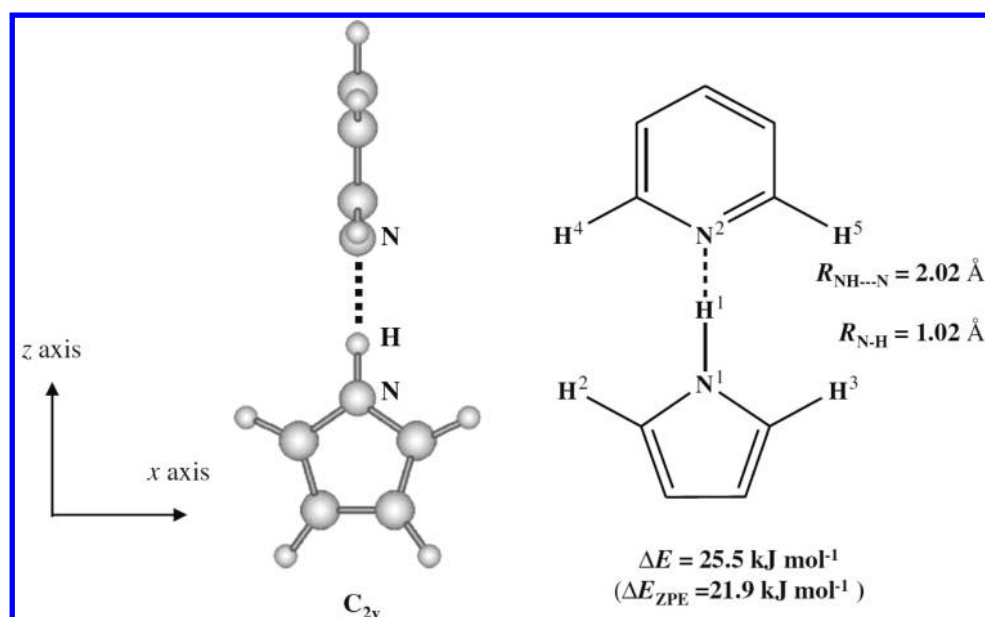


**Figure 19.** Optimized structure for pyrrole–pyridine complex calculated at the DFT//B3LYP/6-311++G(3df,3pd) level. The stabilization energy  $\Delta E = 25.5 \text{ kJ mol}^{-1}$ , or  $21.9 \text{ kJ mol}^{-1}$  after correction of the zero-point energy. The  $\text{NH}\cdots\text{N}$  distance is  $2.02 \text{ \AA}$ , and the  $\text{N-H}$  distances of pyrrole–pyridine complex and pyrrole monomer are  $1.02$  and  $1.00 \text{ \AA}$ , respectively. Reproduced with permission from ref 30. Copyright 2009 Elsevier.

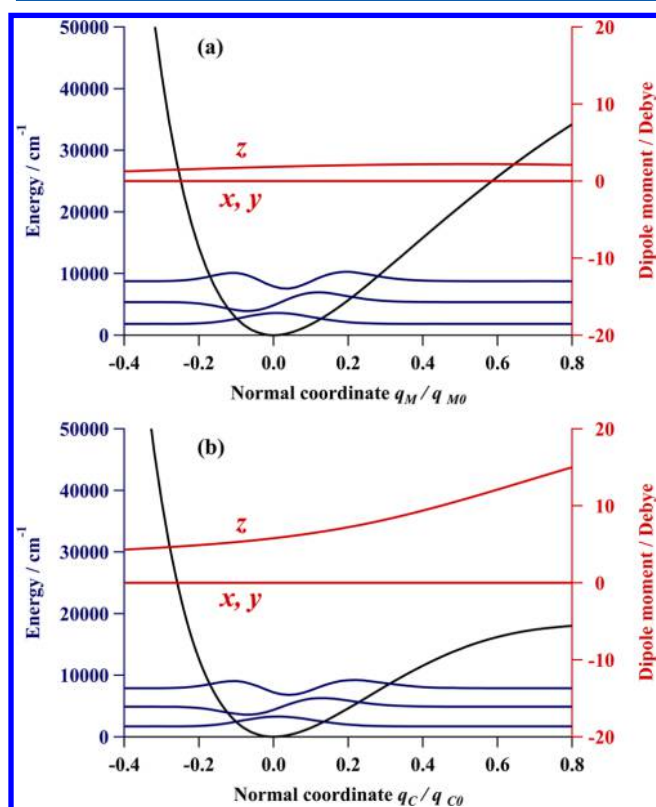


**Figure 20.** Vibrational wave functions and dipole moment functions along potential energy curves of the  $\text{NH}$  stretching mode of (a) pyrrole monomer and (b) pyrrole–pyridine complex calculated at the DFT//B3LYP/6-311++G(3df,3pd) level. Symbols  $q_{M0}$  and  $q_{C0}$  denote units of the normal coordinates for the  $\text{NH}$  stretching mode in the monomer and the complex, respectively. They are represented by the displacement vectors of atoms (see Figure 19) in  $\text{\AA}$  units as follows:  $q_{M0} = \{N^1(0,0,-0.07), H^1(0,0,1.00), H^2(0.01,0,0), H^3(-0.01,0,0)\}$ ;  $q_{C0} = \{N^1(0,0,-0.08), H^1(0,0,1.00), H^2(0.01,0,0), H^3(-0.01,0,0), H^4(0,-0.01,-0.01), H^5(0,0.01,-0.01)\}$ .

calculation points, one can obtain highly accurate numerical solutions without an approximate function. For triatomic or larger molecules, the approximation is not easy. However, several methods to calculate the vibrational spectra have been developed by Carrington et al.,<sup>202</sup> Halonen et al.,<sup>203</sup> and McCoy.<sup>204</sup> In this Review, we have introduced examples of vibrational self-consistent field (VSCF) and vibrational configuration interaction (VCI) methods, which were proposed by Bowman and Gerber as highly accurate analytical methods for calculating anharmonic wavenumbers,<sup>205–208</sup> and these methods have been developed by Christiansen<sup>209</sup> and Barone et al.<sup>210,211</sup> In these methods it is very important to obtain highly accurate potential functions, and not surprisingly the degree of calculations increases rapidly with the number of atoms in the molecule. In recent years there have been significant improvements in the calculation rate of computers and in the technique of parallel computing. In spite of this, the situation for rapid calculations is still not satisfactory. One solution is development of more efficient algorithms that enable one to get potential functions. Yagi et al.<sup>212–217</sup> and Maeda et al.<sup>218,219</sup> separately proposed calculation methods that yield accurate results with a smaller number of operations based on the VSCF method. Yamada and Aida<sup>220,221</sup> presented calculations based on MD. Using these improved methods, Yagi et al.<sup>222</sup> performed numerous quantum chemical calculations including anharmonicity of MIR and NIR spectra. They also studied the changes in the peak positions caused by Fermi resonance and the resulting broadening by hydrogen bonding. The same group extended these studies to larger systems and developed highly accurate methods of calculations.<sup>214</sup>

The determination of vibrational states includes the evaluation of potential energy surface (PES) by electronic state calculations and the solution of vibrational Schrödinger equations. In order to obtain PES, at first one has to calculate the Hessian matrix and anharmonic terms. Recently, marked progress has been made in obtaining both the PES and the solution of the vibrational Schrödinger equation. Yagi et al.<sup>215</sup> divided grid points of PES into points with strong and weak

Table 2. Observed and Calculated Frequencies ( $\text{cm}^{-1}$ ) and Relative Intensities of the Fundamentals and the First Overtones of the NH Stretching Bands of Pyrrole and Pyrrole–Pyridine Complex<sup>a</sup>

	pyrrole				pyrrole–pyridine			
	$\nu$	int.	$2\nu$	int.	$\nu$	int.	$2\nu$	int.
vapor	3531	—	6925	—	—	—	—	—
in $\text{CCl}_4$	3497	1.000	6856	0.023	3266	8.184	—	—
B3LYP/6-311++G(3df,3pd)	3539	1.000	6944	0.057	3206	23.780	6200	0.003
B3LYP/6-31+G**	3547	1.000	6960	0.068	3212	23.634	6212	0.007
B3LYP/6-31G*	3528	1.000	6918	0.113	3235	31.284	6263	0.014

<sup>a</sup>Reproduced with permission from ref 30. Copyright 2009 Elsevier.

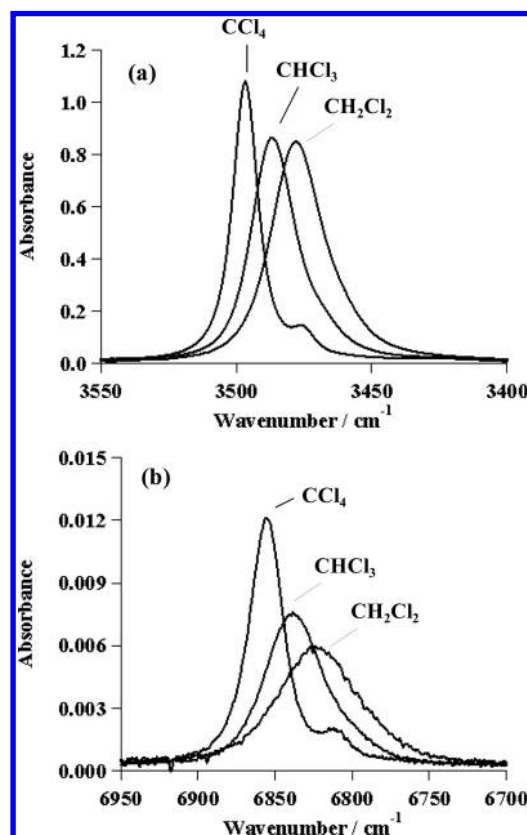


Figure 21. Solvent dependence of (a) the fundamental and (b) the first overtone of the NH stretching mode of pyrrole. Solvents used were  $\text{CCl}_4$ ,  $\text{CHCl}_3$ , and  $\text{CH}_2\text{Cl}_2$ . Concentrations all solutions were 0.04 M. Reproduced with permission from ref 31. Copyright 2011 American Chemical Society.

anharmonicity, and proposed a multiresolution method with optimized accuracy of the electronic-state calculations and grid sizes by the strength of anharmonicity. The same group developed a new method based on the pseudo-degenerate perturbation theory as an efficient method of solving the vibrational Schrödinger equation.<sup>222</sup> These algorithms bring the calculations of vibrational frequencies and absorption intensities of a polyatomic molecule considering anharmonicity close to realization. If only the wavenumbers of the first overtones and combinations of vibrational modes involving anharmonicity need to be calculated, it is possible to do so by using the “anharmonic” option, which was introduced after Gaussian03. One can perform similar calculations by using GAMESS and Multimode software. Akai et al.<sup>223</sup> measured the NIR and IR spectra of acetic acid by using “low-temperature rare gas matrix-isolated IR spectroscopy” and compared the observed wave-

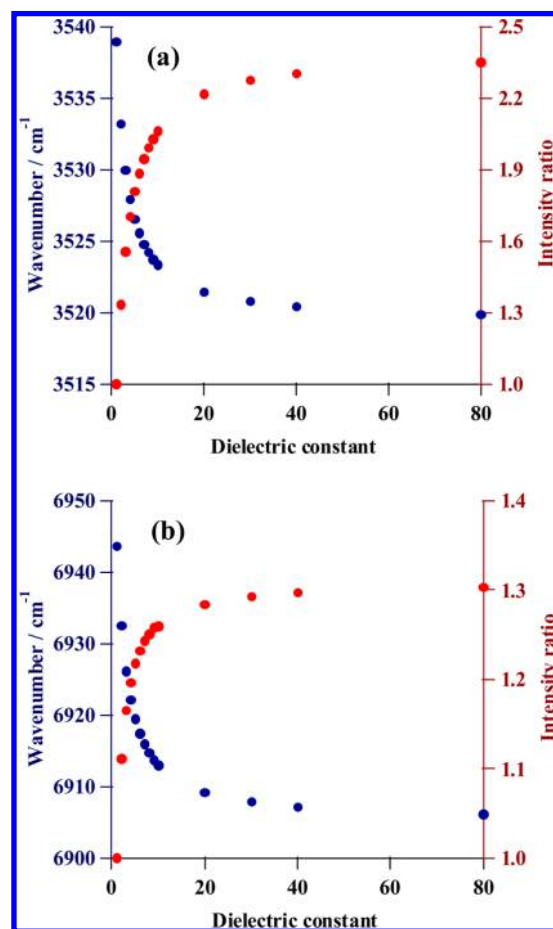
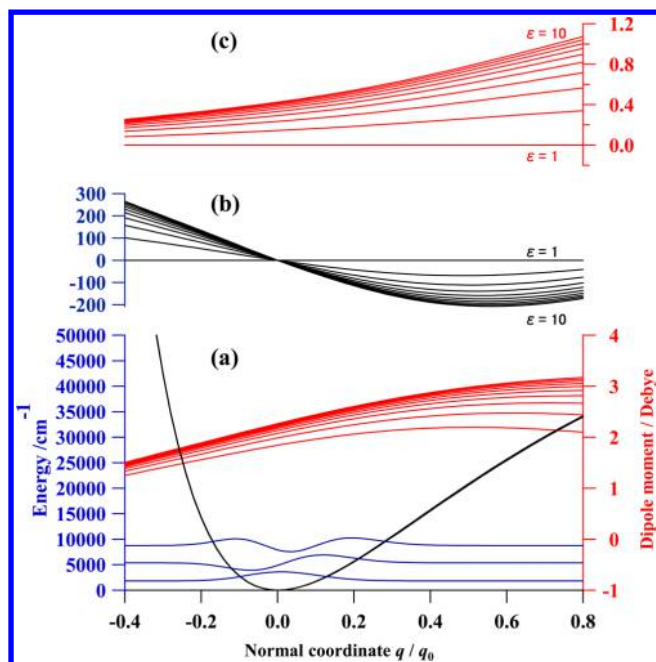


Figure 22. Relationship between the dielectric constant and the wavenumber/intensity ratio of the fundamental NH (a) and the first overtone (b) of pyrrole calculated at the IPCM//DFT/B3LYP/6-311++G(3df,3pd) level. Reproduced with permission from ref 31. Copyright 2011 American Chemical Society.

numbers with the calculated ones. It was also reported by Yoshida et al.<sup>224</sup> that wavenumber linear scaling can reproduce the wavenumbers of the first overtones.

Sandorfy et al.<sup>225</sup> pointed out that there are two methods for the treatment of overtones: one is based on normal coordinates, and the other is based on local coordinates. Normal-mode analysis is usually used for the first overtones. On the other hand, LMM, developed by Mortensen et al.<sup>226</sup> and Child and Lawton<sup>227</sup> in 1981, seems to be better adapted to higher order overtones. As to the local-mode analysis, harmonically coupled anharmonic oscillator LMMs<sup>228</sup> combined with *ab initio* calculated dipole moment functions are the most often applied. Although the experimental absolute





**Figure 23.** (a) Dependences on  $\epsilon$  of the potential energy curve, dipole moment function ( $\epsilon = 1$ –10), and wave function ( $\epsilon = 1$ ) of the NH stretching mode ( $\epsilon = 1$ –10). (b) Difference of the potential energy curve between the calculation result for  $\epsilon = 1$  and a variety of  $\epsilon$ . (c) Difference of the dipole moment function between the calculation result for  $\epsilon = 1$  and a variety of  $\epsilon$ . Reproduced with permission from ref 31. Copyright 2011 American Chemical Society.

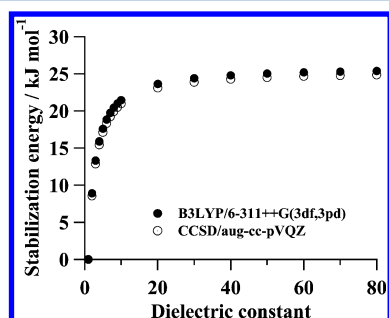


**Figure 24.** Dielectric constant and stabilization energy of hydrogen fluoride. Reproduced with permission from ref 33. Copyright 2012 Elsevier.

intensity for hydrogen bonding species remain only rarely measured for the NIR region, these theoretical studies on intensities and wavenumbers of overtones have been applied to studies on intermolecular interactions. Several research groups have used NIR/IR spectroscopy and quantum chemical calculations to study hydrogen bonding and the solvent dependencies of absorption intensities and wavenumbers of the fundamental and overtones of the OH and NH stretching vibrations, their anharmonicities, and vibrational potentials.

A few groups, including those of Henry and Kjaergaard et al., carried out a comparison of the observed NIR and IR gas-phase spectra with quantum chemical calculations of fundamentals and higher overtones of the CH, OH, NH, and SH stretching modes based on the LMM.<sup>26,27,181,183,229–235</sup> These studies included not only the molecular vibrations of a single molecule but also changes in the molecular vibrations induced by the formation of hydrogen bonds. For example, Kjaergaard et al. measured the NIR spectrum of a MeOH–TMA complex and

the H<sub>2</sub>O dimer in the gas phase.<sup>26,27</sup> They carried out quantum chemical calculations for frequencies and intensities of the OH fundamental and first overtone of MeOH in the complex. It was revealed from these calculations that, after formation of the hydrogen bond, the intensity of the fundamental OH stretching mode of the MeOH became stronger while that of the first overtone became weaker. Takahashi et al. reported theoretical studies on the wavenumbers and absorption intensities of the fundamentals and overtones, including higher order overtones of the OH and CH stretching modes, with LMM approximation.<sup>29,236–238</sup>

Czarnik-Matusiewicz et al. investigated the vibrational potentials of the OH stretching modes of phenol and phenol derivatives by changing a substituent.<sup>99</sup> The first five vibrational transitions of phenol in the gas phase were very well reproduced by the MP2/6-31G\*\* potential of the OH stretching mode. The effect of substituent on the wavenumbers and the intensity of the  $\nu(\text{OH})$  transition was analyzed as a function of the  $\text{pK}_a$  values for 11 different phenol derivatives. Using quantum chemical calculations based on the normal-mode model, Futami et al. investigated the consequences of hydrogen bond formation and solvent effects.<sup>30–33,239</sup> They studied the effects of hydrogen bonding on wavenumber shifts and intensity changes of the NH fundamental and its first overtone for a pyrrole–pyridine complex in CCl<sub>4</sub> by using NIR/IR spectroscopy and DFT calculations. The first overtone of the NH stretching vibration band of free pyrrole was observed at 6856 cm<sup>−1</sup>, but that of the pyrrole–pyridine complex was missing or extremely weak. This result is in good agreement with that of the OH stretching mode of the water dimer and MeOH–TMA complex found by Kjaergaard et al.<sup>26,27</sup> Moreover, they revealed, using similar quantum chemical calculations, that the absorption intensity of the first overtone of the NH stretching mode decreases even in an NH $\cdots\pi$  hydrogen bond.<sup>30</sup> This is a weak hydrogen bond, although the degree of changes in the wavenumbers and absorption intensities is smaller compared with an NH $\cdots\text{N}$  hydrogen bond.<sup>239</sup> Gas-phase MIR and NIR spectra of DMA and pyrrole were recently published by Miller et al.<sup>235</sup> It was revealed that for DMA the intensity of the fundamental NH stretching transition is weaker than the first NH stretching overtone. Moreover, the fundamental NH stretching transition in DMA is less intense than the fundamental transition of pyrrole.

Futami et al. also studied the solvent dependencies on wavenumbers and absorption intensities of the fundamental and the first overtone of the NH stretching vibration of pyrrole in CCl<sub>4</sub>, CHCl<sub>3</sub>, and CH<sub>2</sub>Cl<sub>2</sub> by using NIR/IR spectroscopy and DFT calculations.<sup>30,31,239</sup> They used a self-consistent reaction field (SCRF)/isodensity surface polarized continuum model (IPCM). As shown, the wavenumbers of the NH fundamental and its first overtone decrease in the order of CCl<sub>4</sub>, CHCl<sub>3</sub>, and CH<sub>2</sub>Cl<sub>2</sub>, which is the increasing order of  $\epsilon$ . They concluded that the solvent dependencies of the positions and intensities of the NH stretching bands of pyrrole are quite different from the changes caused by the formation of NH hydrogen bonds. Gonjo et al. extended these studies to the second and third overtones.<sup>32</sup> They studied both wavenumbers and intensity changes of the OH of phenol and 2,6-dihalogenated phenols caused by changes in solvents from the fundamental to the third overtone by Vis/NIR/IR spectroscopy and DFT calculations.

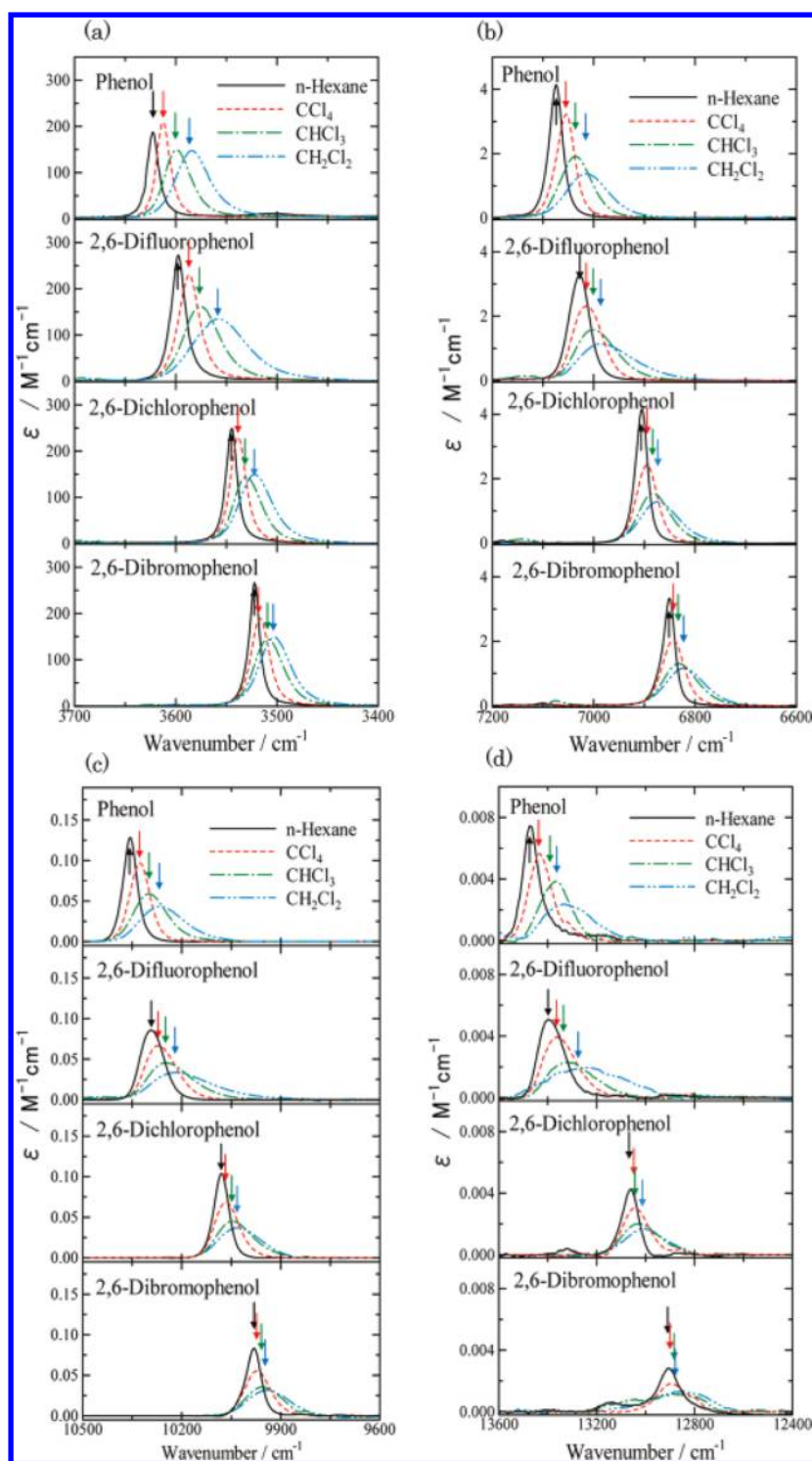


**Figure 25.** Vis/NIR/IR spectra of phenol, 2,6-difluorophenol, 2,6-dibromophenol in *n*-hexane,  $\text{CCl}_4$ ,  $\text{CHCl}_3$ , and  $\text{CH}_2\text{Cl}_2$ : (a) fundamental region, (b) first overtone region, (c) second overtone region, and (d) third overtone region. Reproduced with permission from ref 32. Copyright 2011 American Chemical Society.

## 5.2. Quantum Chemical Calculation Studies of Wavenumbers and Intensities of Overtones, Anharmonicities, Vibrational Potential Functions, and Intermolecular Interactions

For the past 50–60 years, the overtones and combinations of XH ( $\text{X} = \text{C}, \text{N}, \text{O}$ ) stretching modes have been studied by NIR spectroscopy.<sup>1,2,34,35</sup> Band assignments, anharmonicities, hydrogen bonding, and solvent effects have all been investigated to

some extent, even in the 1950s.<sup>1,2,34,35</sup> Mecke and Ziegler worked on the anharmonicity and local mode ideas in the 1930s.<sup>240</sup> Later, Henry reviewed progress in the use of local modes in the description of highly vibrationally excited molecules and an application of the LMM as a probe of molecular structure and conformation.<sup>241,242</sup> Foldes et al. investigated the anharmonicities of the OH and NH stretching vibrations of alcohols and amides in  $\text{CCl}_4$  by measuring their

Table 3. Observed Wavenumbers and Relative Intensities of the Fundamentals and the First, Second, and Third Overtones of OH Stretching Modes of Phenol and 2,6-Dihalogenated Phenols in the Gas Phase and in Four Solvents<sup>a</sup>

“X” in X <sub>2</sub> -PhOH	phase/solvent	fundamental		first overtone		second overtone		third overtone	
		1ν	int	2ν	int	3ν	int	4ν	int
H	gas	3656		7143		10461		13611	
	<i>n</i> -hexane	3622	100	7074	4.43	10358	0.19	13472	0.021
	CCl <sub>4</sub>	3612	140	7055	4.12	10327	0.22	13435	0.018
	CHCl <sub>3</sub>	3600	161	7036	3.92	10298	0.22	13391	0.015
	CH <sub>2</sub> Cl <sub>2</sub>	3586	209	7016	3.71	10267	0.20	13362	0.015
F	gas	3631		7094		10392			
	<i>n</i> -hexane	3598	157	7028	4.58	10292	0.20	13395	0.017
	CCl <sub>4</sub>	3587	188	7015	4.15	10271	0.21	13360	0.016
	CHCl <sub>3</sub>	3576	211	7001	3.99	10248	0.21	13331	0.017
	CH <sub>2</sub> Cl <sub>2</sub>	3558	242	6987	3.98	10219	0.20	13270	0.016
Cl	gas	3571		6957		10157			
	<i>n</i> -hexane	3545	113	6906	3.55	10080	0.16	13063	0.010
	CCl <sub>4</sub>	3538	142	6895	3.48	10067	0.17	13044	0.011
	CHCl <sub>3</sub>	3531	144	6884	3.27	10047	0.16	13041	0.010
	CH <sub>2</sub> Cl <sub>2</sub>	3522	175	6874	3.25	10032	0.15	13008	0.011
Br	gas								
	<i>n</i> -hexane	3522	113	6851	2.99	9980	0.14	12907	0.006
	CCl <sub>4</sub>	3518	126	6843	3.04	9972	0.15	12897	0.007
	CHCl <sub>3</sub>	3509	143	6833	2.89	9957	0.13	12880	0.004
	CH <sub>2</sub> Cl <sub>2</sub>	3503	159	6823	2.84	9947	0.12	12876	0.004

<sup>a</sup>Reproduced with permission from ref 32. Copyright 2011 American Chemical Society.

fundamentals and first and second overtones.<sup>243</sup> Singh et al. studied the solvent and temperature dependencies of anharmonicities for alcohols such as methanol and *tert*-butyl alcohol.<sup>244,245</sup> Furthermore, Detoni et al. compared the wavenumbers of the OH fundamentals of phenol and alcohols in various solvents with the corresponding first overtones and explored the anharmonicity of the intermolecular hydrogen bonds.<sup>246</sup> They showed that the anharmonicity of the phenol OH, which has a strong donor character, increases with the order of solvent basicity, although those of alcohols do not always change in the same order.

Although one can find numerous studies based on fundamentals and first overtones, the works using higher order overtones are quite rare.<sup>32,42</sup> Furthermore, early studies were mainly focused on the wavenumbers and only seldom on the absorption intensities. Over the past two decades, however, this situation has changed radically. Without doubt this can be attributed to the remarkable technical developments in FT-spectrometers that have made it possible to measure highly accurate spectra in terms of both wavenumbers and absorption intensities in the 16000–100 cm<sup>−1</sup> region. This is where bands due to the fundamental and the first, second, and third overtones of the OH, NH, and CH stretching modes appear. Moreover, recent progress in theoretical calculations has also made it possible to compute both the wavenumbers and absorption intensities of not only the fundamentals but also the higher order overtones.<sup>26–33</sup>

A number of studies on the relationship between the MIR absorption intensity and molecular structure as well as intramolecular charge distribution were carried out by Galabov et al.<sup>247–249</sup> As a result of the development of quantum chemical calculations, one can satisfactorily reproduce the relation between molecular structure, frequencies, and

absorption intensities of vibrational modes.<sup>250–253</sup> Molecular vibration analysis based on the harmonic oscillator model cannot reproduce experimental data with sufficient precision. The reason why quantum chemical calculations considering anharmonicity have not yet been explored intensively results from enormous amount of calculations required. Thus, even today, the development of quantum chemical calculations including anharmonicity remains a challenging task.

It is of note that there is significant progress also in experimental studies on anharmonicity. Nishida et al. studied anharmonic coupling of the CH-stretch and CH-bend vibrations of chloroform by NIR electroabsorption (EA) spectroscopy which directly probes the effects of an externally applied electric field on a combination band.<sup>254</sup> Their study indicated that the contribution of the CH-stretch mode to the mechanical anharmonicity is minor, and that the CH-bend mode plays a dominant role in the mechanical part of the vibrational coupling between the two fundamentals. Moreover, their DFT calculations suggested that both the mechanical anharmonicity and electrical anharmonicity of the CH-bend mode may contribute equally to the anharmonic coupling.

### 5.3. Some Examples of NIR Spectroscopy and Quantum Chemical Calculation Studies on Wavenumbers and Absorption Intensities of Overtones and Intermolecular Interactions

**5.3.1. NIR/IR Spectroscopy and a DFT Calculation Study on the Frequencies and Intensities of the Fundamentals and Overtones of the NH Stretching Vibrations of Pyrrole and a Pyrrole–Pyridine Complex.** Futami et al.<sup>30</sup> investigated the frequencies and intensities of the fundamentals and first overtone of the NH stretching bands of pyrrole and a pyrrole–pyridine complex in CCl<sub>4</sub> by means of



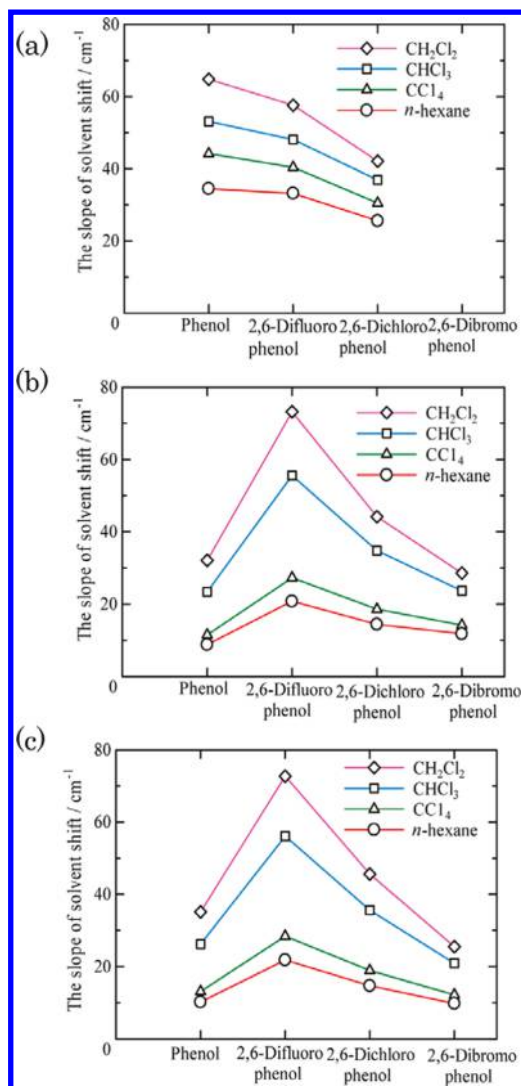


**Figure 26.** Slopes of solvent shifts of phenol, 2,6-difluorophenol, 2,6-dichlorophenol, and 2,6-dibromophenol in *n*-hexane,  $\text{CCl}_4$ ,  $\text{CHCl}_3$ , and  $\text{CH}_2\text{Cl}_2$ . (a) Observed and (b) calculated with base set 6-311++G(3df,3pd). (c) Calculated with base set cc-pVTZ. Reproduced with permission from ref 32. Copyright 2011 American Chemical Society.

NIR/IR spectroscopy and quantum chemical calculations. Special attention was paid to examining the effect of hydrogen bonding on the intensities of the NH fundamental and first overtone. The one-dimensional (1D) Schrödinger equations of the NH stretching vibrations were solved numerically to give both the vibrational energy levels and the wave functions.<sup>30</sup> Futami et al. measured NIR/IR spectra of pyrrole, pyridine, and a pyrrole–pyridine complex in  $\text{CCl}_4$  in the 8000–3000  $\text{cm}^{-1}$  region. A band due to the first overtone of the NH stretching vibration of the free pyrrole was seen at 6856  $\text{cm}^{-1}$ ; however, it was difficult to identify the corresponding band of the pyrrole–pyridine complex. They calculated the molecular vibration potentials and the dipole moment functions of the NH stretching modes of the free pyrrole and pyrrole–pyridine complex in the normal mode. They also estimated the transition probabilities between the vibrational energy levels of the fundamental and the first overtone by solving the 1D Schrödinger equations. These theoretical calculations revealed that the transition dipole moment containing the dipole moment function becomes much smaller upon the formation

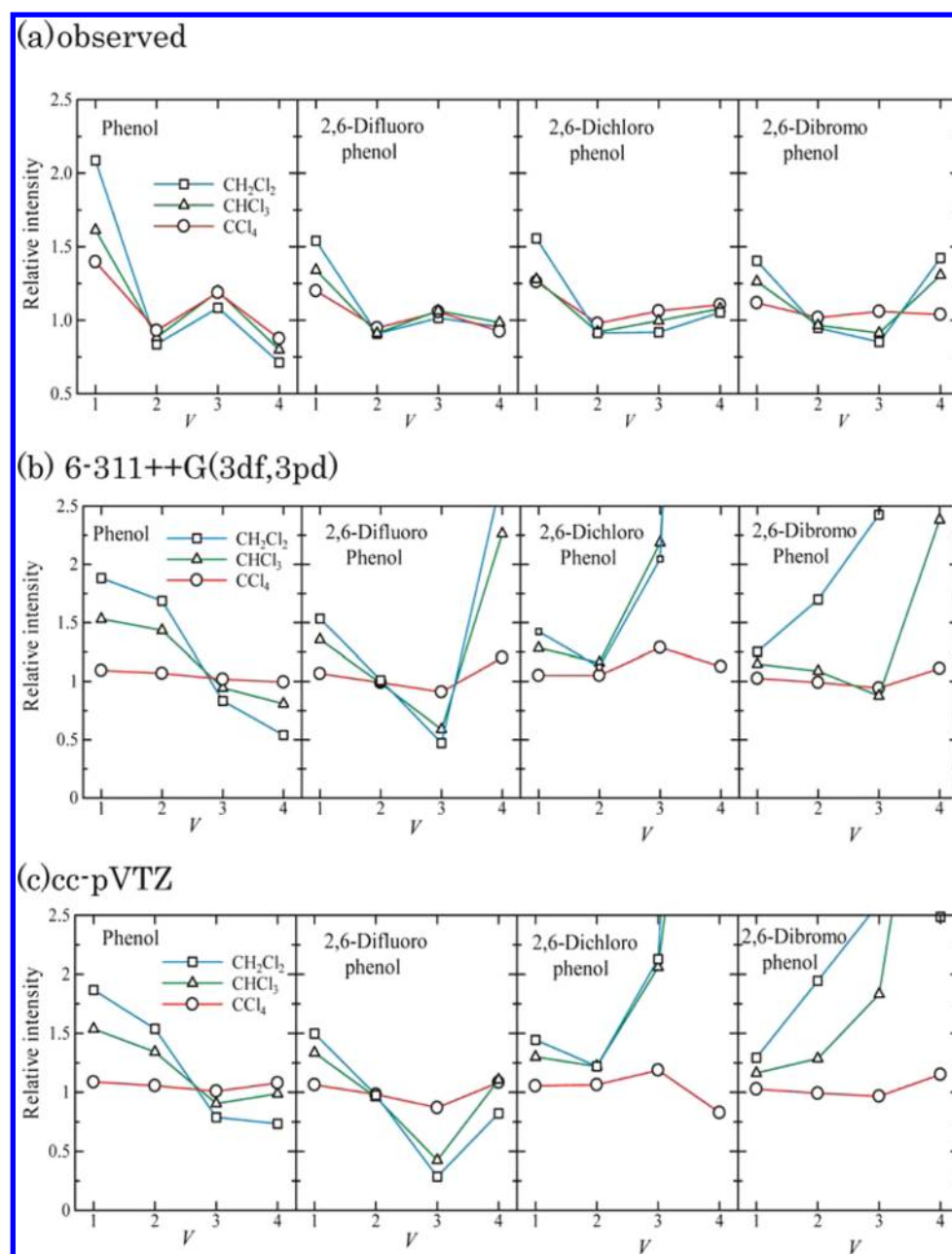
of the complex. This results in the remarkable decrease in intensity of the overtone of the hydrogen-bonded NH group.<sup>255</sup> Details of the DFT calculations were reported in ref 30 and the references cited therein.<sup>256–259</sup>

Figure 17 shows the NIR/IR spectra of the  $\text{CCl}_4$  solutions of (a) pyrrole, (b) pyridine, (c) a mixture of pyrrole and pyridine in  $\text{CCl}_4$  solution, together with the difference spectrum (d) calculated by subtracting spectra (a) and (b) from spectrum (c).<sup>30</sup> The MIR spectrum of the pyrrole solution shows a strong NH stretching band at 3497  $\text{cm}^{-1}$  whereas no band above 3050  $\text{cm}^{-1}$  is observed in the spectrum of the pyridine solution. Of note in Figure 17c is that a weak broad feature is observed near 3265  $\text{cm}^{-1}$ . This may be due to the NH stretching mode of the  $\text{NH}\cdots\text{N}$  hydrogen bond of the pyrrole–pyridine complex. The difference spectrum (Figure 17d) presents evidence that the NH stretching band at 3497  $\text{cm}^{-1}$  of the pyrrole monomer decreases while that at 3265  $\text{cm}^{-1}$ , arising from the complex, increases. As can be seen from Figure 18, the first overtone of the NH stretching mode of the pyrrole monomer is clearly visible at 6856  $\text{cm}^{-1}$ . It should be noted that in Figure 18d only the negative peak at 6856  $\text{cm}^{-1}$  appears.

Figure 19 shows the optimized structure for the pyrrole–pyridine complex calculated at DFT//B3LYP/6-311++G(3df,3pd) level. Futami et al.<sup>30</sup> calculated the vibrational wave functions, dipole moment functions, and potential energy curves of the NH stretching modes of pyrrole monomer and pyrrole–pyridine complex. The dipole moment functions along the axis are shown in Figure 20. Here the *z* axis is taken in the direction of the NH bond. A change in the dipole moment of the NH stretching mode occurs only in the *z* axis. It is of interest (Figure 20) that the potential energy curve and dipole moment function changes result from hydrogen bond formation. The potential energy curve is distorted, and this leads to lowering of the vibrational energy level. The dipole moment function is also distorted, and the direction of the dipole moment vector is reversed.

The harmonic oscillator calculation gives the NH stretching band of pyrrole and pyrrole–pyridine complex at 3678 and 3405  $\text{cm}^{-1}$ , respectively. The 1D Schrödinger equation yields the fundamental and first overtone of the NH stretching mode of the pyrrole monomer at 3539 and 6944  $\text{cm}^{-1}$ , respectively. These frequencies are very close to the observed values (3531 and 6925  $\text{cm}^{-1}$ ) of the pyrrole monomer in the gas phase.<sup>260</sup> The fundamental and first overtone of the NH stretching mode of the pyrrole monomer in  $\text{CCl}_4$  are observed at 3497 and 6856  $\text{cm}^{-1}$ , respectively (Figures 17 and 18). The frequencies of the fundamental and first overtone of the NH stretching mode of the pyrrole–pyridine complex were calculated to be 3206 and 6200  $\text{cm}^{-1}$ , respectively. The experimental frequency of its fundamental is 3266  $\text{cm}^{-1}$ , whereas its first overtone was not observed (Figure 18).

Table 2 summarizes the observed and calculated frequencies and relative intensities of the fundamentals and the first overtones of the NH stretching bands of the pyrrole–pyridine complex.<sup>30</sup> The intensity of the first overtone of the NH stretching band of the pyrrole monomer was calculated to be 0.057 of the intensity of its fundamental based on 1D Schrödinger equation. Since the observed band area of the first overtone of the NH stretching band was only 0.023 of its corresponding fundamental value, the calculation overestimated the intensity of the first overtone by more than twice. On the other hand, the calculated intensity of the first overtone of the NH stretching band of the pyrrole–pyridine complex was 0.003



**Figure 27.** Relative intensities of phenol, 2,6-difluorophenol, 2,6-dichlorophenol, and 2,6-dibromophenol in  $\text{CCl}_4$ ,  $\text{CHCl}_3$ , and  $\text{CH}_2\text{Cl}_2$ : (a) observed, (b) calculated with basis set 6-311++G(3df,3pd), and (c) calculated with basis set cc-pVTZ. The intensities are taken relative to phenol in *n*-hexane. Reproduced with permission from ref 32. Copyright 2011 American Chemical Society.

of the intensity of the pyrrole monomer fundamental (Table 2). This suggests that on hydrogen bond formation the intensity of the first overtone becomes extremely weak; hence, it is very difficult to observe. The reason why the calculation overestimates the intensity increase caused by the formation of the hydrogen bond probably arises from the fact that the solvent effect (here  $\text{CCl}_4$ ) was not taken into consideration.

The solvent dependencies of the frequencies and intensities were investigated for the fundamental and the first overtone of the NH stretching vibration of pyrrole. It was found that the frequencies of the NH fundamental and its first overtone decrease in the order of  $\text{CCl}_4$ ,  $\text{CHCl}_3$ , and  $\text{CH}_2\text{Cl}_2$ , which is the increasing order of  $\epsilon$ .<sup>31</sup> It was also found that their intensities increase in the same order and that this increase is more pronounced for the fundamental than the overtone. Of note is

the fact that the solvent dependencies of the frequencies and intensities of the NH stretching bands of pyrrole were different from their dependencies on the formation of hydrogen bonds.

The solvent dependencies of the fundamental and the first overtone of the NH stretching mode of pyrrole are depicted in Figure 21.<sup>31</sup> As can be seen, both the NH fundamental and the first overtone show a systematic red-shift on going from  $\text{CCl}_4$  to  $\text{CH}_2\text{Cl}_2$ . Simultaneously, the bands become broader and more intense with the increase in the polarity of the solvent. The relative band intensities of the NH fundamental are 1.00, 1.40, and 1.65 for the  $\text{CCl}_4$ ,  $\text{CHCl}_3$ , and  $\text{CH}_2\text{Cl}_2$  solutions, respectively. The corresponding intensities for the first overtone region are 1.00, 1.11, and 1.13. In the case of hydrogen bonds, the intensities of the OH and NH fundamentals increase while those of their first overtones

decrease.<sup>27,30</sup> On the other hand, in the case of solvent dependencies, the intensities of both the NH fundamentals and first overtones increase. For comparison, the dielectric constants of  $\text{CCl}_4$ ,  $\text{CHCl}_3$ , and  $\text{CH}_2\text{Cl}_2$  are 2.2, 4.8, and 8.9, respectively. Figure 21 reveals that both the NH fundamental and its first overtone show a red-shift, and their intensities increase with the increase in  $\epsilon$ . Therefore, Futami et al.<sup>31</sup> calculated the potential of the NH stretching mode and its dipole moment function of pyrrole in solvents with different  $\epsilon$  values by using the SCRF/IPCM method. The calculated wavenumbers and relative intensities versus  $\epsilon$  for the NH fundamental and its first overtone of pyrrole are shown in Figure 22. The NH fundamental and the first overtone shift from 3540 to 3520  $\text{cm}^{-1}$  and from 6944 to 6905  $\text{cm}^{-1}$ , respectively, with the increase in  $\epsilon$  from 1 to 80. The corresponding increase in the intensity was 2.4 and 1.3 for the NH fundamental and the overtone, respectively. The most significant variations take place in the range of  $1 \leq \epsilon \leq 20$  for both the fundamental and the first overtone. From the results that the intensities increase in solvents with a larger  $\epsilon$  for both the fundamental and first overtone and that the fundamental shows a more pronounced intensity change than the first overtone, it can be concluded that the increase in the anharmonicity does not cause the observed intensity changes of the fundamental and first overtone bands.

Figure 23a illustrates the vibrational potential energy curve and the first few vibrational wave functions as well as the dependencies of the dipole moment function on the standard coordinate of the NH stretching mode of pyrrole.<sup>31</sup> Figure 23b,c shows the difference in the vibrational potential energy and that of the dipole moment for the different dielectric constant for  $\epsilon = 1-10$ .<sup>31</sup> Figure 23c reveals that the slope of the dipole moment function becomes larger with  $\epsilon$  and that the minimum of the vibrational potential curve shifts to the positive direction on the normal coordinate, and the anharmonicity of the potential increases gradually. From Figure 23, it is seen that the calculated red-shift of wavenumbers with the increase in  $\epsilon$  originates from the anharmonicity of the vibrational potential and that the intensity increase is due to the gradual rise in the slope of the dipole moment function. It is also clear that the variation in the vibrational potential has an insignificant effect on the absorption intensity changes. The variation in the dipole moment function induced by  $\epsilon$  is large, and this change induces a more significant intensity increase in the fundamental. The variation in the dipole moment function due to the molecular vibration increases with the increase in the induced electric field.

**5.3.2. Quantum Chemical Calculation Study on the Dielectric Constant Dependence of Frequencies and Absorption Intensities of the Fundamental and the First, Second, and Third Overtones of the Stretching Vibration of Hydrogen Fluoride.** Futami et al.<sup>33</sup> investigated the vibrational potentials and dipole moment functions of the hydrogen fluoride in solutions as a function of  $\epsilon$  by using the SCRF/IPCM method. They also calculated the frequencies and absorption intensities of the fundamental and the first, second, and third overtones of the H–F stretching mode as a function of  $\epsilon$ . It was found from the SCRF/IPCM that the vibrational potential and dipole moment function of the HF molecule vary continuously with  $\epsilon$  of the solvent. The calculation also revealed that the intensity of the fundamental increases smoothly with the increase in  $\epsilon$ , but the intensities of the first, second, and third overtones vary irregularly. Figure 24

shows the effect of  $\epsilon$  on the stabilization energy ( $\Delta E$ ) of the HF molecule calculated at the B3LYP/6-311++G(3df,3pd) and CCSD/aug-cc-pVQZ levels.<sup>33</sup> The results shown in Figure 24 demonstrate that the hydrogen fluoride is stabilized with the increase in  $\epsilon$ .

Futami et al.<sup>33</sup> also studied the dependencies of the potential energy curve on the dielectric constant, dipole moment function ( $\epsilon = 1-80$ ), and wave function ( $\epsilon = 1$ ) of the HF stretching mode using the IPCM//DFT/B3LYP/6-311++G-(3df,3pd) and IPCM//CCSD/aug-cc-pVQZ levels. The slope of the dipole moment function also increases with  $\epsilon$ . The anharmonicity of the vibrational potential and that in the slope of the dipole moment function change substantially with the increase in  $\epsilon$  from 1 to 10. A similar trend was also observed for the variation in the stabilization energy. Based on the calculated vibrational potentials and dipole moment functions, the frequencies and absorption intensities of the fundamental and first, second, and third overtones of HF were determined.

**5.3.3. Vis/NIR/IR Spectroscopy Studies of Effects of Hydrogen Bonding on the Frequencies and Intensities of the Fundamental and the First, Second, and Third Overtones of the OH Stretching Mode of Phenol and 2,6-Dihalogenated Phenols.** Vis, NIR, and MIR spectra of phenol, 2,6-difluorophenol, 2,6-dichlorophenol, and 2,6-dibromophenol were measured in the 15600–2500  $\text{cm}^{-1}$  range in *n*-hexane,  $\text{CCl}_4$ ,  $\text{CHCl}_3$ , and  $\text{CH}_2\text{Cl}_2$  to investigate the effects of hydrogen bonding and solvent on the frequencies and intensities of the fundamental and the first, second, and third overtones of the OH stretching vibrations.<sup>32</sup> Phenol, 2,6-difluorophenol, 2,6-dichlorophenol, and 2,6-dibromophenol were subjected to the investigation because phenol forms an intermolecular hydrogen bond between its OH group and the Cl atom of the solvent, while 2,6-dihalogenated phenols possess a weak to strong intramolecular hydrogen bond and a weak to very weak intermolecular hydrogen bond with such solvents. Among the 2,6-dihalogenated phenols, 2,6-difluorophenol has much weaker intramolecular hydrogen bonding and significant intermolecular hydrogen bonding with the solvent. Thus, a comparison of these four phenols enables one to examine the effects of the inter- and intramolecular hydrogen bonds and solvent effects on the wavenumber shifts and changes in absorption intensities of the OH stretching bands.

Vis/NIR/IR spectra in the OH fundamental and the first, second, and third overtone regions of phenol and 2,6-dihalogenated phenols in *n*-hexane,  $\text{CCl}_4$ ,  $\text{CHCl}_3$ , and  $\text{CH}_2\text{Cl}_2$  are shown in Figure 25.<sup>32</sup> The wavenumbers and absorption intensities of the OH stretching vibrations are collected in Table 3.<sup>32</sup> The relative band intensities were estimated by using those of phenol in *n*-hexane as the standards because *n*-hexane is not involved in any hydrogen bonds. As can be seen from Figure 26 and Table 3, the wavenumbers of the OH fundamentals and their overtones decrease in the order of *n*-hexane,  $\text{CCl}_4$ ,  $\text{CHCl}_3$ , and  $\text{CH}_2\text{Cl}_2$ ; this is the increasing order of  $\epsilon$ .

It is well known that the fundamentals and overtones in the gas state are located at higher wavenumbers than those in the solutions because solute–solvent interactions are not expected in the gas phase. The extent of this shift is smaller for solutes with a stronger intramolecular hydrogen bonding. If one compares the four solvents, then the wavenumbers decrease with the increase in  $\epsilon$ . Buckingham et al.<sup>261</sup> defined the “solvent shift” as



$$\Delta\nu \approx \nu_g - \nu_s \quad (12)$$

where  $\nu_g$  and  $\nu_s$  are the wavenumbers of a molecule in the gas and solution states, respectively. The solvent shift has a linear relationship with the vibrational quantum number. Buckingham pointed out that the slope of this relationship indicates the strength of the molecular interaction, i.e., a hydrogen bonding and a solvent effect.<sup>261</sup>

Figure 26a displays the slopes of the observed solvent shifts for phenol, 2,6-difluorophenol, and 2,6-dichlorophenol in *n*-hexane, CCl<sub>4</sub>, CHCl<sub>3</sub>, and CH<sub>2</sub>Cl<sub>2</sub>.<sup>32</sup> It can be seen that the intermolecular interaction between the phenol OH group and a solvent molecule becomes stronger as  $\epsilon$  increases. It should be noted that the slopes of the solvent shifts for *n*-hexane are significantly smaller than those for CCl<sub>4</sub>, which has a weak interaction to a solute. The slopes for 2,6-difluorophenol and 2,6-dichlorophenol are smaller than those for phenol. Therefore, the effects of intermolecular interactions seem to be smaller for 2,6-difluorophenol and 2,6-dichlorophenol than for phenol. This probably results from the competing effect of intramolecular hydrogen bonding between the OH group and the halogen atom from the solvent. Figure 26b,c shows the slopes of the solvent shifts calculated by the 6-311++G(3df,3pd) and cc-pVTZ methods, respectively.<sup>32</sup> The slopes become larger with the increase in  $\epsilon$  as is also the case for the experimental results. In contrast to the experimental results, the calculated slopes become larger going from phenol to 2,6-dichlorophenol and 2,6-difluorophenol. Probably this results from the fact that phenol is involved in intermolecular hydrogen bonding more easily than the 2,6-dihalogenated phenols. However, it should be noted that the intermolecular hydrogen bonding was not considered in the calculations.

The observed relative intensities of the OH stretching bands of phenol, 2,6-difluorophenol, 2,6-dichlorophenol, and 2,6-dibromophenol in CCl<sub>4</sub>, CHCl<sub>3</sub>, and CH<sub>2</sub>Cl<sub>2</sub> versus the vibrational quantum number are displayed in Figure 27a.<sup>32</sup> Interestingly, the relative intensities of the OH stretching vibrations of phenol in CCl<sub>4</sub>, CHCl<sub>3</sub>, and CH<sub>2</sub>Cl<sub>2</sub> increase in the fundamental and the second overtone but decrease in the first and third overtones; i.e., they exhibit the so-called “parity” effect. This effect is more prominent for phenol than for the 2,6-dihalogenated derivatives which form intramolecular hydrogen bonds. Among the 2,6-dihalogenated phenols, 2,6-difluorophenol, with weaker intramolecular hydrogen bonding, shows a clearer parity. Phenol and 2,6-difluorophenol are easily affected by intermolecular hydrogen bonding.

Figure 27b,c displays the relative intensities of phenol and 2,6-dihalogenated phenols in CCl<sub>4</sub>, CHCl<sub>3</sub>, and CH<sub>2</sub>Cl<sub>2</sub> versus the vibrational quantum number calculated by 6-311++G(3df,3pd) and cc-pVTZ, respectively.<sup>32</sup> Both theoretical results deviate significantly from the experimental ones (Figure 27a). This can probably be attributed to the fact that both methods considered only solvent effects and did not take into account the intermolecular hydrogen bonds. The discrepancy between the experimental and theoretical results indirectly suggests that the intermolecular hydrogen bonding plays an important role in the parity.

## 6. CONCLUDING REMARKS

The purpose of this Review was to show both the usefulness and uniqueness of NIR spectroscopy in the study of molecular structure and interactions. At the same time this Review discusses the origin of NIR absorption bands, their intensities,

anharmonicity, and vibrational potentials. The uniqueness of NIR spectroscopy arises mainly from the anharmonicity of the molecular vibrations. Thus, a deeper understanding of anharmonicity and molecular vibrational potentials provides further insight into chemical bonding, molecular structure, and interactions. Current advancement in instrumentation, various methods of spectral analysis, and quantum chemical calculations has stimulated many successful applications of NIR spectroscopy discussed in this Review. For example, the examinations of the gas-phase overtone spectra coupled with the high-level theoretical calculations provided valuable information on the molecular structure and interactions. Recently the first studies of matrix-isolated complexes and ionic liquids by using NIR spectroscopy have been reported. All these works clearly show that the NIR region is not simply an extension of the MIR region—it provides specific information on molecular structure and hydrogen bonding not available from any other spectral range. Besides, the simultaneous analysis of the MIR and NIR spectra often yields information not accessible from the analysis performed on both data sets separately. In analyzing NIR spectra, one should take into account the specific properties that make this spectral region unique and different from the MIR region:

1. The absorption of the overtones and combination bands is much weaker compared with that of the fundamental bands. Hence, NIR spectroscopy is particularly useful for the examination of strongly absorbing samples such as bulk materials, pure liquids, and aqueous solutions.
2. The relative intensities of the free and various hydrogen-bonded species are different in the two spectral regions. As a result, the two spectral regions provide somewhat complementary information on hydrogen bonding.
3. The separation of specific NIR bands is better than that of the corresponding MIR bands, and this effect is more pronounced in the higher overtones region. This offers an opportunity to observe bands not resolved in the MIR spectra.
4. In the higher overtone NIR region the vibrations are well described by the LMM and are less coupled to other modes, thus providing bond-specific information which is to some extent different from that offered by normal-mode models.
5. Application of the  $\nu_2 + \nu_3$  combination band makes it possible to examine the state of water in OH-containing solvents like alcohols and diols.
6. Solvents with functional groups like COO, CON, C $\equiv$ N, C=O, or S=O contribute only weakly to NIR spectra. Hence, NIR spectroscopy is a convenient tool for the study of reactions and molecular interactions in organic solvents with these functionalities.
7. The solvent dependences of the wavenumbers and absorption intensities of the NH (OH) stretching bands of a molecule are quite different from the corresponding changes induced by the formation of the NH (OH)⋯N hydrogen bond.
8. As a result of hydrogen bonding, the overlap integral of the wave function is enhanced, but the transition dipole moment is much diminished. The transition dipole moment contains not only the overlap integral of the wave function but also dipole moment function. This causes a marked decrease in the intensity of the first overtone mode.

In spite of its numerous advantages, NIR spectroscopy is not free from limitations. One of the most important problems in the NIR region is significant width and overlap of numerous overtones and combination bands. As a result, the NIR spectra are relatively complex as compared with the MIR or Raman spectra. To overcome this limitation, one can measure the matrix-isolated or the gas-phase overtone spectra. Both techniques are very useful in studies of the molecular structure and intra- and intermolecular interactions since they provide simpler spectra that one can interpret directly. In the case of liquid samples, the resolution enhancement can be achieved by using the computational methods. Another serious problem in NIR region is the band assignment, additionally complicated by the anharmonicity and Fermi resonances of numerous overtones and combination bands. In this case, the theoretical calculations of the anharmonic spectra appear very helpful. High-level calculations provide very reliable wavenumbers of the overtones and combination bands, making the assignment more straightforward. Sometimes the selective correlation between the NIR and MIR or Raman peaks in the 2D correlation spectra may confirm the assumed assignment. The elimination or significant restriction of the possible resonances one can achieve by measurement of the NIR spectra in the higher overtones region, where the vibrations are well described by the LMM and are less coupled to other modes and to each other. Good-quality spectra in this region can be recorded by using laser photoacoustic spectroscopy.<sup>181</sup> Recently, it has been suggested that the combination of EA spectroscopy and quantum chemical calculations would assist in overcoming problems in NIR spectroscopy such as band complexity and band weakness by looking into the direction of the transition moment.<sup>254</sup>

Finally, we would like to shortly outline prospectives for application of NIR spectroscopy in molecular structure and interaction studies. One needs further a understanding of the origin and properties of the NIR spectra. In particular, our knowledge of the intensities of NIR bands is very limited; we still do not have a correct answer why a band due to the first overtone of the stretching mode of the free OH group of an alcohol is much stronger than that due to the hydrogen-bonded OH group. The knowledge on widths of overtones and combination bands is even poorer. As of yet, very few studies have been carried out on this area. Some pioneering examinations on intensities and widths of NIR bands have been started by a few research groups.<sup>30–33</sup> We have to deepen the understanding of the spectral parameters of overtones and combination bands by using both experimental and theoretical methods. Investigations of anharmonicity and vibrational potential are of special importance, since the anharmonic couplings between different vibrational modes play important roles in intra- and intermolecular interactions and molecular dynamics in the condensed phase. These kinds of studies have recently become active as a result of marked progress in quantum chemical calculations.<sup>30–33</sup> One should note that NIR spectroscopy can solve problems which IR and Raman spectroscopy cannot solve. IR and Raman spectroscopy often cannot directly discriminate the solvent effect from the hydrogen bonding. However, according to our quantum chemical calculations, one can discriminate these two effects by comparing the intensities and band widths of the fundamentals and first overtones.<sup>32</sup> More detailed comparisons between the quantum chemical calculations and experimental measurements are required to understand the accuracy and

limitations. Nonetheless, this combination of methods holds promise in studying molecular structure and intermolecular interaction. Chemometrics and 2D correlation spectra are very powerful tools for separation of different hydrogen-bonded species. However, the normal absorption spectroscopy is not able to separate the contributions from the mechanical and electrical anharmonicity. Thus, in the near future, modulation methods such as coherent two-dimensional spectroscopy and EA spectroscopy that are based on nonlinear phenomena should become vital to solve the mechanical and electrical anharmonicities.

## AUTHOR INFORMATION

### Corresponding Authors

\*E-mail: [mirosław.czarnecki@chem.uni.wroc.pl](mailto:mirosław.czarnecki@chem.uni.wroc.pl).

\*E-mail: [ozaki@kwansei.ac.jp](mailto:ozaki@kwansei.ac.jp).

### Notes

The authors declare no competing financial interest.

### Biographies



Mirosław Czarnecki obtained his M. Sc. (1981) and Ph.D. (1989) degrees in Physical and Theoretical Chemistry from the University of Wrocław. He was a postdoctoral fellow at Kwansei Gakuin University, Japan (1992–1993) and University of Essen, Germany (1995). At present, he is a professor in the Faculty of Chemistry, University of Wrocław, Poland. His current research involves hydrogen bonding, molecular structure, microheterogeneity in binary liquids, effects of inorganic salts on structure of organic phase, liquid crystals, MIR, NIR and Raman spectroscopy, computer-aided spectroscopy, 2D correlation analysis, chemometrics, and theoretical calculations. He is a great fan of running.



Yusuke Morisawa obtained his Ph.D. (2005) in chemistry from Kyoto University. He is currently an Assistant Professor in the Department of

Chemistry, School of Science and Engineering, Kinki University, Higashi-Osaka, Japan. His current research interest is the molecular spectroscopy and analytical applications in the region from THz to FUV. His contributions to NIR spectroscopy involve experimental and quantum chemical calculation studies of overtones including higher overtones. Dr. Morisawa received awards including the 2013 Young Scientist Award of The Spectroscopical Society of Japan. (E-mail: [morisawa@chem.kindai.ac.jp](mailto:morisawa@chem.kindai.ac.jp))



Yoshisuke Futami obtained his Ph.D. (2005) in chemistry from Tokyo University of Agriculture and Technology. At present, he is an associate professor at Department of Biological and Chemical Systems Engineering, National Institute of Technology, Kumamoto College, Japan. His current research focuses on relations between absorption intensities (and frequency) of fundamental and overtones of a molecular vibration and intermolecular interaction (e.g., hydrogen bonding, solvent effect) using IR/NIR spectroscopy and quantum chemistry calculations. (E-mail: [futami@kumamoto-nct.ac.jp](mailto:futami@kumamoto-nct.ac.jp))



Yukihiro Ozaki obtained his Ph.D. (1978) in chemistry from Osaka University. He is currently a professor in the Department of Chemistry, Kwansei Gakuin University, Sanda, Japan. He has been active in the research of a variety of molecular spectroscopy, covering IR, Raman, NIR and far-ultraviolet (FUV) spectroscopy. Of particular note is the fact that he developed research in rather undeveloped areas of molecular spectroscopy such as NIR and FUV spectroscopy. His contributions to NIR spectroscopy involve almost the whole range; (1) developments of NIR spectrometers (e.g., a portable NIR imaging system), experimental techniques, and spectral analysis methods, (2) experimental and quantum chemical calculation studies of overtones including higher overtones and (3) a variety of applications from basic molecular science to practical applications. Prof. Ozaki has received many awards including the 1998 Tomas Hirschfeld Award, the 2001 EAS Award for Achievements in Near Infrared Spectroscopy, the Spectroscopical Society of Japan Award (2002), the 2005 Science and

Technology Award of Japanese Government (Ministry of Education, Culture, Sports, Science and Technology), and Gerald Birth Award of International Conference Diffuse Reflectance Spectroscopy, and Bomem-Michelson Award.

## REFERENCES

- (1) Siesler, H. W.; Ozaki, Y.; Kawata, S.; Heise, H. M., Eds. *Near-Infrared Spectroscopy*; Wiley-VCH: Weinheim, 2002.
- (2) Ozaki, Y.; McClure, W. F.; Christy, A. A., Eds. *Near Infrared Spectroscopy in Food Science and Technology*; Wiley Interscience: New York, 2006.
- (3) Workman, J.; Weyer, L. *Practical Guide to Interpretive Near Infrared Spectroscopy*; CRC Press: Boca Raton, FL, 2007.
- (4) Workman, J.; Weyer, L. *Practical Guide and Spectral Atlas for Interpretive Near-Infrared Spectroscopy*, 2nd ed.; CRC Press: Boca Raton, FL, 2012.
- (5) Ciurczak, E. W.; Drennen, J. K., III *Pharmaceutical and Medical Applications of Near-Infrared Spectroscopy*; CRC Press: Boca Raton, 2002.
- (6) Roberts, C. A. *Near-infrared Spectroscopy in Agriculture*; American Society of Agronomy: Madison, WI, 2004.
- (7) Williams, P. C. *Near-infrared Spectroscopy*; NIR Publications: Chichester, UK, 1996.
- (8) Ozaki, Y. Near-Infrared Spectroscopy — Its Versatility in Analytical Chemistry. *Anal. Sci.* **2012**, 28, 545–563.
- (9) Burns, D. A.; Ciurczak, E. W., Eds. *Handbook of Near-Infrared Spectroscopy*, 3rd ed.; CRC Press: Boca Raton, FL, 2008.
- (10) Osborne, B. G.; Fearn, T. *Near Infrared Spectroscopy in Food Analysis*; Longman Higher Education: Harlow, UK, 1986.
- (11) Figgis, B. N. *Introduction to Ligand Fields*; Krieger Publ. Co.: Melbourne, FL, 1966.
- (12) Villringer, A.; Dirangl, U., Eds. *Optical Imaging of Brain Function and Metabolism 2*; Springer: Berlin, 1997.
- (13) Ciurczak, E. W. In *Handbook of Near-Infrared Analysis*, 3rd ed.; Burns, D. A., Ciurczak, E. W., Eds.; CRC Press: Boca Raton, 2008; p647.
- (14) Morisawa, Y.; Nomura, S.; Sanada, K.; Ozaki, Y. Monitoring of a Calcination Reaction of High Reflective Green-Black (HRGB) Pigments by Using Near-Infrared Electronic Spectroscopy: Calcination Temperature-Dependent Crystal Structural Changes of Their Components and Calibration of the Extent of the Reaction. *Appl. Spectrosc.* **2012**, 66, 665–672.
- (15) Candeia, R. A.; Souza, M. A. F.; Bernardi, M. I. B.; Maestelli, S. C.; Souza, I. M. G. A. G.; Longo, E. MgFe<sub>2</sub>O<sub>4</sub> pigment obtained at low temperature. *Mater. Res. Bull.* **2006**, 41, 183–190.
- (16) Martens, H.; Næs, T. *Multivariate Calibration*; John Wiley & Sons: Chichester, 1989.
- (17) Vandegiste, B. G. M.; Massart, D. L.; Buydens, L. M. C.; De Jong, S.; Lewi, P. L.; Smeyers-Verbeke, J. *Handbook of Chemometrics and Qualimetrics: Part B*; Elsevier: Amsterdam, 1998.
- (18) Mark, H.; Workman, J., Jr. *Chemometrics in Spectroscopy*; Elsevier: Amsterdam, 2007.
- (19) Kramer, R. *Chemometrics Techniques for Quantitative Analysis*; CRC Press: Boca Raton, FL, 1998.
- (20) Varmuza, K.; Filzmoser, P. *Introduction to Multivariate Statistical Analysis in Chemometrics*; CRC Press: Boca Raton, FL, 2009.
- (21) Ozaki, Y.; Noda, I., Eds. *Two Dimensional Correlation Spectroscopy*; AIP Conference Proceedings; American Institute of Physics: Melville, NY, 2000; p 503.
- (22) Noda, I.; Ozaki, Y. *Two Dimensional Correlation Spectroscopy—Applications in Vibrational and Optical Spectroscopy*; John Wiley & Sons, Ltd.: Chichester, UK, 2004.
- (23) Noda, I.; Liu, Y.; Ozaki, Y.; Czarniecki, M. A. Two-Dimensional Fourier Transform Near-Infrared Correlation Spectroscopy Studies of Temperature-Dependent Spectral Variations of Oleyl alcohol. *J. Phys. Chem.* **1995**, 99, 3068–3073.



- (24) Ozaki, Y.; Liu, Y.; Noda, I. Two-dimensional near-infrared correlation spectroscopy study of premelting behavior of Nylon 12. *Macromolecules* **1997**, *30*, 2391–2399.
- (25) Czarnik-Matusewicz, B.; Murayama, K.; Tsenkova, R.; Ozaki, Y. Analysis of Near-Infrared Spectra of Complicated Biological Fluids by Two-Dimensional Correlation Spectroscopy: Protein and Fat Concentration-Dependent Spectral Changes of Milk. *Appl. Spectrosc.* **1999**, *53*, 1582–1594.
- (26) Low, G. R.; Kjaergaard, H. G. Calculation of OH-stretching band intensities of the water dimer and trimer. *J. Chem. Phys.* **1999**, *110*, 9104–9115.
- (27) Howard, D. L.; Kjaergaard, H. G. Vapor Phase Near Infrared Spectroscopy of the Hydrogen Bonded Methanol–Trimethylamine Complex. *J. Phys. Chem. A* **2006**, *110*, 9597–9601.
- (28) Lane, J. R.; Kjaergaard, H. G. XH-stretching overtone transitions calculated using explicitly correlated coupled cluster methods. *J. Chem. Phys.* **2010**, *132*, 174304–11.
- (29) Takahashi, K.; Sugawara, M.; Yabushita, S. Theoretical Analysis of the CH Stretching Overtone Vibration of 1,2-Dichloroethylene. *J. Phys. Chem. A* **2002**, *106*, 2676–2684.
- (30) Futami, Y.; Ozaki, Y.; Hamada, Y.; Wojcik, M. J.; Ozaki, Y. Frequencies and absorption intensities of fundamentals and overtones of NH stretching vibrations of pyrrole and pyrrole–pyridine complex studied by near-infrared/infrared spectroscopy and density-functional-theory calculations. *Chem. Phys. Lett.* **2009**, *482*, 320–324.
- (31) Futami, Y.; Ozaki, Y.; Hamada, Y.; Wojcik, M. J.; Ozaki, Y. Solvent Dependence of Absorption Intensities and Wavenumbers of the Fundamental and First Overtone of NH Stretching Vibration of Pyrrole Studied by Near-Infrared/Infrared Spectroscopy and DFT Calculations. *J. Phys. Chem. A* **2011**, *115*, 1194–1198.
- (32) Gonjo, T.; Futami, Y.; Morisawa, Y.; Wojcik, M. J.; Ozaki, Y. Hydrogen Bonding Effects on the Wavenumbers and Absorption Intensities of the OH Fundamental and the First, Second, and Third Overtones of Phenol and 2,6-Dihalogenated Phenols Studied by Visible/Near-Infrared/Infrared Spectroscopy. *J. Phys. Chem. A* **2011**, *115*, 9845–9853.
- (33) Futami, Y.; Morisawa, Y.; Ozaki, Y.; Hamada, Y.; Wojcik, M. J.; Ozaki, Y. The Dielectric Constant Dependence of Absorption Intensities and Wavenumbers of the Fundamental and Overtone Transitions of Stretching Vibration of the Hydrogen Fluoride Studied by Quantum Chemistry Calculations. *J. Mol. Struct.* **2012**, *1018*, 102–106.
- (34) Abney, C.; Festing, L. C. Atmospheric Absorption in the Infra-Red of the Solar Spectrum. *Proc. R. Soc. London* **1883**, *35*, 80–83.
- (35) Kaye, W. Near-infrared spectroscopy: II. Instrumentation and technique. *Spectrochim. Acta* **1955**, *7*, 181–204.
- (36) Wheeler, O. H. Near Infrared Spectra Of Organic Compounds. *Chem. Rev.* **1959**, *59*, 629–666.
- (37) Hart, J. R.; Norris, K. H.; Golumbic, C. Determination of the Moisture Content of Seeds by Near-Infrared Spectrophotometry of Their Methanol Extracts. *Cereal Chem.* **1962**, *39*, 94–99.
- (38) Massie, D. R.; Norris, K. H. Spectral reflectance and transmittance properties of grain in visible and near infrared. *Trans. ASAE* **1965**, *8*, 598–600.
- (39) Jöbsis, F. F. Noninvasive, infrared monitoring of cerebral and myocardial oxygen sufficiency and circulatory parameters. *Science* **1977**, *198*, 1264–1267.
- (40) Thorpe, M. J.; Moll, K. D.; Jones, R. J.; Safadi, B.; Ye, J. Broadband cavity ringdown spectroscopy for sensitive and rapid molecular detection. *Science* **2006**, *311*, 1595–1599.
- (41) O’Keefe, A.; Deacon, D. A. G. Cavity ring-down optical spectrometer for absorption measurements using pulsed laser sources. *Rev. Sci. Instrum.* **1988**, *59*, 2544–2554.
- (42) Chen, Y.; Morisawa, Y.; Futami, Y.; Czarnecki, M. A.; Wang, H. S.; Ozaki, Y. Combined IR/NIR and Density Functional Theory Calculations Analysis of the Solvent Effects on Frequencies and Intensities of the Fundamental and Overtones of the C = O Stretching Vibrations of Acetone and 2-Hexanone. *J. Phys. Chem. A* **2014**, *118*, 2576–2583.
- (43) Czarnecki, M. A. Two-Dimensional Correlation Analysis of Hydrogen-Bonded Systems: Basic Molecules. *Appl. Spectrosc. Rev.* **2011**, *46*, 67–103.
- (44) Siesler, H. W. In *Near-Infrared Spectroscopy—Principle, Instruments, Applications*; Siesler, H. W., Ozaki, Y., Kawata, S., Heise, H. M., Eds.; Wiley-VCH: Weinheim, 2002; p 247.
- (45) Hu, Y.; Zhang, J.; Sato, H.; Futami, Y.; Noda, I.; Ozaki, Y. C-H...O=C Hydrogen Bonding and Isothermal Crystallization Kinetics of Poly(3-hydroxybutyrate) Investigated by Near-Infrared Spectroscopy. *Macromolecules* **2006**, *39*, 3841–3847.
- (46) Czarnecki, M. A.; Czarnik-Matusewicz, B.; Ozaki, Y.; Iwahashi, M. Resolution Enhancement and Band Assignments for the First Overtone of OH(D) Stretching Modes of Butanols by Two-Dimensional Correlation Spectroscopy. 3. Thermal Dynamics of Hydrogen Bonding in Butan-1-(ol-d) and 2-Methylpropan-2-(ol-d) in the Pure Liquid State. *J. Phys. Chem. A* **2000**, *104*, 4906–4911.
- (47) Czarnik-Matusewicz, B.; Kim, S. B.; Jung, Y. M. A. Study of Urea-dependent Denaturation of  $\beta$ -Lactoglobulin by Principal Component Analysis and Two-dimensional Correlation Spectroscopy. *J. Phys. Chem. B* **2009**, *113*, 559–566.
- (48) Czarnecki, M. A. Two-Dimensional Correlation Spectroscopy: Effect of Normalization of the Dynamic Spectra. *Appl. Spectrosc.* **1999**, *53*, 1392–1397.
- (49) Šašić, S.; Muszynski, A.; Ozaki, Y. A New Possibility of the Generalized Two-Dimensional Correlation Spectroscopy. 1. Sample-Sample Correlation Spectroscopy. *J. Phys. Chem. A* **2000**, *104*, 6380–6387.
- (50) Šašić, S.; Muszynski, A.; Ozaki, Y. A New Possibility of the Generalized Two-Dimensional Correlation Spectroscopy. 2. Sample-Sample and Wavenumber-Wavenumber Correlations of Temperature-Dependent Near-Infrared Spectra of Oleic Acid in the Pure Liquid State. *J. Phys. Chem. A* **2000**, *104*, 6388–6394.
- (51) Šašić, S.; Ozaki, Y. Statistical Two-Dimensional Correlation Spectroscopy: Its Theory and Applications to Sets of Vibrational Spectra. *Anal. Chem.* **2001**, *73*, 2294–2301.
- (52) Czarnecki, M. A. Interpretation of Two-Dimensional Correlation Spectra: Science or Art? *Appl. Spectrosc.* **1998**, *52*, 1583–1590.
- (53) Czarnecki, M. A. Two-Dimensional Correlation Spectroscopy: Effect of Band Position, Width, and Intensity Changes on Correlation Intensities. *Appl. Spectrosc.* **2000**, *54*, 986–993.
- (54) Segtnan, V. H.; Šašić, S.; Isaksson, T.; Ozaki, Y. Studies on the Structure of Water Using Two-Dimensional Near-Infrared Correlation Spectroscopy and Principal Component Analysis. *Anal. Chem.* **2001**, *73*, 3153–3161.
- (55) Šašić, S.; Segtnan, V. H.; Ozaki, Y. Self-Modeling Curve Resolution Study of Temperature-Dependent Near-Infrared Spectra of Water and the Investigation of Water Structure. *J. Phys. Chem. A* **2002**, *106*, 760–766.
- (56) Czarnik-Matusewicz, B.; Pilorz, S.; Hawranek, J. P. Temperature-dependent water structural transitions examined by near-IR and mid-IR spectra analyzed by multivariate curve resolution and two-dimensional correlation spectroscopy. *Anal. Chim. Acta* **2005**, *544*, 15–25.
- (57) Czarnik-Matusewicz, B.; Pilorz, S. Study of the temperature-dependent near-infrared spectra of water by two-dimensional correlation spectroscopy and principal components analysis. *Vib. Spectrosc.* **2006**, *40*, 235–245.
- (58) Czarnecki, M. A.; Wojtków, D. Two-Dimensional FT-NIR Correlation Study of Hydrogen Bonding in the Butan-1-ol/Water System. *J. Phys. Chem. A* **2004**, *108*, 2411–2417.
- (59) Wojtków, D.; Czarnecki, M. A. Effect of Temperature and Concentration on the Structure of tert-Butyl Alcohol/Water Mixtures: Near-Infrared Spectroscopic Study. *J. Phys. Chem. A* **2005**, *109*, 8218–8224.
- (60) Wojtków, D.; Czarnecki, M. A. Effect of Temperature and Concentration on the Structure of sec-Butyl Alcohol/Water Mixtures: Near-Infrared Spectroscopic Study. *J. Phys. Chem. A* **2006**, *110*, 10552–10557.

- (61) Wojtków, D.; Czarnecki, M. A. Two-Dimensional Attenuated Total Reflection Infrared and Near-Infrared Correlation Study of the Structure of Butyl Alcohol/Water Mixtures. *Appl. Spectrosc.* **2007**, *61*, 928–934.
- (62) Czarnecki, M. A.; Wojtków, D. Effect of varying water content on the structure of butyl alcohol/water mixtures: FT-NIR two-dimensional correlation and chemometric studies. *J. Mol. Struct.* **2008**, *883–884*, 203–208.
- (63) Czarnecki, M. A.; Muszyński, A. S.; Troczińska, H. Molecular structure and hydrogen bonding in liquid cyclohexanol and cyclohexanol/water mixtures studied by FT-NIR spectroscopy and DFT calculations. *J. Mol. Struct.* **2010**, *974*, 60–67.
- (64) Haufa, K. Z.; Czarnecki, M. A. Effect of temperature and water content on the structure of 1,2-propanediol and 1,3-propanediol: Near-infrared spectroscopic study. *Vib. Spectrosc.* **2009**, *51*, 80–85.
- (65) Chen, Y.; Ozaki, Y.; Czarnecki, M. A. Molecular structure and hydrogen bonding in pure liquid ethylene glycol and ethylene glycol-water mixtures studied using NIR spectroscopy. *Phys. Chem. Chem. Phys.* **2013**, *15*, 18694–18701.
- (66) Haufa, K. Z.; Czarnecki, M. A. Molecular Structure and Hydrogen Bonding of 2-Aminoethanol, 1-Amino-2-Propanol, 3-Amino-1-Propanol, and Binary Mixtures with Water Studied by Fourier Transform Near-Infrared Spectroscopy and Density Functional Theory Calculations. *Appl. Spectrosc.* **2010**, *64*, 351–358.
- (67) Czarnecki, M. A. Molecular structure and hydrogen bonding in 1,2-diaminopropane and 1,3-diaminopropane and their binary mixtures with water studied by NIR spectroscopy and DFT calculations. *Vib. Spectrosc.* **2012**, *62*, 207–216.
- (68) Adachi, D.; Katsumoto, Y.; Sato, H.; Ozaki, Y. Near-Infrared Spectroscopic Study of Interaction Between Methyl Group and Water in Water-Methanol Mixtures. *Appl. Spectrosc.* **2002**, *56*, 357–361.
- (69) Iwamoto, R. Infrared and Near-Infrared Study of the Interaction of Amide C=O with Water in Ideally Inert Medium. *J. Phys. Chem. A* **2010**, *114*, 7398–7407.
- (70) Iwamoto, R.; Matsuda, T.; Sasaki, T.; Kusanagi, H. Basic Interactions of Water with Organic Compounds. *J. Phys. Chem. B* **2003**, *107*, 7976–7980.
- (71) Iwamoto, R.; Kusanagi, H. Determination of the Hydrate Structure of an Isolated Alcoholic OH in Hydrophobic Medium by Infrared and Near-Infrared Spectroscopy. *J. Phys. Chem. A* **2009**, *113*, 5310–5316.
- (72) Iwahashi, M.; Suzuki, M.; Katayama, N.; Matsuzawa, H.; Czarnecki, M. A.; Ozaki, Y.; Wakisaka, A. Molecular Self-Assembling of Butan-1-ol, Butan-2-ol, and 2-Methylpropan-2-ol in Carbon Tetrachloride Solutions as Observed by Near-Infrared Spectroscopic Measurements. *Appl. Spectrosc.* **2000**, *54*, 268–276.
- (73) Czarnecki, M. A.; Maeda, H.; Ozaki, Y.; Suzuki, M.; Iwahashi, M. Resolution Enhancement and Band Assignments for the First Overtone of OH Stretching Mode of Butanols by Two-Dimensional Near-Infrared Correlation Spectroscopy. Part I: sec-Butanol. *Appl. Spectrosc.* **1998**, *52*, 994–1000.
- (74) Czarnecki, M. A.; Maeda, H.; Ozaki, Y.; Suzuki, M.; Iwahashi, M. Resolution Enhancement and Band Assignments for the First Overtone of OH Stretching Modes of Butanols by Two Dimensional Near-Infrared Correlation Spectroscopy. 2. Thermal Dynamics of Hydrogen Bonding in n- and tert-Butyl Alcohol in the Pure Liquid States. *J. Phys. Chem. A* **1998**, *102*, 9117–9123.
- (75) Czarnecki, M. A.; Ozaki, Y. The temperature-induced changes in hydrogen bonding of decan-1-ol in the pure liquid phase studied by two-dimensional Fourier transform near-infrared correlation spectroscopy. *Phys. Chem. Chem. Phys.* **1999**, *1*, 797–800.
- (76) Czarnecki, M. A. Effect of Temperature and Concentration on Self-Association of Octan-1-ol Studied by Two-Dimensional Fourier Transform Near-Infrared Correlation Spectroscopy. *J. Phys. Chem. A* **2000**, *104*, 6356–6361.
- (77) Czarnecki, M. A.; Orzechowski, K. Effect of Temperature and Concentration on Self-Association of Octan-3-ol Studied by Vibrational Spectroscopy and Dielectric Measurements. *J. Phys. Chem. A* **2003**, *107*, 1119–1126.
- (78) Czarnecki, M. A. Near-Infrared Spectroscopic Study of Hydrogen Bonding in Chiral and Racemic Octan-2-ol. *J. Phys. Chem. A* **2003**, *107*, 1941–1944.
- (79) Czarnecki, M. A. Study on self-association of octanols by two-dimensional FT-NIR correlation spectroscopy. *Vib. Spectrosc.* **2004**, *36*, 237–239.
- (80) Iwahashi, M.; Ikumi, M.; Matsuzawa, H.; Moroi, Y.; Czarnecki, M. A.; Ozaki, Y. Molecular self-assembling of chiral and racemic butan-2-ol in carbon tetrachloride solutions. *Vib. Spectrosc.* **1999**, *20*, 113–119.
- (81) Iwamoto, R.; Matsuda, T.; Kusanagi, H. Contrast effect of hydrogen bonding on the acceptor and donor OH groups of intramolecularly hydrogen-bonded OH pairs in diols. *Spectrochim. Acta, Part A* **2005**, *62*, 97–104.
- (82) Czarnecki, M. A.; Liu, Y.; Ozaki, Y.; Suzuki, M.; Iwahashi, M. Potential of Fourier Transform Near-Infrared Spectroscopy in Studies of the Dissociation of Fatty Acids in the Liquid Phase. *Appl. Spectrosc.* **1993**, *47*, 2162–2168.
- (83) Iwahashi, M.; Hachiya, N.; Hayashi, Y.; Matsuzawa, H.; Suzuki, M.; Fujimoto, Y.; Ozaki, Y. Dissociation of dimeric cis-9-octadecenoic acid in its pure liquid state as observed by near-infrared spectroscopic measurement. *J. Phys. Chem.* **1993**, *97*, 3129–3133.
- (84) Iwahashi, M.; Suzuki, M.; Czarnecki, M. A.; Liu, Y.; Ozaki, Y. Near-IR Molar Absorption Coefficient for the OH-Stretching Mode of cis-9-Octadecenoic Acid and Dissociation of the Acid Dimers in the Pure Liquid State. *J. Chem. Soc., Faraday Trans.* **1995**, *91*, 697–701.
- (85) Koashi, K.; Iwahashi, M.; Ozaki, Y. Band Analysis of Temperature-Dependent Near-Infrared Spectra of Oleic Acid in the Pure Liquid State by the Analytic Geometric Approach. *Appl. Spectrosc.* **2003**, *57*, 1539–1550.
- (86) Šasić, Š.; Katsumoto, Y.; Sato, H.; Ozaki, Y. Applications of Moving Window Two-Dimensional Correlation Spectroscopy to Analysis of Phase Transition and Spectra Classification. *Anal. Chem.* **2003**, *75*, 4010–4018.
- (87) Czarnecki, M. A. Near-infrared spectroscopic study of self-association of octanoic acid. *Chem. Phys. Lett.* **2003**, *368*, 115–120.
- (88) Liu, Y.; Ozaki, Y.; Noda, I. Two-Dimensional Fourier-Transform Near-Infrared Correlation Spectroscopy Study of Dissociation of Hydrogen-Bonded N-Methylacetamide in the Pure Liquid State. *J. Phys. Chem.* **1996**, *100*, 7326–7332.
- (89) Ozaki, Y.; Liu, Y.; Noda, I. Two-Dimensional Infrared and Near-Infrared Correlation Spectroscopy: Applications to Studies of Temperature-Dependent Spectral Variations of Self-Associated Molecules. *Appl. Spectrosc.* **1997**, *51*, 526–535.
- (90) Czarnecki, M. A.; Haufa, K. Z. Effect of Temperature and Concentration on the Structure of N-Methylacetamide-Water Complexes: Near-Infrared Spectroscopic Study. *J. Phys. Chem. A* **2005**, *109*, 1015–1021.
- (91) Ikehata, A.; Hashimoto, C.; Mikami, Y.; Ozaki, Y. Thermal phase behavior of triethylamine-water mixtures studied by near-infrared spectroscopy: band shift of the first overtone of the C-H stretching modes and the phase diagram. *Chem. Phys. Lett.* **2004**, *393*, 403–408.
- (92) Wang, Y.; Murayama, K.; Myojo, Y.; Tsenkova, R.; Hayashi, N.; Ozaki, Y. Two-Dimensional Fourier Transform Near-Infrared Spectroscopy Study of Heat Denaturation of Ovalbumin in Aqueous Solutions. *J. Phys. Chem. B* **1998**, *102*, 6655–6662.
- (93) Ozaki, Y.; Murayama, K.; Wang, Y. Application of two-dimensional near-infrared correlation spectroscopy to protein research. *Vib. Spectrosc.* **1999**, *20*, 127–132.
- (94) Murayama, K.; Czarnik-Matusewicz, B.; Wu, Y.; Tsenkova, R.; Ozaki, Y. Comparison between Conventional Spectral Analysis Methods, Chemometrics, and Two-Dimensional Correlation Spectroscopy in the Analysis of Near-Infrared Spectra of Protein. *Appl. Spectrosc.* **2000**, *54*, 978–985.

- (95) Iwamoto, R.; Matsuda, T. Characterization of Infrared and Near-Infrared Absorptions of Free Alcoholic OH Groups in Hydrocarbon. *Appl. Spectrosc.* **2004**, *58*, 1001–1009.
- (96) Iwamoto, R.; Nara, A.; Matsuda, T. Near-Infrared Combination and Overtone Bands of CH in  $\text{CHX}_3$ ,  $\text{CHX}_2\text{CHX}_2$ , and  $\text{CHX}_2\text{CX}_2\text{CHX}_2$ . *Appl. Spectrosc.* **2005**, *59*, 1393–1398.
- (97) Iwamoto, R.; Nara, A.; Matsuda, T. Near-Infrared Combination and Overtone Bands of the  $\text{CH}_2$  Sequence in  $\text{CH}_2\text{X}_2$ ,  $\text{CH}_2\text{XCHX}_2$ , and  $\text{CH}_3(\text{CH}_2)_5\text{CH}_3$  and their Characteristic Frequency Zones. *Appl. Spectrosc.* **2006**, *60*, 450–458.
- (98) Iwamoto, R. Near-Infrared Spectroscopy as a Useful Tool for Analysis in Solution in Common Organic Solvents. *Appl. Spectrosc.* **2009**, *63*, 354–362.
- (99) Czarnik-Matusewicz, B.; Rospenk, M.; Koll, A.; Mavri, J. Influence of Substituents on the Anharmonicity of  $\nu_s(\text{OH})$  Vibration in Phenol Derivatives Explored by Experimental and Theoretical Approach. *J. Phys. Chem. A* **2005**, *109*, 2317–2324.
- (100) Czarnecki, M. A.; Wojtków, D.; Haufa, K. Rotational isomerism of butanols: Infrared, near-infrared and DFT study. *Chem. Phys. Lett.* **2006**, *431*, 294–299.
- (101) Lachenal, G. Dispersive and Fourier Transform Near-Infrared Spectroscopy of Polymeric Materials. *Vib. Spectrosc.* **1995**, *9*, 93–100.
- (102) Czarnecki, M. A.; Wu, P.; Siesler, H. W. 2D FT-NIR and FT-IR correlation analysis of temperature-induced changes of Nylon 12. *Chem. Phys. Lett.* **1998**, *283*, 326–332.
- (103) Wu, P.; Siesler, H. W.; Dal Maso, F.; Zanier, N. Rheo-optical Fourier-transform NIR spectroscopy of polyamide 11. *Analisis* **1998**, *26*, 61–64.
- (104) Wu, P.; Siesler, H. W. Two-dimensional correlation analysis of variable-temperature Fourier-transform mid- and near-infrared spectra of polyamide 11. *J. Mol. Struct.* **2000**, *521*, 37–47.
- (105) Wu, P.; Yang, Y.; Siesler, H. W. Two-dimensional near-infrared correlation temperature studies of an amorphous polyamide. *Polymer* **2001**, *42*, 10181–10186.
- (106) Siesler, H. W. Near-Infrared Spectroscopy of Polymers. *Makromol. Chem., Macromol. Symp.* **1991**, *52*, 113–129.
- (107) Weyer, L. G.; Lo, S. C. Spectra-Structure Correlations in the Near-Infrared. In *Handbook of Vibrational Spectroscopy*; Chalmers, J. M., Griffiths, P. R., Eds.; Wiley: Chichester, 2002; Vol. 3, p 1817.
- (108) Ozaki, Y.; Katsumoto, Y.; Jiang, J. H.; Liang, Y. Spectral analysis in the NIR region. In *Useful and Advanced Information in the Field of Near Infrared Spectroscopy*; Tsuchikawa, S., Ed.; Research Signpost: Trivandrum, India, 2003; p 1.
- (109) Rinnan, Å.; Berg, F.; Engelsen, S. B. Review of the most common pre-processing techniques for near-infrared spectra. *TrAC, Trends Anal. Chem.* **2009**, *28*, 1201–1222.
- (110) Czarnecki, M. A. Resolution Enhancement in Second-Derivative Spectra. *Appl. Spectrosc.* **2015**, *69*, 67–74.
- (111) Savitzky, A.; Golay, M. J. E. Smoothing and Differentiation of Data by Simplified Least Squares Procedures. *Anal. Chem.* **1964**, *36*, 1627–1639.
- (112) Kauppinen, J. K.; Moffatt, D. J.; Mantsch, H. H.; Cameron, D. G. Fourier Self-Deconvolution: A Method for Resolving Intrinsically Overlapped Bands. *Appl. Spectrosc.* **1981**, *35*, 271–276.
- (113) Noda, I. Two-dimensional infrared (2D-IR) spectroscopy of synthetic and biopolymers. *Bull. Am. Phys. Soc.* **1986**, *31*, 520–524.
- (114) Noda, I. Generalized Two-Dimensional Correlation Method Applicable to Infrared, Raman, and Other Types of Spectroscopy. *Appl. Spectrosc.* **1993**, *47*, 1329–1336.
- (115) Tandler, P. J.; Harrington, P. B.; Richardson, H. Effects of static spectrum removal and noise on 2D-correlation spectra of kinetic data. *Anal. Chim. Acta* **1998**, *368*, 45–57.
- (116) Maasart, D. L.; Vandeginste, B. G. M.; Buydens, L. M. C.; De Jong, S.; Lewi, P. J.; Smeyers-Verbeke, J. *Handbook of Chemometrics and Qualimetrics*, 3rd ed.; Elsevier: Amsterdam, 2003.
- (117) Gemperline, P., Ed. *Practical Guide to Chemometrics*; Taylor & Francis, Boca Raton, FL, 2006.
- (118) Brereton, R. G. *Applied Chemometrics for Scientists*; John Wiley & Sons: Chichester, UK, 2007.
- (119) Geladi, P. Chemometrics in spectroscopy. Part 1. Classical chemometrics. *Spectrochim. Acta, Part B* **2003**, *58*, 767–782.
- (120) Lavine, B.; Workman, J. Chemometrics. *Anal. Chem.* **2008**, *80*, 4519–4531.
- (121) Massart, D.; Kaufman, L. *The Interpretation of Analytical Chemical Data by the Use of Cluster Analysis*; Wiley: New York, 1983.
- (122) Wold, S.; Esbensen, K.; Geladi, P. Principal components analysis. *Chemom. Intell. Lab. Syst.* **1987**, *2*, 37–52.
- (123) Keller, H. R.; Massart, D. L. Evolving factor analysis. *Chemom. Intell. Lab. Syst.* **1991**, *12*, 209–224.
- (124) Tauler, R.; Kowalski, B.; Fleming, S. Multivariate curve resolution applied to spectral data from multiple runs of an industrial process. *Anal. Chem.* **1993**, *65*, 2040–2047.
- (125) Tauler, R.; Izquierdo-Ridorsa, A.; Casassas, E. Simultaneous analysis of several spectroscopic titrations with self-modelling curve resolution. *Chemom. Intell. Lab. Syst.* **1993**, *18*, 293–300.
- (126) Barker, M.; Rayens, W. Partial least squares for discrimination. *J. Chemom.* **2003**, *17*, 166–173.
- (127) Forina, M.; Lanteri, S.; Casale, M. Multivariate calibration. Review article. *J. Chromatogr. A* **2007**, *1158*, 61–93.
- (128) Jiang, J. H.; Berry, R. J.; Siesler, H. W.; Ozaki, Y. Wavelength interval selection in least squares regression with applications to mid-infrared and near-infrared spectroscopic data. *Anal. Chem.* **2002**, *74*, 3555–3565.
- (129) Walrafen, G. E. In *Water, a Comprehensive Treatise*; Francks, F., Ed.; Plenum Press: New York, 1972; Vol. 1, p 208.
- (130) Benson, S. W.; Siebert, D. E. A simple two-structure model for liquid water. *J. Am. Chem. Soc.* **1992**, *114*, 4269–4276.
- (131) Walrafen, G. E.; Hokmabadi, M. S.; Yang, W.-H. Raman isosbestic points from liquid water. *J. Chem. Phys.* **1986**, *85*, 6964–6969.
- (132) Walrafen, G. E.; Hokmabadi, M. S.; Yang, W.-H. Raman investigation of the temperature dependence of the bending  $\nu_2$  and combination  $\nu_2 + \nu_L$  bands from liquid water. *J. Phys. Chem.* **1988**, *92*, 2433–2438.
- (133) Maréchal, Y.  $\text{H}_2\text{O}$  and  $\text{D}_2\text{O}$  spectra from 6000 to  $0\text{ cm}^{-1}$ . *J. Chem. Phys.* **1991**, *95*, 5565–5573.
- (134) Libnau, F. O.; Toft, J.; Christy, A. A.; Kvalheim, O. M. Structure of Liquid Water Determined from Infrared Temperature Profiling and Evolutionary Curve Resolution. *J. Am. Chem. Soc.* **1994**, *116*, 8311–8316.
- (135) Max, J.-J.; Chapados, C. Isotope effects in liquid water by infrared spectroscopy. *J. Chem. Phys.* **2002**, *116*, 4626–4642.
- (136) Larouche, P.; Max, J.-J.; Chapados, C. Isotope effects in liquid water by infrared spectroscopy. II. Factor analysis of the temperature effect on  $\text{H}_2\text{O}$  and  $\text{D}_2\text{O}$ . *J. Chem. Phys.* **2008**, *129*, 064503.
- (137) Wouterson, S.; Emmerichs, U.; Bakker, H. J. Femtosecond mid-IR pump-probe spectroscopy of liquid water: Evidence for a two-component structure. *Science* **1997**, *278*, 658–660.
- (138) Franck, E. U.; Roth, K. Infra-red absorption of HDO in water at high pressures and temperatures. *Discuss. Faraday Soc.* **1967**, *43*, 108–114.
- (139) Efimov, Yu. Ya.; Naberukhin, Yu. I. The fluctuation hypothesis of hydrogen bonding VI. Calculation of the band shapes in infra-red and Raman spectra for normal and heavy water in the region of stretching vibrations. *Mol. Phys.* **1978**, *36*, 973–992.
- (140) Geissler, P. L. Temperature Dependence of Inhomogeneous Broadening: On the Meaning of Isosbestic Points. *J. Am. Chem. Soc.* **2005**, *127*, 14930–14935.
- (141) Ratcliffe, C. I.; Irish, D. E. Vibrational spectral studies of solutions at elevated temperatures and pressures. 5. Raman studies of liquid water up to  $300\text{ }^\circ\text{C}$ . *J. Phys. Chem.* **1982**, *86*, 4897–4905.
- (142) Eaves, J. D.; Loparo, J. J.; Fecko, C. J.; Roberts, S. T.; Tokmakoff, A.; Geissler, P. L. Hydrogen bonds in liquid water are broken only fleetingly. *Proc. Natl. Acad. Sci. U. S. A.* **2005**, *102*, 13019–13022.
- (143) Max, J.-J.; Chapados, C. Isotope effects in liquid water by infrared spectroscopy. IV. No free OH groups in liquid water. *J. Chem. Phys.* **2010**, *133*, 164509.



- (144) Zhukovskii, A. P. Justification of the continuous model of the structure of water by infrared spectroscopy. *J. Struct. Chem.* **1981**, *22*, 356–362.
- (145) Czarnecki, M. A. Frequency shift or intensity shift? The origin of spectral changes in vibrational spectra. *Vib. Spectrosc.* **2012**, *58*, 193–198.
- (146) Luck, W. A. P. The importance of cooperativity for the properties of liquid water. *J. Mol. Struct.* **1998**, *448*, 131–142.
- (147) Luck, W. A. P.; Ditter, W. Alcohol association up to the supercritical region. *Ber. Bunsen-Ges. Phys. Chem.* **1968**, *72*, 365–374.
- (148) Sandorfy, C. *The hydrogen bond—recent developments in theory and experiments*; North-Holland Publ. Co.: Amsterdam, 1976; Chapter 13, p 615.
- (149) Khoshtariya, D. E.; Zahl, A.; Dolidze, T. D.; Neubrand, A.; van Eldik, R. Local Dense Structural Heterogeneities in Liquid Water from Ambient to 300 MPa Pressure: Evidence for Multiple Liquid–Liquid Transitions. *ChemPhysChem* **2004**, *5*, 1398–1404.
- (150) Thompson, W. H.; Snyder, J. R. Mutual Solubilities of Benzene and Water. Equilibria in the Two Phase Liquid - Liquid Region. *J. Chem. Eng. Data* **1964**, *9*, 516–520.
- (151) Connolly, J. F. Solubility of Hydrocarbons in Water Near the Critical Solution Temperatures. *J. Chem. Eng. Data* **1966**, *11*, 13–16.
- (152) Jin, Y.; Ikawa, S. Near-infrared spectroscopic study of water at high temperatures and pressures. *J. Chem. Phys.* **2003**, *119*, 12432–12438.
- (153) Dickens, B.; Dickens, S. H. Estimation of concentration and bonding environment of water dissolved in common solvents using near infrared absorptivity. *J. Res. Natl. Inst. Stand. Technol.* **1999**, *104*, 173–183.
- (154) Alam, M. K.; Callis, J. B. Elucidation of species in alcohol-water mixtures using near-IR Spectroscopy and multivariate statistics. *Anal. Chem.* **1994**, *66*, 2293–2301.
- (155) Puxty, G.; Maeder, M.; Radack, K. P.; Gemperline, P. J. Equilibrium modeling of mixtures of methanol and water. *Appl. Spectrosc.* **2005**, *59*, 329–334.
- (156) Onori, G.; Santucci, A. Dynamical and structural properties of water/alcohol mixtures. *J. Mol. Liq.* **1996**, *69*, 161–181.
- (157) Jin, Y.; Ikawa, S. Near infrared study of water-benzene mixtures at high temperatures and pressures. *J. Chem. Phys.* **2004**, *121*, 2694–2700.
- (158) Jin, Y.; Ikawa, S. Spectroscopic study of mutual solubilities of water and benzene at high temperatures and pressures. *J. Chem. Phys.* **2005**, *122*, 024509.
- (159) Di Michele, A.; Freda, M.; Onori, G.; Santucci, A. Hydrogen bonding of water in aqueous solutions of TMAO and TBA: a near-infrared study. *J. Phys. Chem. A* **2004**, *108*, 6145–6150.
- (160) Balakrishnan, S.; Javid, N.; Weingärtner, H.; Winter, R. Small-angle X-ray scattering and near-infrared vibrational spectroscopy of water confined in aerosol-OT reverse micelles. *ChemPhysChem* **2008**, *9*, 2794–2801.
- (161) Saitow, K.; Kobayashi, K.; Nishikawa, K. How Are Hydrogen Bonds Perturbed in Aqueous NaClO<sub>4</sub> Solutions Depending on the Concentration?: A Near Infrared Study of Water. *J. Solution Chem.* **2004**, *33*, 689–698.
- (162) Sebe, F.; Nishikawa, K.; Koga, Y. Spectrum of excess partial molar absorptivity. Part II: a near infrared spectroscopic study of aqueous Na-halides. *Phys. Chem. Chem. Phys.* **2012**, *14*, 4433–4439.
- (163) Koga, Y.; Sebe, F.; Minami, T.; Otake, K.; Saitow, K.; Nishikawa, K. Spectrum of excess partial molar absorptivity. I. Near infrared spectroscopic study of aqueous acetonitrile and acetone. *J. Phys. Chem. B* **2009**, *113*, 11928–11935.
- (164) Takeuchi, M.; Martra, G.; Coluccia, S.; Anpo, M. Investigations of the structure of H<sub>2</sub>O clusters adsorbed on TiO<sub>2</sub> surfaces by near-infrared absorption spectroscopy. *J. Phys. Chem. B* **2005**, *109*, 7387–7391.
- (165) Takeuchi, M.; Sakamoto, K.; Martra, G.; Coluccia, S.; Anpo, M. Mechanism of photoinduced superhydrophilicity on the TiO<sub>2</sub> photocatalyst surface. *J. Phys. Chem. B* **2005**, *109*, 15422–15428.
- (166) Takeuchi, M.; Martra, G.; Coluccia, S.; Anpo, M. Evaluation of the adsorption states of H<sub>2</sub>O on oxide surfaces by vibrational absorption: near- and mid-infrared spectroscopy. *J. Near Infrared Spectrosc.* **2009**, *17*, 373–384.
- (167) Iwahashi, M.; Hachiya, N.; Hayashi, Y.; Matsuzawa, H.; Liu, Y.; Czarnecki, M. A.; Ozaki, Y.; Horiuchi, T.; Suzuki, M. Self-association of cis-9-octadecen-1-ol in the pure liquid state and in decane solutions as observed by viscosity, self-diffusion, nuclear magnetic resonance, electron spin resonance and near-infrared spectroscopic measurements. *J. Phys. Chem.* **1995**, *99*, 4155–4161.
- (168) Stordrange, L.; Christy, A. A.; Kvalheim, O. M.; Shen, H.; Liang, Y. Study of the self-association of alcohols by near-infrared spectroscopy and multivariate 2D techniques. *J. Phys. Chem. A* **2002**, *106*, 8543–8553.
- (169) Herndon, W. C.; Vincenti, S. P. Hydrogen bonding in optically active and racemic 2-butanol. *J. Am. Chem. Soc.* **1983**, *105*, 6174–6175.
- (170) Palombo, F.; Tassaing, T.; Danten, Y.; Besnard, M. Hydrogen bonding in liquid and supercritical 1-octanol and 2-octanol assessed by near and midinfrared spectroscopy. *J. Chem. Phys.* **2006**, *125*, 094503–1.
- (171) Kuen, D. S.; Feierabend, K. J. Cavity-enhanced overtone spectroscopy of methanol in aprotic solvents: probing solute-solvent interactions and self-associative behavior. *J. Phys. Chem. A* **2014**, *118*, 2942–2951.
- (172) Murthy, A. S.; Davis, R. E.; Rao, C. N. R. Hydrogen bonding: A molecular orbital treatment by the EHT and the CNDO/2 methods of methanol and of formic acid. *Theoret. Chim. Acta* **1969**, *13*, 81–90.
- (173) Turi, L.; Dannenberg, J. J. Molecular orbital study of acetic acid aggregation. 1. Monomers and dimers. *J. Phys. Chem.* **1993**, *97*, 12197–12204.
- (174) Navea, S.; de Juan, A.; Tauler, R. Modeling Temperature-Dependent Protein Structural Transitions by Combined Near-IR and Mid-IR Spectroscopies and Multivariate Curve Resolution. *Anal. Chem.* **2003**, *75*, 5592–5601.
- (175) Wang, J.; Sowa, M. G.; Ahmed, M. K.; Mantsch, H. H. Photoacoustic near-infrared investigation of homo-polypeptides. *J. Phys. Chem.* **1994**, *98*, 4748–4755.
- (176) Robert, P.; Devaux, M. F.; Mouhous, N.; Dufour, E. Monitoring the secondary structure of proteins by near-infrared spectroscopy. *Appl. Spectrosc.* **1999**, *53*, 226–232.
- (177) Izutsu, K.; Fujimaki, Y.; Kuwabara, A.; Hiyama, Y.; Yomota, C.; Aoyagi, N. Near-infrared analysis of protein secondary structure in aqueous solutions and freeze-dried solids. *J. Pharm. Sci.* **2006**, *95*, 781–789.
- (178) Wu, B.; Liu, Y.; Zhang, Y.; Wang, H. Probing Intermolecular Interactions in Ionic Liquid–Water Mixtures by Near-Infrared Spectroscopy. *Chem. - Eur. J.* **2009**, *15*, 6889–6893.
- (179) Wu, B.; Zhang, Y.; Wang, H. Insight into the Intermolecular Interactions in Ionic Liquid–Ethanol–Water Mixtures by Near-Infrared Spectroscopy. *Z. Phys. Chem.* **2009**, *223*, 849–856.
- (180) Wu, B.; Zhang, Y.; Wang, H. Insight into the Intermolecular Interactions in [B<sub>mim</sub>]<sup>+</sup>BF<sub>4</sub><sup>−</sup>/[A<sub>mim</sub>]<sup>+</sup>Cl<sup>−</sup>–Ethanol–Water Mixtures by Near-Infrared Spectroscopy. *J. Phys. Chem. B* **2009**, *113*, 12332–12336.
- (181) Howard, D. L.; Jørgensen, P.; Kjaergaard, H. G. Weak intramolecular interactions in ethylene glycol identified by vapor phase OH-stretching overtone spectroscopy. *J. Am. Chem. Soc.* **2005**, *127*, 17096–17103.
- (182) Howard, D. L.; Kjaergaard, H. G. Influence of intramolecular hydrogen bond strength on OH-stretching overtones. *J. Phys. Chem. A* **2006**, *110*, 10245–10250.
- (183) Miller, B. J.; Howard, D. L.; Lane, J. R.; Kjaergaard, H. G.; Dunn, M. E.; Vaida, V. SH-stretching vibrational spectra of ethanethiol and tert-butylthiol. *J. Phys. Chem. A* **2009**, *113*, 7576–7583.
- (184) Miller, B. J.; Yekutieli, M.; Sodergren, A. H.; Howard, D. L.; Dunn, M. E.; Vaida, V.; Kjaergaard, H. G. Overtone spectra of 2-mercaptoethanol and 1,2-ethanedithiol. *J. Phys. Chem. A* **2010**, *114*, 12692–12700.

- (185) Rong, Z.; Henry, B. R.; Robinson, T. W.; Kjaergaard, H. G. Absolute intensities of CH stretching overtones in alkenes. *J. Phys. Chem. A* **2005**, *109*, 1033–1041.
- (186) Waldrom, R. J.; Kuschel, M.; Kjaergaard, H. G.; Henry, B. R. CH-stretching overtone spectra of cis- and trans-1,3-pentadiene. *J. Phys. Chem. A* **2006**, *110*, 913–920.
- (187) Kjaergaard, H. G.; Henry, B. R. CH Stretching Overtone Spectra and Intensities of Vapor Phase Naphthalene. *J. Phys. Chem.* **1995**, *99*, 899–904.
- (188) Thomsen, D. L.; Axson, J. L.; Schroder, S. D.; Lane, J. R.; Vaida, V.; Kjaergaard, H. H. Intramolecular Interactions in 2-Aminoethanol and 3-Aminopropanol. *J. Phys. Chem. A* **2013**, *117*, 10260–10273.
- (189) Du, L.; Mackeprang, K.; Kjaergaard, H. G. Fundamental and overtone vibrational spectroscopy, enthalpy of hydrogen bond formation and equilibrium constant determination of the methanol-dimethylamine complex. *Phys. Chem. Chem. Phys.* **2013**, *15*, 10194–10206.
- (190) Billinghurst, B. E.; Gough, K. M.; Low, G. R.; Kjaergaard, H. G. CH stretching overtone spectra of trimethyl amine and dimethyl sulfide. *J. Mol. Struct.* **2004**, *687*, 87–99.
- (191) Havey, D. K.; Vaida, V. Near infrared spectroscopy of organic acids: comparing O-H and C-H oscillator frequencies and intensities. *J. Mol. Spectrosc.* **2004**, *228*, 152–159.
- (192) Perchard, J. P.; Mielke, Z. Anharmonicity and hydrogen bonding: I. A near-infrared study of methanol trapped in nitrogen and argon matrices. *Chem. Phys.* **2001**, *264*, 221–234.
- (193) Perchard, J. P.; Romain, F.; Bouteiller, Y. Determination of vibrational parameters of methanol from matrix-isolation infrared spectroscopy and ab initio calculations. Part I – Spectral analysis in the domain 11 000–200 cm<sup>-1</sup>. *Chem. Phys.* **2008**, *343*, 35–46.
- (194) Perchard, J. P. Anharmonicity and hydrogen bonding: II – A near infrared study of water trapped in nitrogen matrix. *Chem. Phys.* **2001**, *266*, 109–124.
- (195) Perchard, J. P. Anharmonicity and hydrogen bonding. III. Analysis of the near infrared spectrum of water trapped in argon matrix. *Chem. Phys.* **2001**, *273*, 217–233.
- (196) Bouteiller, Y.; Perchard, J. P. The vibrational spectrum of (H<sub>2</sub>O)<sub>2</sub>: comparison between anharmonic ab initio calculations and neon matrix infrared data between 9000 and 90 cm<sup>-1</sup>. *Chem. Phys.* **2004**, *305*, 1–12.
- (197) Bouteiller, Y.; Tremblay, B.; Perchard, J. P. The vibrational spectrum of the water dimer: Comparison between anharmonic ab initio calculations and neon matrix infrared data between 14,000 and 90 cm<sup>-1</sup>. *Chem. Phys.* **2011**, *386*, 29–40.
- (198) Tremblay, B.; Madebène, B.; Alikhani, M. E.; Perchard, J. P. The vibrational spectrum of the water trimer: Comparison between anharmonic ab initio calculations and neon matrix infrared data between 11,000 and 90 cm<sup>-1</sup>. *Chem. Phys.* **2010**, *378*, 27–36.
- (199) Parker, M. E.; Steele, D.; Smith, M. J. C. Vibrational absorption intensities in chemical analysis. 9 The near-infrared spectra of methyl branched alkanes. *J. Phys. Chem. A* **1997**, *101*, 9618–9631.
- (200) Kwaśniewicz, M.; Czarnecki, M. A. MIR and NIR group spectra of n-alkanes and 1-chloroalkanes. *Spectrochim. Acta, Part A* **2015**, *143*, 165–171.
- (201) Kelly, J. J.; Barlow, C. H.; Jinguji, T. M.; Callis, J. B. Prediction of gasoline octane numbers by near infrared spectroscopy in the spectral range 680–1235 nm. *Anal. Chem.* **1989**, *61*, 313–320.
- (202) Wang, X.-G.; Carrington, T. New ideas for using contracted basis functions with a Lanczos eigensolver for computing vibrational spectra of molecules with four or more atoms. *J. Chem. Phys.* **2002**, *117*, 6923–6934.
- (203) Venuti, E.; Halonen, L.; Della Valle, R. G. High dimensional anharmonic potential energy surfaces: The case of methane. *J. Chem. Phys.* **1999**, *110*, 7339–7347.
- (204) McCoy, A. B. Diffusion Monte Carlo approaches for investigating the structure and vibrational spectra of fluxional systems. *Int. Rev. Phys. Chem.* **2006**, *25*, 77–107.
- (205) Bowman, J. M. Self-consistent field energies and wavefunctions for coupled oscillators. *J. Chem. Phys.* **1978**, *68*, 608–610.
- (206) Gerber, R. B. A semiclassical self-consistent field (SC SCF) approximation for eigenvalues of coupled-vibration systems. *Chem. Phys. Lett.* **1979**, *68*, 195–198.
- (207) Christoffel, K. M.; Bowman, J. M. Investigations of self-consistent field, scf ci and virtual stateconfiguration interaction vibrational energies for a model three-mode system. *Chem. Phys. Lett.* **1982**, *85*, 220–224.
- (208) Bowman, J. M.; Carter, S.; Huang, X. MULTIMODE: A code to calculate rovibrational energies of polyatomic molecules. *Int. Rev. Phys. Chem.* **2003**, *22*, 533–549.
- (209) Christiansen, O. Selected new developments in vibrational structure theory: potential construction and vibrational wave function calculations. *Phys. Chem. Chem. Phys.* **2012**, *14*, 6672–6687.
- (210) Barone, V. Vibrational zero-point energies and thermodynamic functions beyond the harmonic approximation. *J. Chem. Phys.* **2004**, *120*, 3059–3065.
- (211) Barone, V.; Biczysko, M.; Bloino, J.; Borkowska-Panek, M.; Carnimeo, I.; Panek, P. Toward anharmonic computations of vibrational spectra for large molecular systems. *Int. J. Quantum Chem.* **2012**, *112*, 2185–2200.
- (212) Yagi, K.; Taketsugu, T.; Hirao, K.; Gordon, M. S. Direct vibrational self-consistent field method: Applications to H<sub>2</sub>O and H<sub>2</sub>CO. *J. Chem. Phys.* **2000**, *113*, 1005–1017.
- (213) Yagi, K.; Hirao, K.; Taketsugu, T.; Schmidt, W. M.; Gordon, M. S. Ab initio vibrational state calculations with a quartic force field: Applications to H<sub>2</sub>CO, C<sub>2</sub>H<sub>4</sub>, CH<sub>3</sub>OH, CH<sub>3</sub>CCH, and C<sub>6</sub>H<sub>6</sub>. *J. Chem. Phys.* **2004**, *121*, 1383–1389.
- (214) Yagi, K.; Hirata, S.; Hirao, K. Multiresolution potential energy surfaces for vibrational state calculations. *Theor. Chem. Acc.* **2007**, *118*, 681–691.
- (215) Yagi, K.; Hirata, S.; Hirao, K. Vibrational quasi-degenerate perturbation theory: applications to fermi resonance in CO<sub>2</sub>, H<sub>2</sub>CO, and C<sub>6</sub>H<sub>6</sub>. *Phys. Chem. Chem. Phys.* **2008**, *10*, 1781–1788.
- (216) Yagi, K.; Keçeli, M.; Hirata, S. Optimized coordinates for anharmonic vibrational structure theories. *J. Chem. Phys.* **2012**, *137*, 204118–16.
- (217) Thomsen, B.; Yagi, K.; Christiansen, O. Optimized coordinates in vibrational coupled cluster calculations. *J. Chem. Phys.* **2014**, *140*, 154102–15.
- (218) Maeda, S.; Watanabe, Y.; Ohno, K. A scaled hypersphere interpolation technique for efficient construction of multidimensional potential energy surfaces. *Chem. Phys. Lett.* **2005**, *414*, 265–270.
- (219) Ohno, K.; Maeda, S. Ab initio anharmonic calculations of vibrational frequencies of benzene by means of efficient construction of potential energy functions. *Chem. Phys. Lett.* **2011**, *503*, 322–326.
- (220) Yamada, T.; Aida, M. Fundamental absorption frequencies and mean structures at vibrational ground state from quasi-classical direct ab initio MD: Triatomic molecule. *Chem. Phys. Lett.* **2008**, *452*, 315–320.
- (221) Yamada, T.; Aida, M. Structures of Molecules in Ground and Excited Vibrational States from Quasiclassical Direct ab Initio Molecular Dynamics. *J. Phys. Chem. A* **2010**, *114*, 6273–6283.
- (222) Yagi, K.; Karasawa, H.; Hirata, S.; Hirao, K. First-Principles Quantum Calculations on the Infrared Spectrum and Vibrational Dynamics of the Guanine-Cytosine Base Pair. *ChemPhysChem* **2009**, *10*, 1442–1444.
- (223) Akai, N.; Katsumoto, Y.; Ohno, K.; Aida, M. Vibrational anharmonicity of acetic acid studied by matrix-isolation near-infrared spectroscopy and DFT calculation. *Chem. Phys. Lett.* **2005**, *413*, 367–372.
- (224) Yoshida, H.; Takeda, K.; Okamura, J.; Ehara, A.; Matsuura, H. A New Approach to Vibrational Analysis of Large Molecules by Density Functional Theory: Wavenumber-Linear Scaling Method. *J. Phys. Chem. A* **2002**, *106*, 3580–3586.
- (225) Sandorfy, C.; Buchet, R.; Lachenal, G. Principles of Molecular Vibrations for Near-Infrared Spectroscopy. In *Near Infrared Spectros-*

copy in *Food Science and Technology*; Ozaki, Y., McClure, W. F., Christy, A. A., Eds.; Wiley Interscience: New York, 2006; p 11.

(226) Mortensen, O. S.; Henry, B. R.; Mohammadi, M. A. The effects of symmetry within the local mode picture: A reanalysis of the overtone spectra of the dihalomethanes. *J. Chem. Phys.* **1981**, *75*, 4800–4808.

(227) Child, M. S.; Lawton, R. T. Local and normal vibrational states: a harmonically coupled anharmonic-oscillator model. *Faraday Discuss. Chem. Soc.* **1981**, *71*, 273–285.

(228) Child, M. S.; Halonen, L. Overtone Frequencies and Intensities in the Local Mode Picture. *Adv. Chem. Phys.* **1984**, *57*, 1–58.

(229) Henry, B. R.; Siebrand, W. Anharmonicity in Polyatomic Molecules. The CH - Stretching Overtone Spectrum of Benzene. *J. Chem. Phys.* **1968**, *49*, 5369–5676.

(230) Swanton, D. J.; Henry, B. R. A theoretical basis for the correlation between bond length and local mode frequency. *J. Chem. Phys.* **1987**, *86*, 4801–4807.

(231) Goswami, P. C.; Swanton, D. J.; Henry, B. R. Evidence for vibronic coupling contributions to overtone intensities in alkyl phenyl ketones. *J. Chem. Phys.* **1987**, *86*, 5281–5287.

(232) Kjaergaard, H. G.; Yu, H.; Schattka, B. J.; Henry, B. R.; Tarr, A. W. Intensities in local mode overtone spectra: Propane. *J. Chem. Phys.* **1990**, *93*, 6239–6248.

(233) Kjaergaard, H. G.; Howard, D. L.; Schofield, D. P.; Robinson, T. W.; Ishiuchi, S.; Fujii, M. OH- and CH-Stretching Overtone Spectra of Catechol. *J. Phys. Chem. A* **2002**, *106*, 258–266.

(234) Du, L.; Lane, J. R.; Kjaergaard, H. G. Identification of the dimethylamine-trimethylamine complex in the gas phase. *J. Chem. Phys.* **2012**, *136*, 184305–8.

(235) Miller, B. J.; Du, L.; Steel, T. J.; Paul, A. J.; Sodergren, A. H.; Lane, J. R.; Henry, B. R.; Kjaergaard, H. G. Absolute Intensities of NH-Stretching Transitions in Dimethylamine and Pyrrole. *J. Phys. Chem. A* **2012**, *116*, 290–296.

(236) Takahashi, K.; Sugawara, M.; Yabushita, S. Theoretical Analysis on the Fundamental and Overtone OH Stretching Spectra of Several Simple Acids and Alcohols. *J. Phys. Chem. A* **2003**, *107*, 11092–11101.

(237) Takahashi, K.; Sugawara, M.; Yabushita, S. Effective One-Dimensional Dipole Moment Function for the OH Stretching Overtone Spectra of Simple Acids and Alcohols. *J. Phys. Chem. A* **2005**, *109*, 4242–4251.

(238) Takahashi, H.; Yabushita, S. Theoretical Analysis of Weak Adjacent Substituent Effect on the Overtone Intensities of XH (X = C, O) Stretching Vibrations. *J. Phys. Chem. A* **2013**, *117*, 5491–5502.

(239) Futami, Y.; Ozaki, Y.; Hamada, Y.; Ozaki, Y. Frequencies and absorption intensities of the fundamental and the first overtone of NH stretching vibrations of pyrrole-acetylene and pyrrole-ethylene complexes studied by density-functional-theory calculation. *Vib. Spectrosc.* **2014**, *72*, 124–127.

(240) Mecke, R.; Ziegler, R. Das Rotationsschwingungsspektrum des Acetylens ( $C_2H_2$ ). *Eur. Phys. J. A* **1936**, *101*, 405–417.

(241) Henry, B. R. The local mode model and overtone spectra: a probe of molecular structure and conformation. *Acc. Chem. Res.* **1977**, *10*, 207–213.

(242) Henry, B. R. Use of local modes in the description of highly vibrationally excited molecules. *Acc. Chem. Res.* **1987**, *20*, 429–435.

(243) Foldes, A.; Sandorfy, C. Anharmonicity and hydrogen bonding: Part III. Examples of strong bonds. General discussion. *J. Mol. Spectrosc.* **1966**, *20*, 262–275.

(244) Singh, S.; Schiöberg, D.; Luck, W. A. P. Dipole Moment Derivatives of Free and Hydrogen Bonded O-H Bond of Methanol. *Spectrosc. Lett.* **1981**, *14*, 141–155.

(245) Singh, S.; Fritzsche, M.; Kümmerle, I.; Luck, W. A. P.; Zheng, H. Y. Variation of Dipole Moment Function of O-H Bond of t-Butanol with the Nature of Solvent and Its Temperature. *Spectrosc. Lett.* **1985**, *18*, 283–299.

(246) Detoni, S.; Hadzi, D.; Juranji, M. A study of proton donor-acceptor systems in the overtone region. *Spectrochim. Acta, Part A* **1974**, *30*, 249–253.

(247) Galabov, B.; Dudev, T.; Orville-Thomas, W. J. Interpretation and prediction of vibrational intensities in infrared spectra: fluorinated methanes. *J. Mol. Struct.* **1986**, *145*, 1–13.

(248) Dudev, T.; Galabov, B.; Orville-Thomas, W. J. Interpretation of infrared intensities of some simple hydrides. *J. Mol. Struct.* **1987**, *157*, 289–294.

(249) Bobadova-Parvanova, P.; Galabov, B. Ab Initio Molecular-Orbital Study of Hydrogen-Bonded Complexes of Carbonyl Aliphatic Compounds and Hydrogen Fluoride. *J. Phys. Chem. A* **1998**, *102*, 1815–1819.

(250) Durig, J. R.; Klaassen, J. J.; Panikar, S. S.; Darkhalil, I. D.; Ganguly, A.; Guirgis, G. A. Conformational and structural studies of 2,2-difluoroethylamine from temperature dependent infrared spectra of xenon solution and *ab initio* calculations. *J. Mol. Struct.* **2011**, *993*, 73–85.

(251) Durig, J. R.; Panikar, S. S.; Glenn, K. A.; Zheng, Y. Y.; Guirgis, G. A. Infrared and Raman spectra, conformational stability and vibrational assignment of 1-chloro-1-silacyclopentane. *Vib. Spectrosc.* **2011**, *55*, 250–257.

(252) Nagashima, N.; Kudoh, S.; Nakata, M. Infrared and UV–visible absorption spectra of hexafluoroacetylacetone in a low-temperature argon matrix. I. Structure of a non-chelated enol-type isomer. *Chem. Phys. Lett.* **2003**, *374*, 59–66.

(253) Futami, Y.; Chin, M. L. S.; Kudoh, S.; Takayanagi, M.; Nakata, M. Conformations of nitro-substituted spiropyran and merocyanine studied by low-temperature matrix-isolation infrared spectroscopy and density-functional-theory calculation. *Chem. Phys. Lett.* **2003**, *370*, 460–468.

(254) Nishida, J.; Shigeto, S.; Yabumoto, S.; Hamaguchi, H. Anharmonic coupling of the CH-stretch and CH-bend vibrations of chloroform as studied by near-infrared electroabsorption spectroscopy. *J. Chem. Phys.* **2012**, *137*, 234501–9.

(255) Wójcik, M. J.; Nakamura, H.; Iwata, S.; Tatara, W. Theoretical study of multidimensional proton tunneling in the excited state of tropolone. *J. Chem. Phys.* **2000**, *112*, 6322–6358.

(256) Frisch, M. J.; et al. GAUSSIAN09, Revision B.05; Gaussian, Inc.: Pittsburgh, PA, 2003.

(257) Becke, A. D. Density-functional thermochemistry. III. The role of exact exchange. *J. Chem. Phys.* **1993**, *98*, 5648–5652.

(258) Lee, C.; Yang, W.; Parr, R. G. Development of the Colle-Salvetti correlation-energy formula into a functional of the electron density. *Phys. Rev. B: Condens. Matter Mater. Phys.* **1988**, *37*, 785–789.

(259) Johnson, B. R. New numerical methods applied to solving the one-dimensional eigenvalue problem. *J. Chem. Phys.* **1999**, *67*, 4086–4093.

(260) Mellouki, A.; Liévin, J.; Herman, M. The vibrational spectrum of pyrrole ( $C_4H_5N$ ) and furan ( $C_4H_4O$ ) in the gas phase. *Chem. Phys.* **2001**, *271*, 239–266.

(261) Buckingham, A. D. Solvent effects in vibrational spectroscopy. *Trans. Faraday Soc.* **1960**, *56*, 753–760.